

MIT/WHOI 2007-16

**Massachusetts Institute of Technology
Woods Hole Oceanographic Institution**



**Joint Program
in Oceanography/
Applied Ocean Science
and Engineering**



DOCTORAL DISSERTATION

Influence Of Hydrodynamics On The Larval Supply To
Hydrothermal Vents On The East Pacific Rise

by

Diane K. Adams

June 2007

20070927453

MIT/WHOI

2007-16

Influence Of Hydrodynamics On The Larval Supply To
Hydrothermal Vents On The East Pacific Rise

by

Diane K. Adams

Massachusetts Institute of Technology
Cambridge, Massachusetts 02139

and

Woods Hole Oceanographic Institution
Woods Hole, Massachusetts 02543

June 2007

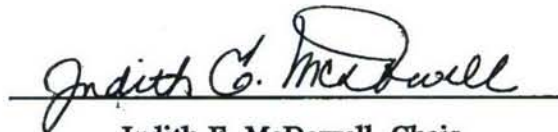
DOCTORAL DISSERTATION

Funding was provided by a National Defense Science and Engineering Graduate Fellowship, the WHOI Academic Programs Office, a WHOI Ocean Venture Fund award, the Ocean Life Institute, the Deep Ocean Exploration Institute, and National Science Foundation grants OCE0424953 and OCE9712233 to L.S. Mullineaux

Reproduction in whole or in part is permitted for any purpose of the United States Government. This thesis should be cited as: Diane K. Adams, 2007. Influence of Hydrodynamics on the Larval Supply to Hydrothermal Vents on the East Pacific Rise. Ph.D. Thesis. MIT/WHOI, 2007-16.

Approved for publication; distribution unlimited.

Approved for Distribution:

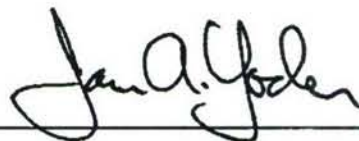


Judith E. McDowell, Chair

Department of Biology



Paola Malanotte-Rizzoli
MIT Director of Joint Program



James A. Yoder
WHOI Dean of Graduate Studies

Influence of hydrodynamics on the larval supply to hydrothermal vents on the East Pacific Rise

by

Diane K Adams

Bachelors of Science, University of California, Santa Barbara, 2001

Submitted in partial fulfillment of the requirements for the degree of

Doctor of Philosophy

at the

MASSACHUSETTS INSTITUTE OF TECHNOLOGY

and the

WOODS HOLE OCEANOGRAPHIC INSTITUTION

June 2007

© 2007 Diane K Adams, All rights reserved.

The author hereby grants to MIT and WHOI permission to reproduce and distribute publicly paper and electronic copies of this thesis document in whole or in part.

Author 

Department of Biology
Massachusetts Institute of Technology
and Woods Hole Oceanographic Institution
May 25, 2007

Certified by 

Lauren S. Mullineaux
Senior Scientist, Woods Hole Oceanographic Institution
Woods Hole Oceanographic Institution

Accepted by 

Ed DeLong
Chair Joint Committee for Biological Oceanography
Massachusetts Institute of Technology
and Woods Hole Oceanographic Institution

Influence of hydrodynamics on the larval supply to hydrothermal vents on the East Pacific Rise

by

Diane K Adams

Submitted to the Department of Biology
on May 25, 2007, in partial fulfillment of the
requirements for the degree of
Doctor of Philosophy

Abstract

Examination of the scales at which larval supply varies spatially and temporally, and correlation with concurrent physical observations can provide insights into larval transport mechanisms that contribute to structuring marine benthic communities. In order to facilitate field studies, this thesis first provides new morphological and genetic identifications for hydrothermal vent gastropod larvae along the northern East Pacific Rise. Daily and weekly variability in the supply of hydrothermal vent gastropod larvae to two hydrothermal vents, 1.6 km apart on the East Pacific Rise, were quantified concurrently with current velocity observations. The magnitude and temporal pattern of larval supply differed between vent sites, despite their close proximity. A strong correlation between along-axis flow and daily larval supply suggested that larval supply occurred primarily via along-axis transport between local sources 1-2 km apart. However, weekly larval supply appeared to be driven by larger spatial scales through losses associated with cross-axis flows and the passage of mesoscale eddies. Tracer movement within a quasi-geostrophic eddy model was consistent with the observations of decreased larval supply concurrent with an eddy observed via satellite altimetry. The tracer movement also indicated that deep eddy-induced flow could facilitate a long-distance dispersal event, enhancing dispersal between vents 100s km apart.

Thesis supervisor: Lauren S. Mullineaux
Title: Senior Scientist
Woods Hole Oceanographic Institution

Acknowledgments

I dedicate this thesis to my family - past, present and future. My grandparents fostered an innate curiosity and creativity within me that my parents then turned towards the sea. They cultured my love for the ocean throughout my life, from tidepooling as a toddler, dinner discussions afterschool, to emails during my first research cruise doing 'real' science. My devoted and unyielding husband constantly reminds me of the joys of life, within and outside of science. His unwavering support has kept me (relatively) sane throughout this often grueling, often wonderful, journey of graduate school. I can not possibly thank you enough.

My curiosity and creativity has flourished as a graduate student due to the collaborative effort of many supportive and brilliant colleagues who have provided guidance, knowledge, laughs, and resources that allowed me to complete this document. Foremost, I'd like to offer my sincere appreciation to my advisor, Lauren Mullineaux. You have been indispensable as a mentor, colleague, and voice of reason; and you were patient and understanding, even when I was too stubborn to listen to the voice of reason. Since my dissertation was interdisciplinary in nature, I also relied heavily upon my thesis committee and many members of WHOI to collect, interpret, and understand my data. Thank you to Glenn Flierl for allowing me to use your model and taking the time and effort to explain the model and physics to me, a biologist. Additionally, I'd like to thank Irene Garcia Berdeal, Karl Helfrich, Terry Joyce, Bill Lavelle, Jim Ledwell, Steven Lentz, Joe Pedlosky, and Jack Whitehead for helpful discussions that enlightened my understanding of fluid dynamics and physics in general. I appreciate Jesús Pineda's attention to my work that assured that I 'did it the right way', and thank you to Andy Solow for the statistics help that made sure that it *was* right. I am grateful to Tim Shank for wonderful discussions about science and numerous cruise opportunities, without which I might not have retrieved my thesis data and samples. John Kemp, Steve Manganini, Todd Morrison, Rick Trask, Sandy Williams, and Scott Worrirow provided the engineering know-how, instrumentation and hardware needed to collect the bulk of the data and samples for my thesis - thank you all. I'd like to acknowledge Marv Lilley, Costa Vetriani, and Karen Von Damm who as chief scientists provided me a bunk and ship time for my thesis work. I am also indebted to the captains and crew of the *RV Atlantis* and the pilots and crew of the *DSV Alvin* for their outstanding professionalism and kindness which made the at-sea operations a success - the moorings and instruments that went into the water

also came back out. I would especially like to thank Pat Hickey, Bruce Strickrott, Gavin Eppard, and Anthony Tarantino for their help on impossible projects and the good times at sea which made the long workdays bearable. I would also like to thank Stace Beaulieu, Susan Mills, Carly Strasser, Kate Buckman, Breea Govenar, Rhian Waller, and Abby Fusaro for making life more fun and for their assistance at-sea and in the lab. I would like to extend thanks to my labmates, Heidi Fuchs, Lara Gulmann, Rob Jennings, Susan Mills, Nathalie Reyns and a special thank you to Carly Strasser who was forced to read numerous versions of this document and to share my woes and triumphs. I'd finally like to acknowledge the wonderful job that the administrative staff and the Academic Programs Office did to take care of me and to make sure that I could focus on the science. Thank you all and anyone else I may have missed.

Financial support was provided by a National Defense Science and Engineering Graduate Fellowship, the WHOI Academic Programs Office, a WHOI Ocean Venture Fund award, the Ocean Life Institute, the Deep Ocean Exploration Institute, and NSF grants OCE0424953 and NSF OCE9712233 to L.S. Mullineaux.

Contents

1	Introduction	15
1.1	Thesis Organization	18
2	Morphological and molecular identification of gastropod larvae	23
2.1	Introduction	23
2.2	Methods	25
2.2.1	Sample Collection	25
2.2.2	Morphological Identification	26
2.2.3	Identification of a Defined Group of Species - RFLP Design	27
2.2.4	Identification with No Morphological Information - Expanding the Sequence Database	30
2.2.5	Application to Larval Samples	31
2.3	Results	32
2.3.1	Morphological Identification and Descriptions	32
2.3.2	Identification of a Defined Group of Species - RFLP Design	35
2.3.3	Identification with No Morphological Information - Expanding the Sequence Database	36
2.3.4	Application to Larval Samples	39
2.4	Discussion	40
2.4.1	The Staged Approach to Larval Identification	40
2.4.2	Daily Larval Collections	46
2.4.3	Egg Capsules	47
2.5	Supplemental Material	51
3	Gastropod larval flux to hydrothermal vents influenced by spatial and temporal variability in currents on small scales	57
3.1	Abstract	57
3.2	Introduction	58
3.3	Methods	61
3.3.1	Study Sites	61
3.3.2	Sample Collection	62
3.3.3	Correlation between Larval Flux and Transport	65
3.4	Results	68

3.4.1	Larval Fluxes	68
3.4.2	Currents	71
3.4.3	Larval Flux and Hydrodynamics	75
3.5	Discussion	76
3.5.1	Transport from a Larval Source	76
3.5.2	Implications for Larval Sampling	80
3.5.3	Ecological Implications of Variable Supply	81
3.6	Supplemental Material	82
3.6.1	Correction for Autocorrelation	82
4	Larval transport contributes to successful larval dispersal and larval loss	91
4.1	Introduction	91
4.2	Methods	93
4.2.1	Experimental Design	93
4.2.2	Along-Axis Transport	96
4.2.3	Cross-Axis Transport	98
4.2.4	Sea Level Anomalies	100
4.3	Results	103
4.3.1	Current Velocities	103
4.3.2	Variation in Larval Flux	103
4.3.3	Cross-Axis Transport	107
4.3.4	Along-Axis Transport	107
4.3.5	Sea Level Anomalies	109
4.4	Discussion	109
4.5	Supplemental Material	117
5	Mesoscale eddies extend into the deep-sea: implications for larval dispersal	123
5.1	Introduction	123
5.2	Methods	126
5.2.1	Observations	126
5.2.2	Quasi-Geostrophic Model	128
5.3	Results	134
5.3.1	Sea Surface Observations	134
5.3.2	Quasi-Geostrophic Model	135
5.4	Discussion	145
5.4.1	Applicability to Tehuantepec and Papagayo Eddies	145
5.4.2	Vertical Structure	150
5.4.3	Ridge Interactions	152
5.4.4	Implications for Dispersal	153

6	Conclusion	159
6.1	Summary of Results	159
6.2	Recovery from Disturbance	161
6.3	Mesoscale Eddies	162

List of Figures

2-1	Flow chart of staged identification procedure	26
2-2	Identification of <i>Gorgolettis spiralis</i>	29
2-3	Identification of <i>Echinopelta fistulosa</i>	33
2-4	Morphological Similarity of Peltospirids	34
2-5	RFLP to Identify species of Lepetodrilus	36
2-6	RFLP to Identify Unknown Peltospirids	37
2-7	Morphology of Vent Families	45
2-8	Lenticular Egg Capsules	47
2-9	Sequence Alignment to Identify Egg Capsules	52
2-10	Sequence Alignment of <i>Lepetodrilus</i> spp.	53
2-11	Sequence Alignment of Peltospiridae	54
2-12	Neighbor Joining Tree	55
3-1	Maps of 9° N area	59
3-2	Diagram of Collection Sites and Possible Larval Sources	62
3-3	Progressive Vector Diagrams	64
3-4	Current Velocities and Tidal Motions	67
3-5	Spatial Variability between East Wall and Choo Choo	69
3-6	Along-axis Transport and Larval Flux at East Wall	72
3-7	Larval Flux of Individual Taxa at East Wall	73
3-8	Along-axis Transport and Larval Flux at Choo Choo	77
3-9	Larval Flux of Individual Taxa at Choo Choo	78
3-10	First Order Autoregressive Series	83
3-11	Full Current Velocity Record	84
4-1	Map of Mooring Deployments near 9° N, East Pacific Rise	92
4-2	Transport Measure	96
4-3	Progressive Vector Diagrams	99
4-4	Current Velocities at East Wall 170 mab	100
4-5	Flux of Vent Gastropod Larvae	104
4-6	Species-Specific Larval Flux of Vent Gastropods	104
4-7	Flux of Probable Vent Gastropod Larvae	105
4-8	Species-Specific Larval Flux of Probable Vent Gastropods	105
4-9	Along-axis Transport of <i>Laeviphitus</i> sp.	109
4-10	Sea Level Anomaly	112
4-11	Currents vs. Δ Sea Level	112

5-1	Map of the Region Influenced by Tehuantepec and Papagayo Eddies .	125
5-2	Trajectories of Four Anticyclonic Eddies	133
5-3	Development of a Deep Cyclonic Eddy	136
5-4	Vertical Shear	137
5-5	Effect of Radius and Swirl Speed on Trajectories	138
5-6	Upper Layer Propagation over a Ridge	139
5-7	Stream Function at Depth - Ridge Topography	140
5-8	Stream Function at Depth - Flat Bottom	141
5-9	Tracing Ridge Interactions at Depth	142
5-10	Tracer at Depth over a Flat Bottom	143
5-11	Observed vs. Modeled Current Velocities at the Ridge Axis	144
5-12	Tracer Concentration Time Series - on the Ridge Axis	146
5-13	Tracer Concentration Time Series - Flat Bottom	147
5-14	Advection of Tracer Patches with Ridge	148
5-15	Advection of Tracer Patches with a Flat Bottom	149

List of Tables

2.1	Northern EPR Vent Gastropod 18S and 16S Sequences	38
2.2	Daily collections of gastropod larvae	39
2.3	Morphology of Northern East Pacific Rise Gastropod Larvae	41
3.1	Correlation of Current Velocities	65
3.2	Species Collected	70
3.3	Correlation between Transport and Larval Fluxes at East Wall	74
3.4	Correlation between Transport and Larval Fluxes at Choo Choo	79
3.5	Correlations to Evaluate Trap Efficiency	80
4.1	Correlation of Current Velocities	98
4.2	Gastropod Species Collected	102
4.3	Correlation between Cross-Axis Transport and Larval Fluxes	107
4.4	Correlation between Along-Axis Transport and Larval Fluxes	110
4.5	Larval Flux at East Wall Weeks 1-11	118
4.6	Larval Flux at East Wall Weeks 12-21	119
4.7	Larval Flux at Choo Choo Weeks 1-11	120
4.8	Larval Flux at Choo Choo Weeks 12-21	121
5.1	Satellite Observations of Tehuantepec and Papagayo Eddies	127
5.2	Summary of Tehuantepec and Papagayo Eddy Characteristics	131

Chapter 1

Introduction

Most marine and terrestrial ecosystems are seldom in an equilibrium state. Within a set of interacting communities, only a few communities may reach equilibrium, while other communities will be at various non-equilibrium states. It is difficult to reach equilibrium, because natural and anthropogenic disturbances continuously disrupt allocation of resources and biological interactions during the progression to an equilibrium state. Trees in the tropical rainforest are killed or broken by strong winds, landslides, insect infestations, lightning, and farming; coral reefs are damaged during hurricanes, freshwater floods, heavy sedimentation, predatory outbreaks, and bleaching events [4]. Disturbances such as these prevent the competitive dominant from creating a monoculture. As a site recovers from a major disturbance, the community will progress along a successional sequence of changing species composition depending on colonization and competition capabilities. A mosaic of local communities or patches at various successional stages, from initial colonization to equilibrium, enhances the species diversity of the ecosystem as a whole. Initial recovery from disturbance and the subsequent evolution of benthic marine communities depend on the extent and frequency of disturbance and the availability of recruits to colonize the disrupted area, and post-settlement mortality (e.g. [1, 8, 31]). Small areas (meters) can be colonized quickly by vegetative growth and migration of local individuals into the disturbed space. Larger areas of disturbance (tens of meters to kilometers) take longer to recover due to greater reliance on the dispersal of propagules (larvae, seeds and spores) from outside populations. Temporal and spatial variability in the availability of dispersive propagules could delay recovery or potentially alter the trajectory of the community. Recovery of large areas may follow the successional trajectory of

the previous community or diverge and establish ‘alternative stable states’ [18, 19, 30]. Understanding the recovery and trajectory of communities after a disturbance is essential for the effective management and conservation of ecological resources.

Hydrothermal vent ecosystems provide a system for understanding the role of dispersive propagules in the recovery from disturbance and the successional processes that follow. The majority of the species inhabiting the vents are endemic, sessile, benthic invertebrates, so recovery from large disturbances occurs primarily through the arrival dispersive propagules, in this case larvae. While some shallow water benthic communities that rely on dispersal of larvae can take many years to recover from a disturbance [1, 7, 37], hydrothermal vents along the East Pacific Rise (EPR) become densely populated with new colonists in six months to a year [28]. The remote location of hydrothermal vents ensures that the disturbances are primarily natural rather than anthropogenic; therefore the observed species responses will be adapted for natural disturbance over a long evolutionary period. These species responses may inform the potential for response to the qualitatively new disturbances imposed by humans in other systems [4, 15].

Hydrothermal vent communities occur along the mid-ocean ridge, essentially situated on top of a chain of underwater volcanoes. The shallow magma chamber heats seawater and catalyzes reactions with the crust that create chemically altered fluid that escapes at hydrothermal vents. The hydrothermal fluid is rich in hydrogen sulfide [9, 10, 35], the essential ingredient for the chemical reaction that forms the basis of life at vents [2, 17, 33]. While the shallow magma chamber provides many of the essential chemicals for vent life, during underwater volcanic eruptions, the shallow magma chamber contributes to the demise of vent life. Along the relatively fast-spreading EPR, eruptions occur on decadal time scales, obliterating vent communities and creating new seafloor over kilometers to tens of kilometers [14, 28, 32]. New, vacant vent habitat emerges where fissures and cracks in the new seafloor allow hydrothermal vent fluid to escape.

Nascent vents after the 1991 eruption at the East Pacific Rise were colonized by dispersive propagules within 6 months. Only dispersive larvae could have contributed to colonization, since almost all local communities were eliminated and no species with vegetative growth or propagule stores (i.e. seed banks) are known to occur at vents. The quick recovery was surprising, as rapid recovery after a major disturbance has been primarily observed for algal species [6, 37] which have propagules that generally

disperse locally, within a few km [26], compared to many benthic invertebrate with feeding larvae which disperse widely, over tens to hundreds of km [29]. Recoveries of benthic invertebrate species tend to be much longer due to high variation in larval supply and recruitment [7, 37].

Succession at hydrothermal vents can also proceed rapidly with changes in the dominant megafauna every few years [28]. The change in dominant fauna has been largely attributed to changes in the physical and chemical environment. The hydrothermal fluid evolves over time, usually from a hot, sulfide rich fluid to a cooler, low sulfide fluid [34, Love in prep]. Species that were not competitive previously, due to physiological tolerances, could become the competitive dominant as the hydrothermal fluid cools and hydrogen sulfide concentrations decrease. Limitation of space with the appropriate physio-chemical conditions is believed to drive strong biological interactions - competition, interference and facilitation - that then further structure the macrofaunal communities [12, 13, 23, 25]. In shallow water, the strength of benthic interactions can be determined by the availability of larvae [11, 21, 22, 27]. If larval recruitment to the benthos is low, space may not be a limiting factor; whereas, if larval recruitment to the benthos is high, space will likely become a limiting factor for which competition is high and on which predation is high due to an increased contact rate. Despite the established role of dispersive propagules in shallow water environments and the fact that dispersive larvae serve as the primary source of individuals to each vent, spatial and temporal variation in larval supply has not been directly examined as a factor contributing to colonization or succession at hydrothermal vents. Relatively little is known about the dispersal and availability of larvae of vent species, compared to shallow water counterparts.

Larval dispersal only has been investigated indirectly at hydrothermal vents along the EPR. Numerous population genetic studies suggest that vent species have high gene flow over hundreds of km, and thus have highly dispersive larvae [5, 16, 36, 38]. Estimates of dispersal distance based on simple passive dispersal models also suggest that larvae are dispersed long distances, tens to hundreds of kilometers [3, 20]. On the other hand, the distribution of larval abundances near vents suggests that larvae may not be dispersed long distances. Larval abundances near a vent were higher than abundances away from a vent [24].

Observations of initial colonization and benthic succession also allude to contradictory larval dispersal distances. Since eruptions disrupt vent communities over a

few to tens of kilometers, larvae must be dispersed long-distances to colonize nascent habitat. During long-distance dispersal, mean larval concentrations would decrease for a given area. Larvae could be diluted through diffusion and advective mixing into a dilute larval pool, which would decrease larval concentration by spreading larvae over a larger area. Alternatively, larvae could remain aggregated and dispersed in small patches, which would decrease larval concentration by decreasing the frequency of larval supply to a given location. However, high abundances of larvae are required at a vent site to quickly accumulate benthic abundances and biomass after an eruption, and to establish numerical and spatial dominance during successional changes. If vent larvae disperse long-distances, initial colonization would be facilitated but recovery would be slow, similar to that observed for many shallow water benthic invertebrates. On the other hand, if larvae are locally retained, colonization would be impeded, but once initial colonization occurred the communities would quickly recover.

In order to address this apparent contradiction in larval dispersal, this dissertation investigated the temporal and spatial variation in larval supply to hydrothermal vents and the hydrodynamic processes that influence that variation in supply. Characterizing the temporal and spatial variation of larval supply will provide insight into the temporal and spatial scales of larval dispersal. Furthermore, I correlated larval supply with currents, to understand the mechanisms controlling the variation larval supply.

1.1 Thesis Organization

The goals of this thesis were to quantify the spatial and temporal variation in the larval supply of vent gastropods near $9^{\circ} 50'$ N on the East Pacific Rise and to investigate the hydrodynamic processes that establish the observed variations. Before the larval supply of vent gastropods can be determined, larvae of vent origin must be identifiable. I expanded our ability to identify hydrothermal vent gastropods near 9° N, East Pacific Rise using a combination of morphological and molecular techniques in Chapter 2. A sequence database deposited in GenBank will facilitate difficult morphological identifications in the future and contributes to the 'bar-coding' effort for chemosynthetic communities. Chapter 3 characterizes the variation in larval supply on small temporal (days) and spatial (1.6 km) scales. Correlations between larval supply and current velocities suggest that larval transport was limited and that the

majority of larvae originate from local (< 1-2 km) vent communities. Chapter 4 characterizes the weekly variation in larval supply and tested the generality of the results from Chapter 3. Based on current velocity observations in Chapter 4, the effect of mesoscale eddies generated in the Gulfs of Tehuantepec and Papagayo on deep-sea currents and transport was investigated through satellite observations and a quasi-geostrophic model in Chapter 5. Together the chapters provide a description of larval transport and supply to hydrothermal vents on multiple temporal (days and weeks) and spatial (kilometers to hundreds of kilometers) scales.

Bibliography

- [1] Bertness, M., Trussell, G., Ewanchuk, P., & Silliman, B. (2002). Do alternate stable community states exist in the Gulf of Maine rocky intertidal zone? *Ecology*, 83:3434–3448.
- [2] Cavanaugh, C. (1983). Symbiotic chemoautotrophic bacteria in marine invertebrates from sulfide-rich habitats. *Nature*, 302:58–61.
- [3] Chevaldonné, P., Jollivet, D., Vangriesheim, A., & Desbruyeres, D. (1997). Hydrothermal-vent alvinellid polychaete dispersal in the Eastern Pacific. 1. Influence of vent site distribution, bottom currents, and biological patterns. *Limnology and Oceanography*, 42(1):67–80.
- [4] Connell, J. (1978). Diversity in tropical rain forests and coral reefs. *Science*, 199:1302–1310.
- [5] Craddock, C., Hoeh, W. R., Lutz, R. A., & Vrijenhoek, R. C. (1995). Extensive gene flow among mytilid (*Bathymodiolus thermophilus*) populations from hydrothermal vents of the eastern Pacific. *Marine Biology*, 124(1):137–146.
- [6] Dayton, P., Tegner, M., Parnell, P., & Edwards, P. (1992). Temporal and spatial patterns of disturbance and recovery in a kelp forest community. *Ecological Monographs*, 62:421–445.
- [7] Dethier, M. (1984). Disturbance and recovery in intertidal pools: Maintenance of mosaic patterns. *Ecological Monographs*, 54:99–118.
- [8] Dugeon, S. & Petraitis, P. (2001). Scale-dependent recruitment and divergence of intertidal communities. *Ecology*, 82:991–1006.
- [9] Edmond, J. M., von Damm, K. L., McDuff, R. E., & Measures, C. I. (1982). Chemistry of hot springs on the East Pacific Rise and their effluent dispersal. *Nature*, 297(5863):187–191.

- [10] Emond, J. M. & von Damm, K. L. (1992). Hydrothermal activity in the deep sea: Intractable problems and lots of questions. *Oceanus*, 35(1):76–85.
- [11] Gaines, S. & Roughgarden, J. (1985). Larval settlement rate - a leading determinant of structure in an ecological community of the marine intertidal zone. *Proceedings of the National Academy of Sciences of the United States of America*, 82(11):3707–3711.
- [12] Govenar, B., Freeman, M., Bergquist, D. C., Johnson, G. A., & Fisher, C. R. (2004). Composition of a one-year-old *Riftia pachyptila* community following a clearance experiment: Insight to succession patterns at deep-sea hydrothermal vents. *Biological Bulletin*, 207(3):177–182.
- [13] Govenar, B., Le Bris, N., Gollner, S., Glanville, J., Aperghis, A. B., Hourdez, S., & Fisher, C. R. (2005). Epifaunal community structure associated with *Riftia pachyptila* aggregations in chemically different hydrothermal vent habitats. *Marine Ecology Progress Series*, 305:67–77.
- [14] Haymon, R. M., Fornari, D. J., Von Damm, K. L., Lilley, M. D., Perfit, M. R., Edmond, J. M., Shanks, W. C., I., Lutz, R. A., Grebmeier, J. M., Carbotte, S., Wright, C. D., McLaughlin, E., Smith, M., Beedle, N., & Olson, E. (1993). Volcanic eruption of the mid-ocean ridge along the East Pacific Rise crest at 9° 45' - 52' N: Direct submersible observations of seafloor phenomena associated with an eruption event in April, 1991. *Earth and Planetary Science Letters*, 119(1-2):85–101.
- [15] Hughes, T. (1994). Catastrophes, phase shifts, and large-scale degeneration of Caribbean coral reef. *Science*, 265(5178):1547–1551.
- [16] Hurtado, L. A., Lutz, R. A., & Vrijenhoek, R. C. (2004). Distinct patterns of genetic differentiation among annelids of eastern Pacific hydrothermal vents. *Molecular Ecology*, 13(9):2603–2615.
- [17] Jannasch, H., Wirsén, C., Molyneux, S., & Langworthy, T. (1988). Extremely thermophilic fermentative archaeobacteria of the genus *Desulfurococcus* from deep-sea hydrothermal vents. *Applied and Environmental Microbiology*, 54:1203–1209.
- [18] Johnson, C. & Mann, K. (1988). Diversity, patterns of adaptation and stability in Nova Scotian kelp beds. *Ecological Monographs*, 58:129–154.
- [19] Knowlton, N. (1992). Thresholds and multiple stable states in coral reef community dynamics. *American Zoologist*, 32:674–682.
- [20] Marsh, A., Mullineaux, L. S., Young, C. M., & Manahan, D. T. (2001). Larval dispersal potential of the tubeworm *Riftia pachyptila* at deep-sea hydrothermal vents. *Nature*, 411:77–80.
- [21] Menge, B. (1991). Relative importance of recruitment and other causes of variation in rocky intertidal community structure. *Journal of Experimental Marine Biology and Ecology*, 146:69–100.

- [22] Menge, B. A. (2000). Recruitment vs. postrecruitment processes as determinants of barnacle population abundance. *Ecological Monographs*, 70:265–288.
- [23] Mullineaux, L. S., Mills, S. W., & Goldman, E. (1998). Recruitment variation during a pilot colonization study of hydrothermal vents (9° 50' N, East Pacific Rise). *Deep Sea Research*, 45:1–3.
- [24] Mullineaux, L. S., Mills, S. W., Sweetman, A. K., Beaudreau, A. H., Metaxas, A., & Hunt, H. L. (2005). Vertical, lateral and temporal structure in larval distributions at hydrothermal vents. *Marine Ecology Progress Series*, 293:1–16.
- [25] Mullineaux, L. S., Peterson, C. H., Micheli, F., & Mills, S. (2003). Successional mechanism varies along a gradient in hydrothermal fluid flux at deep-sea vents. *Ecological Monographs*, 73(4):523–542.
- [26] Reed, D., Laur, D., & Ebeling, A. (1988). Variation in algal dispersal and recruitment - the importance of episodic events. *Ecological Monographs*, 58:321–335.
- [27] Roughgarden, J., Gaines, S., & Possingham, H. (1988). Recruitment dynamics in complex life cycles. *Science*, 241(4872):1460–1466.
- [28] Shank, T. M., Fornari, D. J., Von Damm, K. L., Lilley, M. D., Haymon, R. M., & Lutz, R. A. (1998). Temporal and spatial patterns of biological community development at nascent deep-sea hydrothermal vents (9° 50' N, East Pacific Rise). *Deep-Sea Research (Part 2, Topical Studies in Oceanography)*, 45:465–515.
- [29] Shanks, A., Grantham, B., & Carr, M. (2003). Propagule dispersal distance and the size and spacing of marine reserves. *Ecological Applications*, 13:S159–169.
- [30] Simenstad, C., Estes, J., & Kenyon, K. (1978). Aleuts, sea otters, and alternative stable-state communities. *Science*, 200:403–411.
- [31] Sousa, W. (1979). Disturbance in marine intertidal boulder fields: the nonequilibrium maintenance of species diversity. *Ecology*, 60:1225–1239.
- [32] Tolstoy, M., Cowen, J., Baker, E., Fornari, D., Rubin, K., Shank, T., Waldhauser, F., Bohnenstiel, D., Forsyth, D., Holmes, R., Love, B., Perfit, M., Weekly, R., Soule, S., & Glazer, B. (2006). A sea-floor spreading event captured by seismometers. *Science*, 314(5807):1920–1922.
- [33] Van Dover, C. L. & Trask, J. L. (2000). Diversity at deep-sea hydrothermal vent and intertidal mussel beds. *Marine Ecology Progress Series*, 195:169–178.
- [34] Von Damm, K. L., Buttermore, L. G., Oosting, S. E., Bray, A. M., Fornari, D. J., Lilley, M. D., & Shanks, W. C., I. (1997). Direct observation of the evolution of a seafloor 'black smoker' from vapor to brine. *Earth and Planetary Science Letters*, 149(1-4):101–111.

- [35] Von Damm, K. L., Grant, B., & Edmond, J. M. (1983). Preliminary report on the chemistry of hydrothermal solutions at 21 degree North, East Pacific Rise. *Hydrothermal Processes At Seafloor Spreading Centers*, 12:369–390.
- [36] Vrijenhoek, R. C., Shank, T. M., & Lutz, R. (1998). Gene flow and dispersal in deep-sea hydrothermal vent animals. *Cahier de Biologie Marine*, 39:363:366.
- [37] Witman, J. (1987). Subtidal coexistence: storms, grazing, mutualism, and the zonation of kelps and mussels. *Ecological Monographs*, 57:167–187.
- [38] Won, Y., Young, C. R., Lutz, R. A., & Vrijenhoek, R. C. (2003). Dispersal barriers and isolation among deep-sea mussel populations (Mytilidae: *Bathymodiolus*) from eastern Pacific hydrothermal vents. *Molecular Ecology*, 12(1):169–184.

Chapter 2

Morphological and molecular identification of gastropod larvae

2.1 Introduction

Larval dispersal of benthic organisms can contribute to processes controlling gene flow, maintenance of populations, and community dynamics. Dispersal appears to be especially important for the success of sessile species inhabiting hydrothermal vents [12]. Suitable habitat for vent endemic species is patchily distributed, often separated by hundreds of meters to hundreds of kilometers of uninhabitable area. Individual vent habitats have been observed to be created and senesce on time scales of decades to years [8], which may represent only a few generations for many species. Planktonic larval dispersal can bridge the disparate habitats and deliver recruits to newly formed and existing vent communities to maintain species and facilitate gene flow.

Gastropods are a useful model group to address questions involving larval dispersal such as: how do larval development and behavior, and hydrodynamics combine to disperse and/or retain individuals [10, 15]; and what is the impact of dispersal and recruitment on community structure and dynamics. Gastropods are well suited for these questions due to their abundance in the benthos [33] and in the water column as larvae [19, 23]. Gastropods play an integral role in succession and community structure by inhibiting recruitment through grazing [20, 24]. Larval supply is known to affect subsequent benthic interactions and community structure in coastal environments [18, 32], and may be equally important in vent habitats. Gastropod species differ in their larval feeding mode (e.g. planktotrophic or lecithotrophic) and broad-

cast mode (e.g. broadcast spawning, brooding or delayed release from egg capsules) [13, 12]. Each of these developmental modes could have an impact on the retention and dispersal potential of larvae [31]. Gastropods are present in all vent biogeographic regions [29] and over the range of physiochemical habitats at vents, from the surface of black smoker chimneys to the ambient periphery [5, 21, 33]. However, gastropod species within a family and genus often differ in their geographical range [38] despite similarities in the mode of larval development [11].

Studies to understand the role of dispersal at hydrothermal vents have been limited by the ability to identify planktonic larvae to the species level [19, 23]. Larval identifications have traditionally relied on culturing of larvae and metamorphosis of collected larvae to an identifiable juvenile stage. To date, only *Riftia pachyptila* larvae have been cultured from embryos [15] and *Bythograea thermydron* megalopae have been observed to metamorphose through multiple juvenile stages in laboratory experiments [4]. No vent organisms have been successfully cultured through the entire lifecycle. Identifications of vent larvae have instead relied on similarities between larval and adult morphology, larval structures preserved in adult morphology [6, 22] and, more recently, molecular identification [1, 4, 26].

Comparisons of preserved protoconch (the larval shell) morphology in adult and juvenile gastropods to field-collected larvae has enabled the morphological identification of some but not all larval vent gastropods to species [22]. Most embryos and trochophores do not have morphological characteristics that allow for species-level identification. Currently fewer than half of the gastropod species (17 of 41 species) inhabiting the north East Pacific Rise (NEPR), from 21° N to 9° N EPR and Galápagos Rift, can be unequivocally identified at the larval stage using morphological characteristics of the protoconch. Seventeen species found along the NEPR have species-specific morphological descriptions of the larval shell in the current literature e.g. [22, 38]. Larval morphology is distinct at the species level for all of the species of Sutilizonidae and Neomphalidae known to occur in the northern EPR. On the other hand, the majority of the Lepetodrilidae (7 out of 8 species) and Peltospiridae (8 out of 12 species) and all of the Caenogastropoda (4 species) cannot be distinguished morphologically to the species level. Protoconchs on identified juvenile *Lepetodrilus cristatus* (see Fig 2a-c unnamed archeogastropod in [12]), *L. ovalis* (see Fig 1b unnamed archaeogastropod in [13]) and *L. elevatus* [22] exhibit strong morphological similarity between species preventing species level identifications. Images

of protoconchs on specimens of *Neolepetopsis densata* [38], *Gorgoleptis emarginatus* and *Peltoospira operculata* [22] are not diagnostic because specimens of closely related species are not available for comparison. Seventeen species do not have any protoconch morphological data.

A main goal of the present study is to develop an efficient and economical method for identifying vent gastropod larvae. I use a staged approach that involves visual examination of larval shell morphology, followed when necessary, by molecular genetic analysis (Fig 2-1). Gastropod specimens can be divided into three categories based on morphology alone - those with larval shell morphology that is distinct at the species level, those with larval shell morphology distinct only at the family or genus level, and those with uninformative larval shell morphology (hereto referred to as 'unknowns'). From the morphological categorization, the appropriate molecular techniques are used for each grouping to obtain a species level identification. This approach takes advantage of easily obtained morphological information and optimizes the efficiency of molecular genetic identifications.

I have three objectives to increase the efficiency and economy of the staged approach. The first objective is to expand the number of species that can be identified solely by larval shell morphology. The second objective is to develop a fast and inexpensive molecular genetic method that is useful for identifying species whose larval shell morphology is informative, but not distinct at the species level. The third objective is to expand a sequence database of identified gastropod species that can be compared to sequences of unknowns - embryos, trochophore larvae, and shelled larvae whose morphologies do not allow for classification.

To demonstrate the effectiveness of this three-step approach, it is used to identify field collected larval and benthic samples.

2.2 Methods

2.2.1 Sample Collection

Adult, juvenile and larval gastropods were collected by *DSV Alvin*. Adult and juvenile gastropods used in morphological studies were collected on basalt blocks (10 cm each side) or from washings of mussel, tubeworm and sulfide collections during seven cruises to the EPR, 9° 50' N area between 1994 and 2004. Larvae were collected in the same region, near active vent sites, via Mclane WTS-LV plankton pumps between 1998

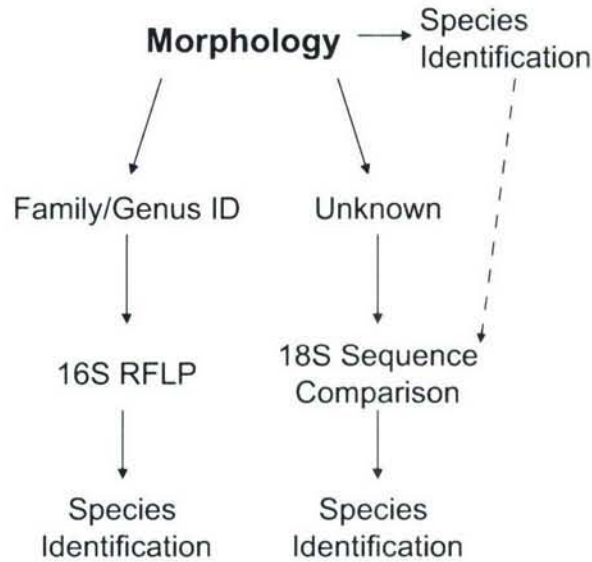


Figure 2-1: Flow chart of staged identification procedure. Some of the morphological identifications were further verified through 18S sequence comparisons, as indicated by the dashed line.

and 2000. All specimens used for morphology were preserved in 80% ethanol. For molecular development, adult gastropods were collected from washings of mussel, tubeworm and sulfide collections from the EPR, 9° 29' - 9° 51' N and 21° N between 2000 and 2005. Specimens were sorted and identified onboard the *RV Atlantis* before freezing at -70° C.

2.2.2 Morphological Identification

To expand the suite of species that can be identified by larval shell morphology, I compiled morphological descriptions from the literature to identify gaps in our knowledge and imaged protoconchs retained on juveniles from species lacking larval descriptions. Diagnostic features used for morphological characterization and identification include shell size (maximum diameter), sculpture and shape, and aperture flare and shape (e.g. sinuous, or straight margin). I focused on obtaining descriptions for the genus *Lepetodrilus* and for the family Peltospiridae, whose species are abundant and ecologically important. Juveniles and adults were collected for scanning electron microscopy (SEM) imaging of retained protoconchs. Juveniles and small adults (hereto referred collectively as juveniles) were screened under a dissecting scope for the preservation of an intact protoconch. Juveniles of *Clypeosectus delectus*, *Echinopelta fistulosa*, *Gorgolettis spiralis*, *Lepetodrilus cristatus*, *L. elevatus*, *L. ovalis*, *L. pustulosus*, *Nodopelta*

rigneae, *N. subnoda*, and *Peltospira operculata* were found with intact protoconchs. If SEM images of protoconchs retained on juveniles yielded taxonomically informative descriptions, larvae were also imaged with SEM to document larval shell characteristics that were not apparent on the juveniles due to juvenile growth or corroded protoconch sculpture.

For SEM, juvenile gastropods with intact larval protoconchs and larvae were cleaned in a diluted 3:1 (Chlorox) bleach solution at 50° C for five minutes, air dried, and then mounted on circular glass slides using a small amount of white glue. Slides were glued to SEM stubs with silver polish. Specimens were silver-coated in a SAMSPUTTER 2a automatic sputter-coating machine and imaged on a JEOL JSM-840 Scanning Electron Microscope. For each species, juveniles were imaged until an informative SEM image was obtained or all available specimens of that species with an intact protoconch were used. In all, 16 juveniles and 45 larvae were imaged with SEM.

2.2.3 Identification of a Defined Group of Species - RFLP Design

Restriction fragment length polymorphism assays (RFLPs) were developed as a cost effective molecular method for identifying specimens within a well defined species group. RFLPs are an inexpensive alternative to sequencing. RFLPs use restriction enzymes to cut PCR products into unique banding patterns. The restriction enzyme(s) cut at different locations, because the sequence of the gene or gene fragment amplified in the PCR differs among species. The differences in enzyme cutting locations create banding patterns that can be assigned to different species. This method is most efficient for identification of a finite number of candidate species for which species-specific banding patterns are characterized. Protoconchs within the genus *Lepetodrilus* [22] and within the family Peltospiridae [22] can be assigned to the genus and family level, respectively, based on similar sculpture, shape, aperture and size visualized under the light microscope. *Lepetodrilus* species and peltospirids represent 11 of the morphologically unidentifiable species at the larval stage on the NEPR. These two groups are well suited for a cost effective assay due to high abundance in the benthos [3, 34] and as larvae in the plankton [23].

I developed RFLP assays for the genus *Lepetodrilus* and unidentifiable species of the family Peltospiridae (*Echinopelta fistulosa*, *Hirtapelta hirta*, *Nodopelta heminoda*,

N. rigneae, *N. subnoda*, *P. delicata*, and *P. operculata*) using part of the mitochondrial 16S rDNA gene. The goal was to develop an RFLP that identifies all species within the genus *Lepetodrilus* known to occur at the EPR, near 9° 50' N and a second RFLP that identifies all unidentifiable species of the family Peltospiridae known to occur at the EPR, near 9° 50' N. The mitochondrial 16S rDNA gene was chosen because of its established use in gastropod phylogenetics [2, 27]. An initial attempt to use part of the nuclear 18S rDNA gene was abandoned given the lack of sufficient nucleotide variability among species within the same genus (see Section 2.3.3).

Part of the 16S gene was amplified and sequenced for two adult individuals each of *Lepetodrilus cristatus*, *L. elevatus*, *L. ovalis*, *L. pustulosus*, *Peltospira operculata*, *P. delicata*, *Echinopelta fistulosa* and *Nodopelta subnoda*. Only one individual of each *N. rigneae* and *N. heminoda* were available for amplification and sequencing. No *Hirtapelta hirta* specimens were available, but the partial 16S sequence from GenBank (AY163397) was included in the alignment and RFLP design. *Lepetodrilus tevnianus* and *Peltospira lamellifera* are the only morphologically unidentifiable species in the Northern EPR region from these two groups not included in the study, because no specimens were available. The absence of these species is not likely to compromise the ability to identify to species near 9° 50' N since *L. tevnianus* had only been recorded from 11° N and only three specimens of *P. lamellifera*, all from the 13° N area, have ever been recorded.

All PCR reactions were performed in an Eppendorf Master Gradient thermocycler in 25 μ l reaction containing 0.75 - 1.00 μ l genomic DNA extracted using a DNAeasy Kit (Qiagen), 1x buffer (Promega), 1mM MgCl₂, 250 μ M each dNTP, 500 nM each primer, and 1 unit of Taq DNA polymerase (Promega). *Lepetodrilus* spp. were amplified and sequenced using the “universal” primers, 16sar-L (forward) and 16sbr-H (reverse) [25]. The peltospirids were amplified and sequenced using the 16sar-L forward primer and a new reverse primer, Pelt16sR: 5' GCTTCTRCACCMACCTGGAAATC. Failure to amplify *N. rigneae* using 16sar-L and 16sbr-H necessitated the design of the new primer for the peltospirids following protocols and software provided by Primer3 ([http : //frodo.wi.mit.edu/cgi - bin/primer3/primer3_www.cgi](http://frodo.wi.mit.edu/cgi-bin/primer3/primer3_www.cgi)). Amplifications were performed using the following cycling parameters: 2 minutes initial denaturation at 96° C followed by 30 cycles of 30 s at 94° C, 30 s at 48° C, and 1 min at 72° C. PCR products were visualized on a 1.5% agarose gel with ethidium bromide using the ChemImager or AlphaImager system (Alpha Innotech Corporation). PCR products

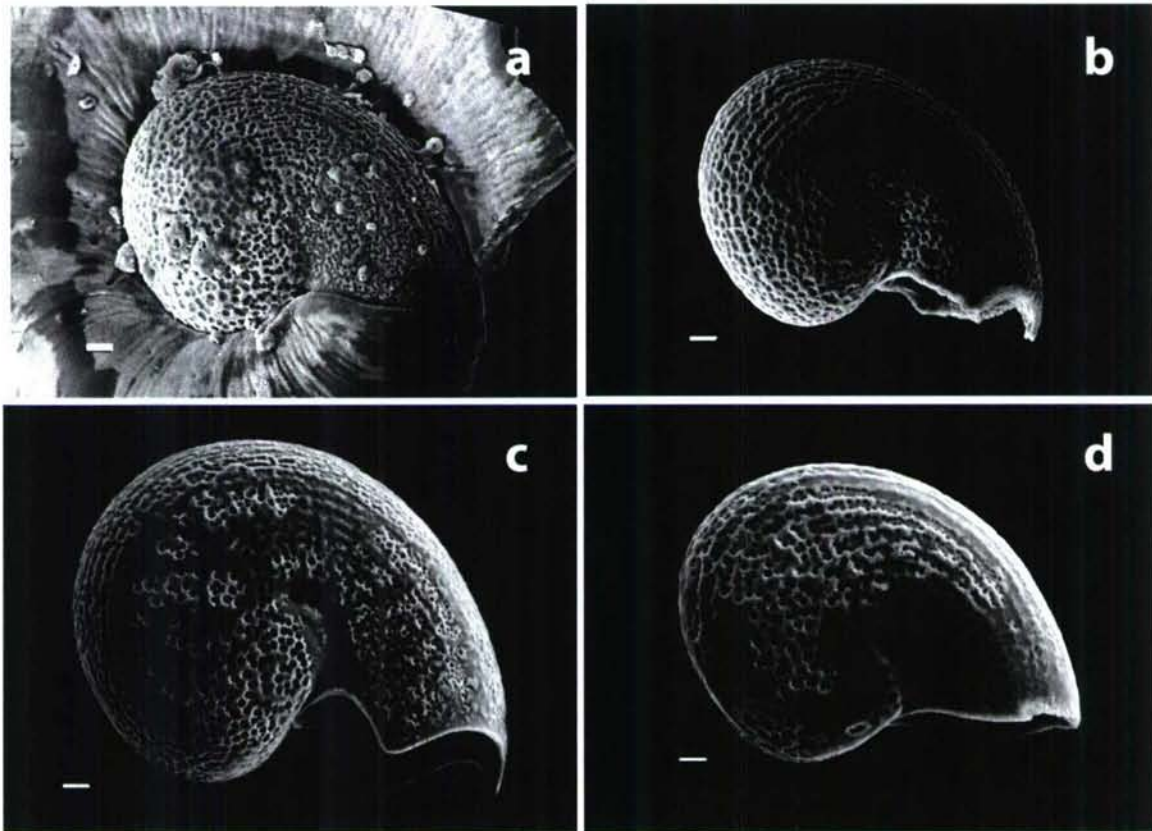


Figure 2-2: SEM images of juvenile and larval *Gorgolectis spiralis* and closely related species. (a) *G. spiralis* protoconch on juvenile. A broader view of the juvenile shell is not shown due to breakage during sample preparation. (b) *G. spiralis* larva. (c) *G. emarginatus* larva. (d) *Clypeosectus delectus* larva. Scale bars are 10 μm for all shells.

were purified using the QiaQuick PCR Purification Kit (Qiagen) before sequencing on an ABI 377 or 3730xl sequencer (Applied Biosystems). Sequences were edited in EditView (Applied Biosystems) and aligned using Sequencher v. 4.2.2 (Gene Codes Corp.) and MacClade [14]. Restriction enzymes were chosen by viewing cut sites using Sequencher v. 4.2.2 (Gene Codes Corp.)

All restriction enzyme digestions were performed in 15 μ l reactions containing 500-1000 ng of DNA, 5 units of each restriction enzyme, 1x buffer (enzyme specific, provided by Promega or New England Biolabs), and 100 μ M BSA. Digestions were visualized on a 2% agarose gel containing ethidium bromide using the ChemImager or AlphaImager system (Alpha Innotech Corporation).

Fifteen individuals of each species, except *H. hirta*, *N. rigneae* and *N. heminoda*, from at least two ridge segments (e.g. 9° 50' N and 21° N) were digested as described above to test for false negatives and false positives. Initial morphological screening into the two taxonomic groups, the genus *Lepetodrilus* and unknown peltospirids, eliminates false positive identification of species not included in the RFLP design.

2.2.4 Identification with No Morphological Information – Expanding the Sequence Database

In order to expand the database for comparison with sequences from unidentified larvae, partial nuclear 18S rDNA sequences were obtained from all available adult gastropods species from the 9° 50' N area (Table 2.1). The nuclear 18S rDNA gene was chosen to take advantage of existing sequences in GenBank and because of the established use of the 18S region in gastropod phylogeny [7]. Adults were compared to the reference collection at the Los Angeles County Natural History Museum or identified by Anders Warén at the Swedish Museum of Natural History, if identification required confirmation. Genomic DNA was purified using the DNAeasy Kit (Qiagen). Part of the 18S rDNA gene was amplified and sequenced using polymerase chain reaction with the primers AGM-18F (forward): 5' GCCAGTAGTCATATGCTTGCTC and AGM-18R (reverse): 5' AGACTTGCCCTCCAATRGATCC [7] using the procedure and PCR conditions described in the previous section Restriction Fragment Length Polymorphisms. Sequences were aligned for comparison using Sequencher v. 4.2.2 (Gene Codes Corp.) and MacClade [14]. Parsimony trees and neighbor-joining trees were made in PAUP 4.0 [28]. To assess the confidence or robustness of the sequence data, bootstrap analyses were performed using 500 replicates.

2.2.5 Application to Larval Samples

The staged procedure developed in this study was applied to identify larvae from a sub-set of time-series sediment trap collections near 9° 50' N EPR. Larvae were collected daily in a 21 sample Mclane MARKFLUX time-series sediment trap moored 4 meters above bottom at a location 10 m south of the Choo Choo vent site (9° 49.60' N, 104° 17.37' W, 2512 m) during the November 2004 AT11-20 cruise. The trap opening is 0.5 m² and is covered by baffle with a cell diameter of 2.5 cm. Samples were preserved in a saturated salt - 20% DMSO solution [9] to preserve morphology and DNA. Larvae from four of the samples were sorted using a Zeiss Stemi 2000-C dissecting scope and then identified morphologically to species using a Zeiss AxioStar Plus compound scope.

Those larvae not identifiable to species were sorted into three groups for molecular identification: *Lepetodrilus* spp., peltospirids and unknowns. *Lepetodrilus* spp. were identified based on small size, 170-190 μ m, punctate sculpture, and a straight aperture margin that is even with the axis of coiling. Unfortunately, *L. pustulosus* has not been successfully imaged and juveniles are difficult to identify [38]; thus the morphology is assumed based on the consistency of size, shape and sculpture characteristics within *Lepetodrilus* species on the EPR, Galápagos, Juan de Fuca, and Mid Atlantic Ridges and within the family in general [22, 38]. Peltospirids were identified based on ridged ornamentation and shape (Fig 2-3 and 2-4).

Genomic DNA was extracted from each sorted larva using the QiaAmp DNA Micro Kit (Qiagen), a Chelex extraction [35], or by dropping larvae directly into the PCR solution. As described in Section 2.2.3, the partial 16S gene was PCR amplified from successful extractions as described previously using the 16sar-H and 16sbr-L primers for the *Lepetodrilus* spp. and 16sar-H and Pelt16sR primers for the peltospirids. The PCR products were digested as described in Restriction Fragment Length Polymorphisms section to determine the species identification. A selection of the 'unknowns' was PCR amplified for the 18S gene for direct sequence comparisons to determine the species identification.

The identification procedure was also applied to unidentified egg capsules to demonstrate the utility of the technique on other early-stage specimens without morphological descriptions. Egg capsules were collected on caged and uncaged basalt colonization blocks placed on the seafloor as part of a larger colonization study [20, 24]. Nine blocks collected during the May 1998 cruise contained egg capsules with em-

bryos and developing veligers. The blocks with egg capsules had been placed in within vestimentiferans and mussels with and without cages (6 mm mesh described in [20]). Blocks placed in the periphery did not contain egg capsules. Larvae in the egg capsules had not yet formed identifiable shells preventing morphological identification, therefore, they were identified by direct 18S sequence comparisons. Sequences obtained from the egg capsules were compared directly to the gastropod 18S sequences from known adults using Sequencher v. 4.2.2 (Gene Codes Corp.) and MacClade [14]. The shape, size and number of embryos per capsule were characterized for 20 egg capsules under a Zeiss Stemi 2000-C dissecting scope.

2.3 Results

2.3.1 Morphological Identification and Descriptions

SEM images yielded new protoconch descriptions for three species, *Gorgolettis spiralis*, *Echinopelta fistulosa* and *Nodopelta subnoda*. The protoconch of *G. spiralis* is characterized by a small size ($\sim 150 \mu\text{m}$) and an overall coarse punctuate sculpture which forms close parallel rows away from the axis (Fig 2-2a, b). This description of the *G. spiralis* protoconch allows it to be differentiated from the *G. emarginatus* protoconch (Fig 2-2c) which is similar in shape, sculpture, and aperture [22], but is larger in size ($\sim 180 \mu\text{m}$). Based on sorting thousands of vent larvae, a difference of $30 \mu\text{m}$ in size is diagnostic for identification (SM and DA personal observation). *G. spiralis* is distinguished from another close relative, *Clypeosectus delectus* (Fig 2-2d), by the scalloped aperture. Additional images of *C. delectus* protoconchs on two juveniles (not shown) confirm the previous protoconch description and larval identification.

In the Peltospiridae, the protoconch of *E. fistulosa* (Fig 2-3) is distinct at the species level, but the protoconch of *N. subnoda* (Fig 2-4) is not. Both protoconchs were similar to protoconchs of previously described peltospirids based on the presence of ridges. *E. fistulosa* protoconchs can be easily distinguished from other members of the peltospirid family by the limitation of ridges to near the apex and indentations or “shelves” at the axis of coiling. The protoconch of *N. subnoda* (Fig 2-4 a, b) is not distinguishable to species due to a high degree of similarity to that of *P. operculata* (Fig 2-4c). Both species are characterized by smooth parallel ridges and moderate size (215-220 μm).

Protoconchs on the remaining juveniles were not informative. An additional 11

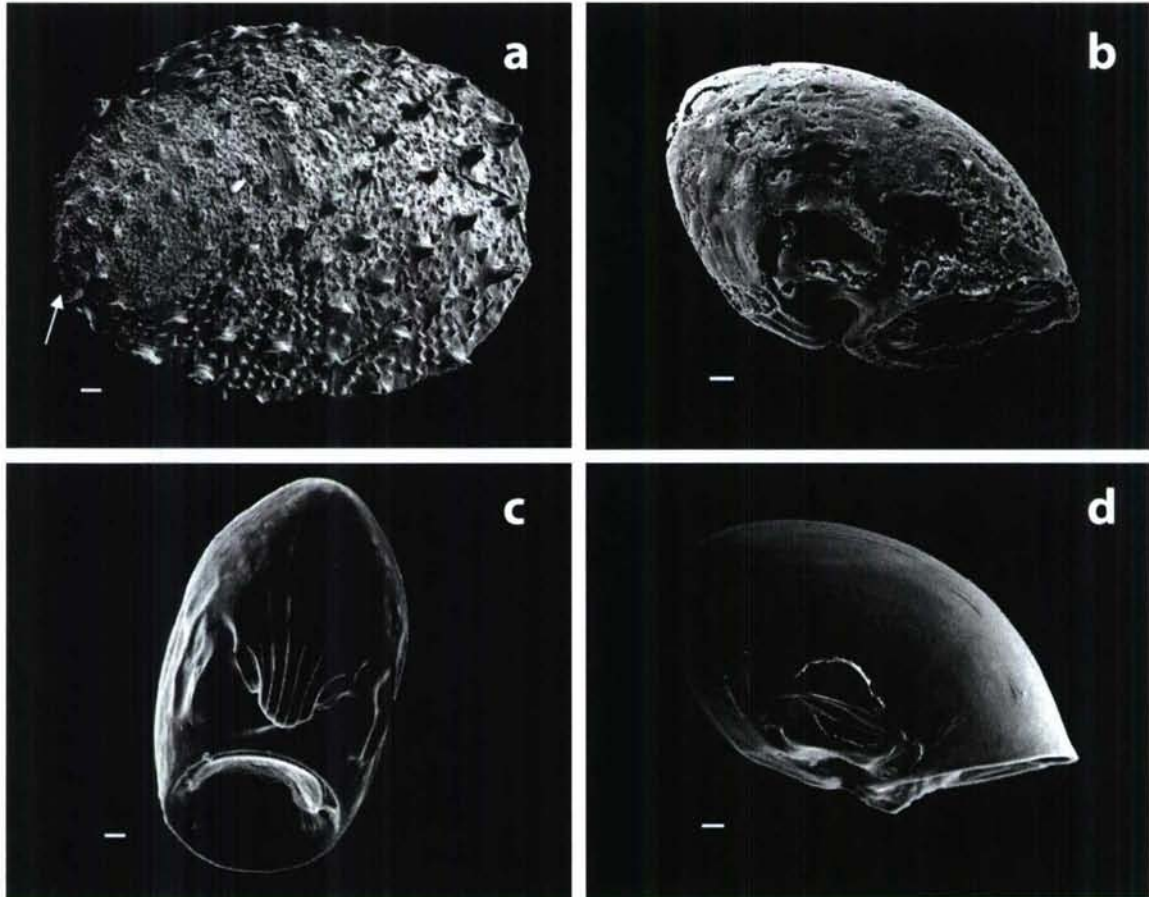


Figure 2-3: SEMs of juvenile and larval *Echinopelta fistulosa*. (a) *E. fistulosa* juvenile. The white arrow denotes the location where the protoconch was previously attached. (b) Protoconch detached during manipulations of *E. fistulosa* juvenile pictured in a. Two *E. fistulosa* larvae are pictured to show the ridged sculpture restricted to the axis (c) and the indentations on the sides in the same orientation as the protoconch from the juvenile (d). Scale bars are 10 μm for all shells except a (100 μm).

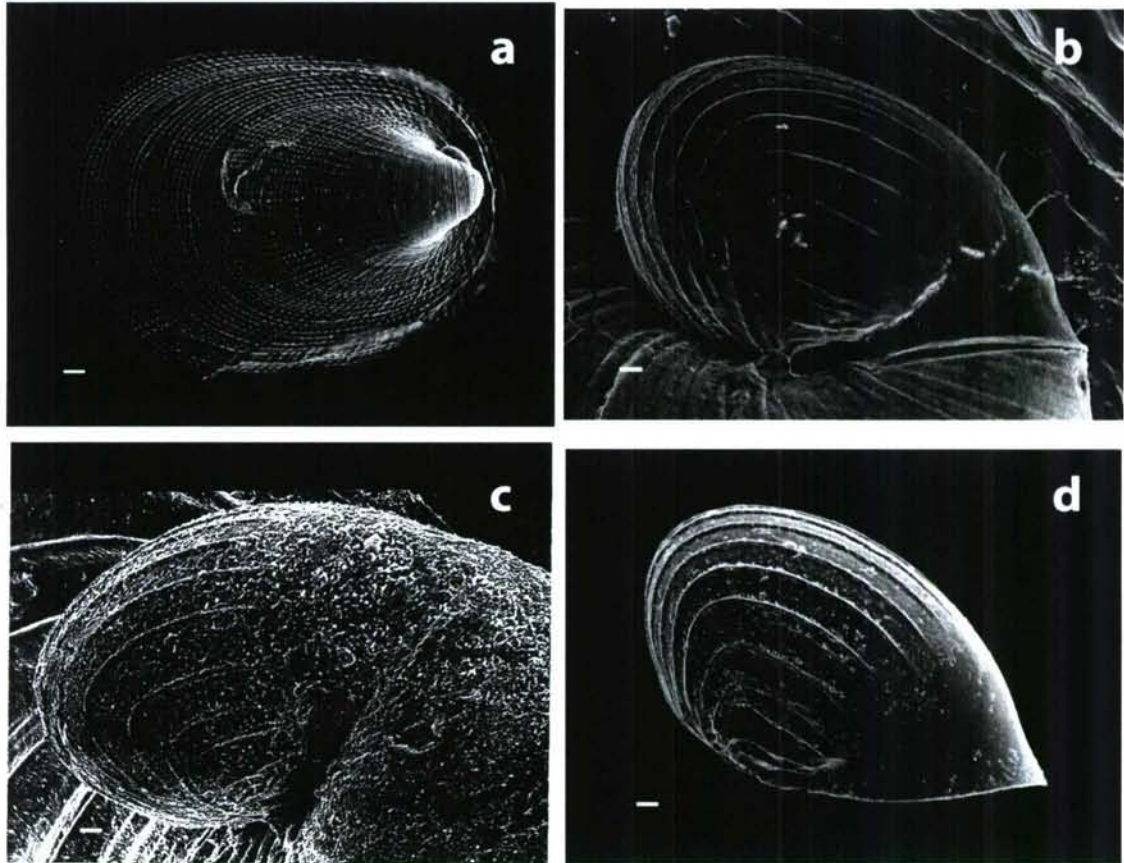


Figure 2-4: SEMs of juveniles and larvae in the family Peltospiridae. (a) *Nodopelta subnoda* juvenile. (b) *N. subnoda* protoconch attached to juvenile pictured in a. (c) *Peltospira operculata* protoconch on a juvenile, repictured from [22]. (d) Peltospirid larva that closely resembled both *N. subnoda* and *P. operculata* in shape and sculpture. Scale bars are 10 μm for all shells except A (100 μm).

intact protoconchs on juveniles, *Lepetodrilus cristatus*, *L. elevatus*, *L. ovalis*, *L. pustulosus*, *Nodopelta rigneae*, *N. subnoda*, and *Peltospira operculata* were found and imaged. Images of *N. rigneae*, *N. subnoda*, and *P. operculata* were uninformative due to corrosion or other damage. *Lepetodrilus* spp. exhibited the previously described punctuate sculpture but lacked visible species-specific characteristics.

Morphological characteristics of the protoconch of 27 vent gastropods from the EPR 9° 50' N area were compiled from the literature and from new descriptions from SEM images presented in this study (Table 2.3). With the new morphological descriptions, 20 descriptions are diagnostic to the species level, five descriptions are diagnostic to the genus level, and two descriptions are diagnostic to the family level. All descriptions from the literature, except for *Phymorhynchus* sp. were from protoconchs preserved on identified or identifiable juveniles. The larval description of *Phymorhynchus* sp. is based upon veligers found within egg capsules collected on the Galápagos Rift morphologically identified as belonging to the genus *Phymorhynchus* [6]. Unnamed archaeogastropods in Lutz et al (1986) [12] and Lutz et al (1984) [13] have been since described and are identifiable as *L. cristatus* and *L. ovalis*, respectively. Unnamed *Rimula?* in Turner et al 1985, figure 11a-c [30] has since been identified as *Temnozaga parilis*. The specimen in Mullineaux et al (1996) [22] figure 1F, 1I was mistakenly identified as *Lepetodrilus ovalis* instead of *L. elevatus*.

2.3.2 Identification of a Defined Group of Species - RFLP Design

For the *Lepetodrilus* spp. and peltospirid groups, 16S rDNA sequences from morphologically identifiable adults and juveniles contained suitable variation among species to design species-specific RFLP assays (GenBank accession numbers listed in Table 2.1, Fig 2-10). Species-specific banding patterns were obtained for *L. cristatus*, *L. elevatus*, *L. ovalis*, and *L. pustulosus* by digesting the initial PCR product with the restriction enzymes Sty I, Stu I, and Dra I (Promega) together, using Buffer B, for 3-4 hours at 37° C (Fig 2.3.2). Due to decreased efficiency (75-100%) of Sty I in Buffer B (Promega), digestion of PCR products from *L. ovalis* often resulted in the expected diagnostic cut bands as well as a remaining uncut band. Inclusion of Stu I is optional but makes an additional cut which facilitates identification of *L. cristatus*.

Diagnostic banding patterns were obtained for the peltospirids (Fig 2-6) by digesting the initial PCR product with Dra I (New England Biolabs) for 3-4 hours at



Figure 2-5: Restriction fragment length polymorphism assays showing species-specific banding patterns using Dra I, Stu I, and Sty I. Le, *Lepetodrilus elevatus*; Lo, *L. ovalis*; Lp, *L. pustulosus*; Lc, *L. cristatus*. 100 bp ladder is included as size standard.

37° C and, if necessary, with Ssp I and EcoR V (New England Biolabs) in buffer 3 for 3-4 hours at 37° C in parallel. The first Dra I digestion identifies *Peltoispira operculata*, *P. delicata*, *Echinopelta fistulosa*¹ and *H. hirta* to species and the genus *Nodopelta* but does not distinguish among *Nodopelta* species. The second Ssp I and EcoR V digestion of the initial PCR product was only necessary to distinguish among *Nodopelta* species.

Digestions to test for false positives and negatives produced the expected banding patterns for all adult individuals from each species with the exception of *Peltoispira delicata* and a single specimen of *Lepetodrilus cristatus*. Ssp I and EcoR V digestion of three individuals of *P. delicata* produced the banding patterns expected for *P. operculata*. However, the banding patterns in the initial Dra I digestion produced the expected banding patterns for both *P. delicata* and *P. operculata*.

2.3.3 Identification with No Morphological Information – Expanding the Sequence Database

Diagnostic 18S rDNA sequences were obtained from 39 adult gastropods representing 19 species (Table 2.1). Genbank contained two different sequences of the 18S rDNA region for each of *Eulepetopsis vitrea* and *Peltoispira operculata*. To resolve possible sequence errors in these and other species, all of the existing GenBank sequences, ex-

¹*Echinopelta fistulosa* was included in the RFLP because it was not morphologically identifiable at the time of RFLP development

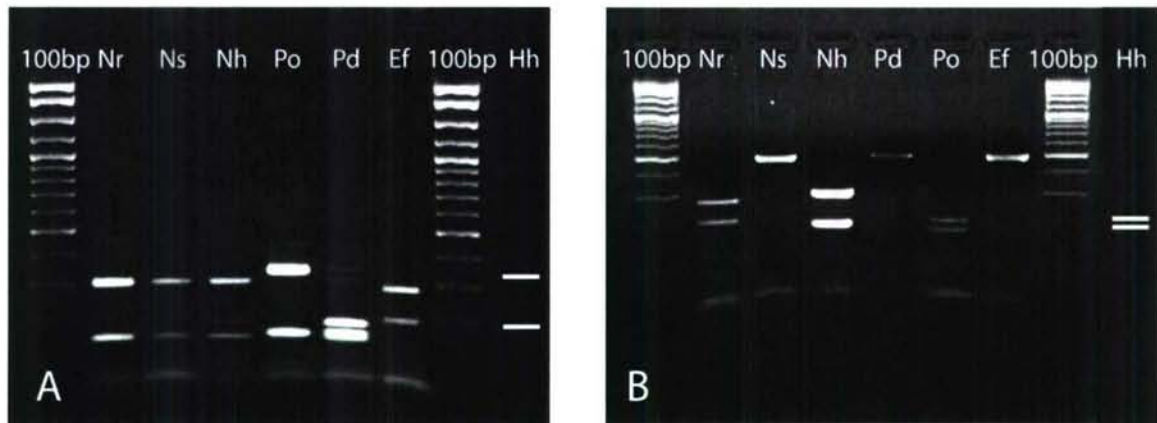


Figure 2-6: Restriction fragment length polymorphism assays showing species-specific banding patterns for Dra I (A) and Ssp I with EcoR V (B). Nh, *Nodopelta heminoda*; Nr, *N. rigneae*; Ns, *N. subnoda*; Pd, *Peltospira delicata*; Po, *P. operculata*; Hh, *Hirtapelta hirta*. *H. hirta* digestions are predicted patterns inferred from sequence data, since no specimens were available. 100 bp ladder is included as size standard.

cept for *Melanodrymia aurantiaca* (specimens were not available), were verified with additional sequences in the present study. GenBank sequences and their accession numbers that were identical to sequences obtained during the present study are included in Table 2.1. Sequences for 13 new species were added to the public database, bringing the total number of vent gastropod species near 9° 50' N EPR with 18S rDNA sequences to 20 (Table 2.1).

Genetic variation of the partial 18S sequence (~ 550 bp) was sufficient to differentiate among the vent gastropod species except among *Lepetodrilus* spp. Neomphalids showed the highest divergence amongst species with greater than 15 bp (max 33 bp) differences between species pairs. Genera within Peltospiridae differed by at least 7 bp and up to 19 bp, but differences among species within genera were lower, 2-9 bp. The pairwise difference between *Peltospira delicata* and *P. operculata* was 4 bp and between *Nodopelta heminoda* and *N. subnoda* was 2 bp. Lepetodrilids differ from all other families by greater than 45 bp sequence divergence, however differentiation within the family was very low. *Lepetodrilus elevatus*, *L. ovalis* and *L. pustulosus* were identical over 540 bp and differed from *Gorgolettis spiralis* and from *L. cristatus* by only one base pair. In the Caenogastropoda, *Gymnobela* sp. A and *Phymorhynchus major* varied by only one base pair. (See Section 2.5 for Sequence Alignments and Phylogenetic Tree)

Species	GenBank Accession #	
	18S	16S
Subclass Patellogastropoda		
Family Neolepetopsidae		
<i>Eulepetopsis vitrea</i>	AF046052 (3)	U86355
<i>Neolepetopsis densata</i>		
<i>Neolepetopsis occulta</i>		
<i>Neolepetopsis verruca</i>		
Subclass Vetigastropoda		
Family Trochidae		
<i>Bathymargarites symplector</i>	AY090810 (2)	DQ093477
Family Lepetodrilidae		
<i>Clypeosectus delectus</i>		
<i>Gorgoleptis emarginatus</i>		
<i>Gorgoleptis spiralis</i>	EF549668 (1)	
<i>Lepetodrilus cristatus</i>	EF549671 (2)	EF549687 (2)
<i>Lepetodrilus elevatus</i>	AY145381 (2)	U86348 (2)
<i>Lepetodrilus ovalis</i>	AY923887 (2)	U86351 (2)
<i>Lepetodrilus pustulosus</i>	AY923886 (3)	EF549690 (2)
<i>Lepetodrilus temnianus</i>		
Family Sutilizonidae		
<i>Sutilizona theca</i>		
<i>Temnozaga parilis</i>		
Family Fissurellidae		
<i>Cornisepta leviniae</i>		
Subclass Uncertain		
Superfamily Neomphaloidea		
Family Neomphalidae		
<i>Cyathermia naticoides</i>	AY090803 (2)	DQ093472
<i>Lacunoides exquisitus</i>		
<i>Melanodrymia aurantiaca</i>	AY090805	
<i>Melanodrymia galeronae</i>		
<i>Neomphalus fretterae</i>	AY090806 (2)	
<i>Pachydermia laevis</i>	EF549673 (2)	
<i>Planorbidella planispira</i>		
<i>Solutigyra reticulata</i>		
Family Peltospiridae		
<i>Ctenopelta porifera</i>		
<i>Echinopelta fistulosa</i>	EF549677 (2)	EF549691 (2)
<i>Hirtopelta hirta</i>		AY163397
<i>Lirapex granularis</i>		
<i>Lirapex humata</i>		
<i>Nodopelta heminoda</i>	EF549675 (1)	EF549692 (1)
<i>Nodopelta rigneae</i>	EF549676 (1)	EF549693 (1)
<i>Nodopelta subnoda</i>	EF549674 (2)	EF549694 (2)
<i>Peltospira delicata</i>	AY923893 (3)	EF549695-6 (6)
<i>Peltospira lamellifera</i>		
<i>Peltospira operculata</i>	AY090807 (3)	EF549697 (6)
<i>Rhynchopelta concentrica</i>	AF534988 (2)	
Subclass Caenogastropoda		
Family Conidae		
<i>Gymnobela</i> sp. A	EF549685 (3)	
<i>Phymorhynchus major</i>	EF549684 (1)	
Family Provannidae		
<i>Provanna ios</i>		
<i>Provanna muricata</i>		

Table 2.1: GenBank accession numbers for north EPR vent gastropods. Accession numbers in **bold** were contributed by this study. All existing 18S sequences in GenBank, except for *Melanodrymia aurantiaca* and *Hirtopelta hirta*, were verified by additional sequences. 16S sequences in GenBank were verified for the Lepetodrilidae and Peltospiridae. The number of individuals sequenced is in parentheses ().

Species	Date				Total
	13-Nov	14-Nov	15-Nov	16-Nov	
<i>B. symplector</i>		1			1
<i>C. delectus</i>		1			1
<i>C. naticoides</i>	5	10	2	1	18
<i>G. spiralis</i>	1				1
<i>P. operculata</i>			1		1
Unknown peltospirid		1			1
<i>Lepetodrilus</i> spp.		1		2	3
Unknown benthic sp. A	1	2	1	1	5
<i>Laeviphitus</i> sp.	2	4	2		8
Unknown	1	1			2
Daily Total	10	21	6	4	41

Table 2.2: Abundances of gastropod larvae at Choo Choo vent site, 9° 49.60' N East Pacific Rise, each day collected over a 0.5 m² area. The first four species were identified to species morphologically. *Peltospira operculata* was identified using RFLP. The morpho-types Unknown Benthic sp. A and *Laeviphitus* sp. were sequenced but were not successfully assigned to species.

2.3.4 Application to Larval Samples

Forty-one gastropod larvae, collected in the sediment trap over the course of four days, were analyzed to demonstrate the staged approach (Table 2.2). Twenty-one of the specimens could be identified as either *Bathymargarites symplector*, *Clypeosectus delectus*, *Cyathernia naticoides*, and *Gorgoleptis spiralis* under a light microscope by morphology alone. *Cyathernia naticoides* (n=18) was the most abundant species collected. The remaining 20 specimens that could not be identified to species morphologically were divided into 3 morpho-groups, *Lepetodrilus* spp., peltospirids, and unknown for further identification.

The *Lepetodrilus* spp. and peltospirids were suitable for RFLP analyses (Fig 2-6), however, genomic extractions failed to yield sufficient DNA for PCR for all but one individual. An unknown peltospirid was identified as *P. operculata*.

Two distinct morpho-types in the unknown group, *?Laeviphitus* sp. and Unknown Benthic sp. A (sensu [23]), were sequenced for identification by direct comparison of 18S rDNA. These morpho-types were chosen due to their relatively high abundances in the collection. Neither *?Laeviphitus* sp. nor Unknown Benthic sp. A matched any gastropod species within the current 18S database for gastropods along the Northern EPR. Additionally, morphological identifications of *Cyathernia naticoides* and *Bathymargarites symplector* were verified through direct 18S rDNA sequence comparison

of one individual each.

The sequence database was used to identify to species lenticular egg capsules (Fig 2-8) collected on colonization blocks. Comparison of partial 18S rDNA sequences from the lenticular egg capsules showed that the capsules were laid by the conid gastropod *Gymnobela* sp. A. Sequences from six egg capsules, including yellow, pink and transparent capsules, had a 100% match over 540 bp with each other and adult *Gymnobela* sp. A, but differed from *Phymorhynchus major* by only one base pair (Supplemental Material 2-9). The lenticular egg capsules occurred in abundances ranging from 1 to 390 egg capsules per block with densities up to 1.6 capsules per cm². Egg capsules are 2.0-3.0 mm (average 2.6 mm) in diameter, harbor approximately 90-200 embryos, and have a pink, yellow or transparent coloration.

2.4 Discussion

2.4.1 The Staged Approach to Larval Identification

Thirty-two of the 41 gastropod species inhabiting the northern EPR (NEPR) can be identified to species at the larval stage using a combination of morphological and molecular techniques. This is nearly double the number of previously identifiable gastropod species. Twenty-five of the 26 gastropod species known to occur specifically in the 9° 50' N area can be identified to species, an increase of 14 species. Only *Provanna ios* has no morphological or molecular information, due to scarce collection and poor preservation of the larval shell on juveniles and adults. New SEM protoconch descriptions of *Gorgoleptis spiralis*, *Echinopelta fistulosa* and *Nodopelta subnoda* increases the total of morphological protoconch descriptions for NEPR gastropods to 20 diagnostic to the species level, five diagnostic to the genus level, and two diagnostic to the family level. The RFLP assays allow for identification of four species within the genus *Lepetodrilus* and six species of peltospirids. 18S rDNA sequences for 20 species are available in GenBank, providing a 'bar code' with which to identify NEPR gastropod species at any stage.

Morphological and molecular techniques have advantages and disadvantages such that the combination of the two is better than either alone. The level of morphological identification in Table 2.3 is based on identification under a dissection and/or compound light microscope. Morphological identification under a light microscope requires very little equipment and thus has a low direct cost. In addition, more than

Table 2.3: Summary of known protoconch and egg capsule characteristics for vent gastropods on the Northern East Pacific Rise. Taxonomic placement and range as in Warén and Bouchet [38] with modifications to the range based on authors' unpublished collections. The taxonomic level to which the morphological characters are discriminatory for each species is listed under 'Morph ID'. **Bold** type represents new information contributed by this study. The size is the maximum length of the shell in micrometers or the maximum diameter of the egg capsule in millimeters, if preceded by EC. Gal: Galápagos, fl. flare and sl. slightly.

Species	Range	Level of			General Protoconch Description			Source	Figure
		Morph ID	Size μm	Sculpture/Shape	Aperture				
Subclass Patellogastropoda									
Family Neolepetopsidae									
<i>Eulepetopsis vitrea</i>	21° N-17° S, Gal	Species	250	Deep side indentations, flattened, smooth curvature	straight fl.	[17]	2-7a		
<i>Neolepetopsis densata</i>	12°-13° N, Gal	Genus	230	Surface looks grainy in light microscopy		[38]			
<i>Neolepetopsis occulta</i>	21° N			Deep side indentations, punctuate at apex, knobbed apex					
<i>Neolepetopsis verruca</i>	21° N								
Subclass Vetigastropoda									
Family Trochidae									
<i>Bathymargarites symplector</i>	21° N-17° S	Species	240 PI, +	Smooth PI, outer axial striations on PII	sinuous fl.	[37]	2-7b		
<i>Moelleriopsis</i> sp.	13° N								
Family Lepetodrilidae									
<i>Clypeosectus delectus</i>	21° N-17° S, Gal	Species	175	Coarse punctate, forms close rows at curve	sl. sinuous	[22]	2-2d		
<i>Gorgoleptis emarginatus</i>	21°-9° N	Species	180	Coarse punctate, forms close rows at curve	scalloped	[22]	2-2c		
<i>Gorgoleptis spiralis</i>	13°-9° N	Species	150	Coarse punctate, forms close rows at curve	scalloped	Thesis	2-2a,b		
<i>Lepetodrilus cristatus</i>	21°-9° N, Gal	Genus		Punctate	straight	[12]			
<i>Lepetodrilus elevatus</i>	21° N-17° S, Gal	Genus	170-180	Punctate	straight	[22]			
<i>Lepetodrilus ovalis</i>	21° N-17° S, Gal	Genus	170-180	Punctate	straight	[13]			
<i>Lepetodrilus pustulosus</i>	21° N-17° S, Gal								
<i>Lepetodrilus tenuianus</i>	11° N								

continued on next page

Species	General Protoconch Description				Aperture	Source	Figure
	Level of Morph ID	Range	Size μm	Sculpture/Shape			
Family Sutilizonidae							
<i>Sutilizona theca</i>	13° N	Species	250	Deep punctate, in lineations following shell curve	sl. sinuous	[16]	
<i>Temnozaga parilis</i>	21° N	Species	170	Smooth	straight	[36]	
Family Fissurellidae							
<i>Cornisepta levinae</i>	13° N				sinuous fl.	[22]	
Subclass Uncertain					ridge above		
Superfamily Neomphaloidea					sinuous ext.	[38]	
Family Neomphalidae					sinous fl.	[30]	
<i>Cyathermia naticoides</i>	21°-9° N	Species	240	Initial bold reticulate web, distal smooth	straight	[36]	2-7d
<i>Lacunoides exquisitus</i>	Gal	Species	160	Initial irregular net, distal smooth, bulbous shape	sinuous fl.	[22]	
<i>Melanodrymia aurantiaca</i>	21° N-17° S, Gal	Species	250	Fine irregular reticulate, full	ridge above		
<i>Melanodrymia galeronae</i>	13° N	Species	250	Very fine reticulate net, full	sinuous ext.	[38]	
<i>Neomphalus fretterae</i>	21°-9° N, Gal	Species	260	Initial fine irregular reticulate, distal smooth	sinous fl.	[30]	
<i>Pachydermia laevis</i>	21° N-17° S	Species	250	Reticulate web fading at aperture	straight fl.	[36]	
<i>Planorbidella planispira</i>	21°-9° N	Species	215	Initial coarse irregular net, distal smooth, broad curvature	straight	[36]	
<i>Solutigra reticulata</i>	21°-13° N	Species	210	Initial irreg net, distal smooth, rounded curve	straight	[36]	
Family Peltospiridae							
<i>Ctenopelta porifera</i>	13°-9° N	Species	325	Ridged parallel, irregular near apex, end abruptly at half	scalloped	[37]	
<i>Echinopelta fistulosa</i>	21°-9° N	Species	210	Ridges only at apex, deep side indentations	straight	Thesis	2-3
<i>Hirtopelta hirta</i>	21°-13° N						
<i>Lirapex granularis</i>	21°-9° N	Species	220	Ridges fade towards axis, punctate apex	straight	[22, 36]	
<i>Lirapex humata</i>	21° N	Species	180	Strong ridges irregular spaced at apex	straight	[22, 36]	
<i>Nodopelta heminoda</i>	21°-9° N						
<i>Nodopelta rigneae</i>	13°-9° N						
<i>Nodopelta subnoda</i>	9° N-17° S	Family	215	Smooth parallel ridges	straight	Thesis	2-4a, b
<i>Peltospira delicata</i>	13°-9° N						
<i>Peltospira lamellisfera</i>	13° N						
<i>Peltospira operculata</i>	21°-9° N	Family	220	Smooth parallel ridges	straight	[22, 36]	2-4c
<i>Rhynchopelta concentrica</i>	21° N-17° S	Species	290	Irregular ridges, shelf at axis	straight	[22, 36]	

continued on next page

Species	Range	Level of Morph ID	General Protoconch Description			Source	Figure
			Size μm	Sculpture/Shape	Aperture		
Subclass Caenogastropoda							
Family Conidae							
<i>Gynnobela</i> sp. A	13°-9° N	EC Species	EC 2-3 mm	Egg capsules: lenticular, transparent, yellow or pink, elliptical escape aperture		Thesis	2-8
<i>Phymorhynchus</i> sp. (<i>P. major</i>)	21°-9° N, Gal (13°-9° N)	Genus	EC 14-16 mm	Egg capsules: lenticular, white to transparent, elongated escape aperture (s-shaped)			
			235	Larvae: Spiral raised ridges in direction of growth crossed by perpendicular riblets			
Family Provannidae							
<i>Provanna ios</i>	21° N-17° S, Gal						
<i>Provanna muricata</i>	21° N, Gal						

25 specimens can be identified in an hour. Specimens are not destroyed in the identification process and can be used in the future.

Molecular identification techniques, though currently more costly and time consuming, contribute to new morphological descriptions and complement morphological identification techniques when morphology alone is insufficient. Molecular techniques require more specialized and expensive equipment and reagents. The procedure requires more steps, with each step ranging in time commitment from 15 minutes to 4 hours. The longer steps do not require continuous labor and attention but make the entire process from sample to sequence or RFLP assay take 2-3 days. Multiple samples can be processed during this time period. The use of RFLPs eliminates sequencing, thus reducing the overall cost. The restriction enzymes Ssp I and EcoR V are more expensive than Dra I, therefore I suggest performing the Dra I digest for the peltospirids first and then performing an Ssp I and EcoR V digest only if necessary to distinguish among *Nodopelta* species. This will also prevent the potential for false identification of *Peltoospira delicata* as *P. operculata*. *Peltoospira* spp. are more common in adult collections than *Nodopelta* spp. at the 9° 50' N area (T. Shank unpublished data, DA personal observation) and *Hirtapelta hirta* are not known from the 9° 50' N area [38]; therefore it is reasonable to predict that *Peltoospira* spp. larvae, identifiable with the Dra I digestion, will be more common than other unknown peltospirids in the plankton.

Lepetodrilus spp. and the peltospirids are two groups of species that exemplify the need to combine molecular and morphological techniques. SEM imaging of unknown peltospirid and *Lepetodrilus* sp. larvae and additional *Lepetodrilus* spp. juveniles yielded no additional information about species-specific protoconch characters. The similarity between *Peltoospira operculata* and *Nodopelta subnoda* protoconchs and amongst the *Lepetodrilus* spp. protoconchs in SEM images indicates that morphology is not, at present, a useful tool for identifying these species in the larval stage. Given the high degree of similarity in shape, sculpture and size between *N. subnoda* and *P. operculata*, it is unlikely that other members of these two genera, *N. rigneae*, *N. heminoda* *P. lamellifera* and *P. delicata*, will be easy to differentiate based on protoconch morphology. Additional imaging of juvenile specimens of the unknown peltospirids could yield species-specific descriptions such as that for *Echinopelta fistulosa*; however, peltospirids were rare in the collections from nine cruises screened in this study and, like other gastropods, have a high occurrence of protoconch loss and

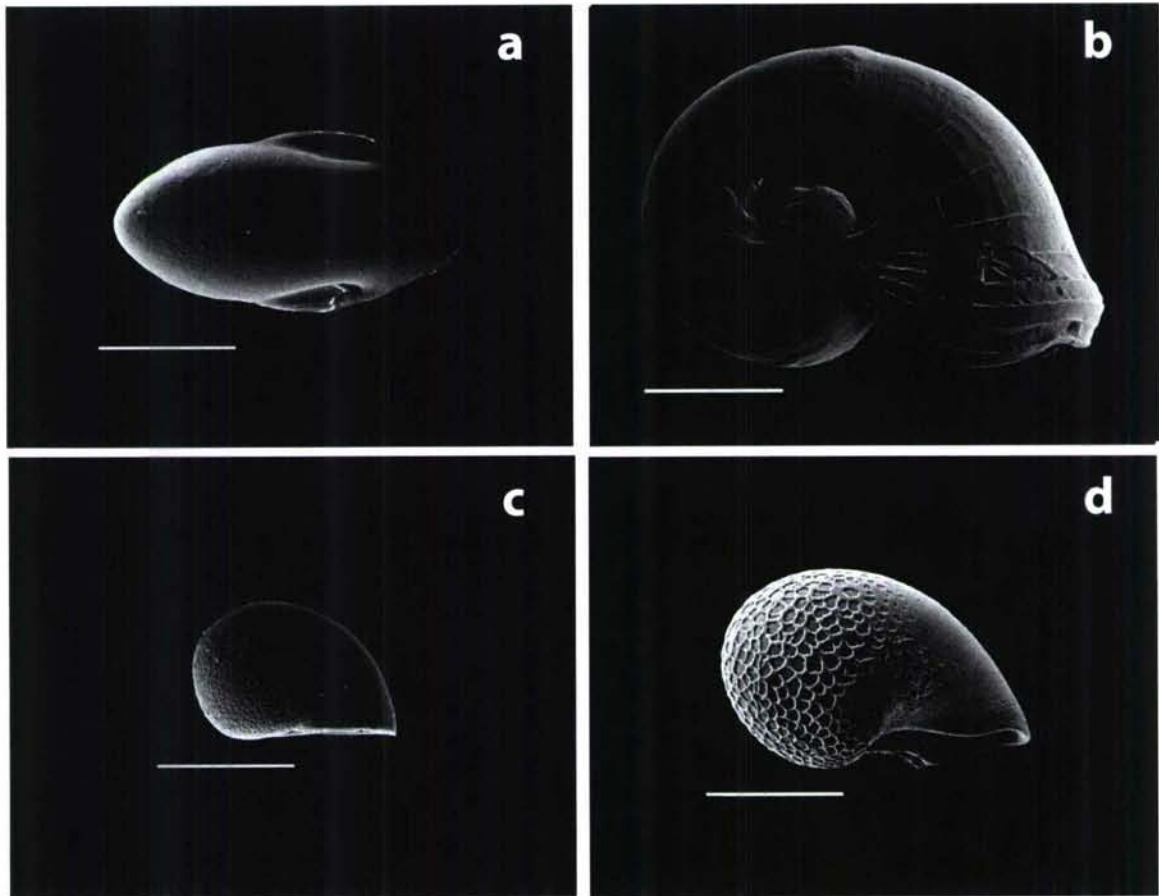


Figure 2-7: Scanning electron micrographs of larvae representing different families. (a) *Euleptopsis vitrea* larva, family Neoleptopsidae. (b) *Bathymargaties symplector* larva with PII growth, family Trochidae. (c) *Lepetodrilus* sp. larva, family Lepetodrilidae. (d) *Cyathermia naticoides* larva, family Neomphalidae. Scale bars are 100 μm for all shells.

damage. The available morphological information does, however, allow for grouping into defined groups such that RFLP assays can be used.

Genetics may also be needed for identifications of early stages of the Caenogastropods. In the present study, the egg capsules of one species of caenogastropod in the NEPR, *Gymnobela* sp. A, were identified to species and described morphologically after molecular identification. Other egg capsules and veligers have been described morphologically by Gustafson and colleagues [6] but have not been definitively assigned to a species. The protoconch and teloconch of caenogastropods quickly corrode such that additional morphological descriptions from retained protoconchs are unlikely. *Gymnobela* sp. A has not yet been described as a species due to high levels of corrosion of examined specimens [38]. Even juveniles with intact protoconchs may not yield species-specific protoconch descriptions because descriptions of juvenile shells are also rare. Direct sequence comparison can help generate morphological descriptions of Caenogastropods' and other gastropods' protoconchs by identifying juveniles, by identifying egg capsules containing developed veligers, and by directly identifying planktonic larvae. More molecular work on the caenogastropods is needed.

Similarity between species and lack of descriptions are just some of the problems that prevent morphological identification. Specimens in an embryo, egg case or trochophore stage, or with a damaged shell, may have no taxonomically informative morphology. These specimens can still be identified using genetics, as demonstrated in the present study by the identification of the under-developed *Gymnobela* sp. A veligers within egg cases.

2.4.2 Daily Larval Collections

Identification of larvae from sediment trap collections demonstrated the utility of the combined morphological and molecular approach. Larval collections varied daily in abundance and species composition (Table 2.2). The high abundance of Unknown Benthic sp. A and *?Laeviphitus* sp. which are unknown as adults and did not match any sequences in the database is intriguing. Species of *Laeviphitus* have not been found on the EPR as adults, but the genus was originally described from larvae, and the PI and PII on larval specimens from this study and Mullineaux et al. 2005 [23] closely resemble other *Laeviphitus* spp. larvae. *?Laeviphitus* larvae may exhibit high abundances near vents due to the increased food supply in the plankton but not reside at vents as adults. Unknown Benthic sp. A does not have PII growth suggesting a non-

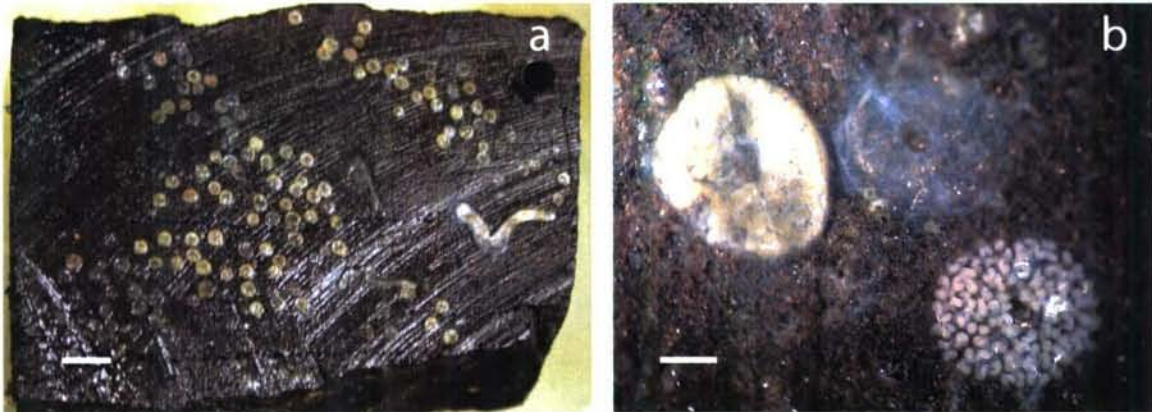


Figure 2-8: Light micrographs of the lenticular egg capsules. (A) Egg capsules density deposited on a basalt block. The arched striations on the block are from cutting the blocks. Scale bar is 1 cm. (B) Close up of three egg capsules at different stages. The right case is yellow with yolky globular embryos inside. The empty middle capsule clearly shows the oval escape aperture from which the larvae escaped. The bottom right capsule is pinkish and contains developing larvae with bilobed velums but no fully developed shell. Scale bar is 1 mm.

feeding larval form, so increased food supply does not explain the high abundances for this morpho-species. Alternatively, adults of ?*Laeviphitus* and Unknown Benthic sp. A may be present in the vent periphery which is not well sampled.

Difficulties in DNA extraction prevented the identification of one unknown peltospirid and three *Lepetodrilus* spp. The identified *Peltospira operculata* and a *Lepetodrilus* were extracted within 3 months of collection, whereas attempts to extract DNA from the other larvae occurred > 6 months after collection. DNA could have been too degraded after 6 months to successfully amplify in PCR reactions. Extractions of *Lepetodrilus* spp. may not have been successful, even within 3 months, due to their relative small size. DNA was successfully extracted from larger larvae, such as *Cyathernia naticoides* and *Laeviphitus* sp. Additionally, a fresh water rinse may have lysed cells, resulting in loss of DNA. Alternative preservatives and sampling techniques could yield sufficient amounts of high quality DNA for identification of unknown larvae using RFLP and direct sequence comparisons.

2.4.3 Egg Capsules

The lenticular egg capsules (Fig 2-8) were identified molecularly to belong to *Gymnobela* sp. A. Sequences from the egg capsules and *Gymnobela* sp. differed from *Phymorhynchus major* by one base pair (see Supplement 2-9). The habitat in which the

egg capsules were collected is consistent with their designation as *Gymnobela* sp. A. *Gymnobela* sp. A have been collected in mussel aggregations near active venting where the egg capsules were found. Blocks placed in the periphery, where *Phymorhynchus major* has been predominantly observed, did not contain any lenticular egg capsules. Additionally, the 6 mm mesh cages would have prevented larger gastropods, like *Phymorhynchus major* (up to 72 mm) [38], from entering and depositing eggs. The smaller size of *Gymnobela* sp. A, 12 mm (maximum length [38]), would allow the gastropod to enter the cages and is consistent with the size of the egg capsules. *Phymorhynchus* sp. is believed to deposit large, 14-16 mm diameter, lenticular egg capsules found on the Galápagos Rift [6]. The egg capsules have similar shapes which supports the close phylogenetic relationship between the two species, but the different sizes and adult distributions suggest that the egg capsules collected on the basalt blocks belonged to *Gymnobela* sp. A.

Identification of the *Gymnobela* sp./ A egg capsules is an example of how molecular identification contributes to our understanding of life histories and the ecology of vent gastropods. *Gymnobela* sp. A is a species for which little life history data were previously known due to poor preservation of larval and juvenile shells on adult specimens. This early life-history information allows us to compare *Gymnobela* sp. A to other gastropod species with different larval dispersal potential, i.e. planktotrophic larvae and non-planktotrophic lecithotrophic larvae. Comparisons of the genetics, benthic ecology and larval supply at the species level for species with different life histories may provide additional insights into the role of larval dispersal in structuring benthic communities.

Bibliography

- [1] Comtet, T., Jollivet, D., Khripounoff, A., Segonzac, M., & Dixon, D. R. (2000). Molecular and morphological identification of settlement-stage vent mussel larvae, *Bathymodiolus azoricus* (Bivalvia: Mytilidae), preserved in situ at active vent fields on the Mid-Atlantic Ridge. *Limnology and Oceanography*, 45(7):1655–1661.
- [2] Douris, V., Cameron, R., Rodakis, G., & Lecanidou, R. (1998). Mitochondrial phylogeography of the land snail *Albinaria* in Crete: Long-term geological and short-term vicariance effects. *Evolution*, 52(1):116–125.
- [3] Dreyer, J., Knick, K., Flickinger, W., & Van Dover, C. (2005). Development of

- macrofaunal community structure in mussel beds on the northern East Pacific Rise. *Marine Ecology Progress Series*, 302:121–134.
- [4] Epifanio, C. E., Perovich, G., Dittel, A. I., & Cary, S. C. (1999). Development and behavior of megalopa larvae and juveniles of the hydrothermal vent crab *Bythograea thermydron*. *Marine Ecology Progress Series*, 185:147–154.
- [5] Govenar, B., Freeman, M., Bergquist, D. C., Johnson, G. A., & Fisher, C. R. (2004). Composition of a one-year-old *Riftia pachyptila* community following a clearance experiment: Insight to succession patterns at deep-sea hydrothermal vents. *Biological Bulletin*, 207(3):177–182.
- [6] Gustafson, R. G., Littlewood, D. T. J., & Lutz, R. A. (1991). Gastropod egg capsules and their contents from deep-sea hydrothermal vent environments. *Biological Bulletin*, 180(1):34–55.
- [7] Harasewych, M. & McArthur, A. (2000). A molecular phylogeny of the Patellogastropoda (Mollusca: Gastropoda). *Marine Biology*, 137:183–194.
- [8] Haymon, R. M., Fornari, D. J., Von Damm, K. L., Lilley, M. D., Perfit, M. R., Edmond, J. M., Shanks, W. C., I., Lutz, R. A., Grebmeier, J. M., Carbotte, S., Wright, C. D., McLaughlin, E., Smith, M., Beedle, N., & Olson, E. (1993). Volcanic eruption of the mid-ocean ridge along the East Pacific Rise crest at 9° 45' - 52' N: Direct submersible observations of seafloor phenomena associated with an eruption event in April, 1991. *Earth and Planetary Science Letters*, 119(1-2):85–101.
- [9] Khripounoff, A., Comtet, T., Vangriesheim, A., & Crassous, P. (2000). Near-bottom biological and mineral particle flux in the Lucky Strike hydrothermal vent area (Mid-Atlantic Ridge). *Journal of Marine Systems*, 2:101–118.
- [10] Lutz, R., Jablonski, D., Rhoads, D., & Turner, R. (1980). Larval dispersal of a deep-sea hydrothermal vent bivalve from the Galapagos rift. *Marine Biology*, 57:127–133.
- [11] Lutz, R. A. (1988). Dispersal of organisms at deep-sea hydrothermal vents: A review. *Oceanologica acta*, Proceedings of the Symposium Hydrothermal Vents of the East Pacific Rise. Biology and Ecology:23–29.
- [12] Lutz, R. A., Bouchet, P., Jablonski, D., Turner, R. D., & Warén, A. (1986). Larval ecology of mollusks at deep-sea hydrothermal vents. *American Malacological Bulletin*, 4(1):49–54. Conference International Symposium on the Ecology of Larval Molluscs.
- [13] Lutz, R. A., Jablonski, D., & Turner, R. D. (1984). Larval development and dispersal at deep-sea hydrothermal vents. *Science*, 226(4681):1451–1454.
- [14] Maddison, D. & Maddison, W. (2000). MacClade.

- [15] Marsh, A., Mullineaux, L. S., Young, C. M., & Manahan, D. T. (2001). Larval dispersal potential of the tubeworm *Riftia pachyptila* at deep-sea hydrothermal vents. *Nature*, 411:77–80.
- [16] McLean, J. (1989). New archaeogastropod limpets from hydrothermal vents - new family Peltospiridae, new superfamily Peltospiracea. *Zoologica Scripta*, 18:49–66.
- [17] McLean, J. (1990). Neolepetopsidae, a new docoglossate limpet family from hydrothermal vents and its relevance to Patellogastropod evolution. *Journal of Zoology*, 222:485–528.
- [18] Menge, B. A. (2000). Recruitment vs. postrecruitment processes as determinants of barnacle population abundance. *Ecological Monographs*, 70:265–288.
- [19] Metaxas, A. (2004). Spatial and temporal patterns in larval supply at hydrothermal vents in the northeast Pacific Ocean. *Limnology and Oceanography*, 49(6):1949–1956.
- [20] Micheli, F., Peterson, C. H., Johnson, G. A., Mullineaux, L. S., Mills, S. W., Sancho, G., Fisher, C. R., & Lenihan, H. S. (2002). Predation structures communities at deep-sea hydrothermal vents. *Ecological Monographs*, 72(3):365–382.
- [21] Mills, S., Mullineaux, L., & Tyler, P. (2007). Habitat associations in gastropod species at East Pacific Rise hydrothermal vents (9° 50' N). *Biological Bulletin*. in press.
- [22] Mullineaux, L. S., Kim, S. L., Pooley, A., & Lutz, R. A. (1996). Identification of archaeogastropod larvae from a hydrothermal vent community. *Marine Biology*, 124(4):551–560.
- [23] Mullineaux, L. S., Mills, S. W., Sweetman, A. K., Beaudreau, A. H., Metaxas, A., & Hunt, H. L. (2005). Vertical, lateral and temporal structure in larval distributions at hydrothermal vents. *Marine Ecology Progress Series*, 293:1–16.
- [24] Mullineaux, L. S., Peterson, C. H., Micheli, F., & Mills, S. (2003). Successional mechanism varies along a gradient in hydrothermal fluid flux at deep-sea vents. *Ecological Monographs*, 73(4):523–542.
- [25] Palumbi, S. R. (1996). Nucleic acids II: The polymerase chain reaction. In: *Molecular systematics.*, D. Hillis, C. Mortiz, & B. Mable, ed., pages 205–248. Sinauer Associates.
- [26] Pradillon, F., Schmidt, A., Peplies, J., & Dubilier, N. (2007). Species identification of marine invertebrate early stages by whole-larvae *in situ* hybridisation of 18S ribosomal RNA. *Marine Ecology Progress Series*, 333:103–116.

- [27] Reid, D., Rumbak, E., & Thomas, R. (1996). DNA, morphology, and fossils: phylogeny and evolutionary rates of the gastropod genus *Littorina*. *Philosophical Transactions of the Royal Society of London Series B-Biological Sciences*, 351(1342):877–895.
- [28] Swofford, D. (2003). PAUP* Phylogenetic Analysis Using Parsimony (*and Other Methods). version 4.0.
- [29] Tunnicliffe, V., McArthur, A., & McHugh, D. (1998). A biogeographical perspective of the deep-sea hydrothermal vent fauna. *Advances in Marine Biology*, 34:353–442.
- [30] Turner, R. D., Lutz, R., & Jablonski, D. (1985). Modes of molluscan larval development at deep-sea hydrothermal vents. *Bulletin of the Biological Society of Washington*, 6:167–184.
- [31] Tyler, P. A. & Young, C. M. (1999). Reproduction and dispersal at vents and cold seeps. *Journal of the Marine Biological Association of the United Kingdom*, 2:193–208.
- [32] Underwood, A. & Keough, M. J. (2001). *Marine Community Ecology*, chapter Supply-Side Ecology: The Nature and Consequences of Variations in Recruitment of Intertidal Organisms, pages 183–200. Sinauer Associates, Inc.
- [33] Van Dover, C. L. (2002). Community structure of mussel beds at deep-sea hydrothermal vents. *Marine Ecology Progress Series*, 230:137–158.
- [34] Van Dover, C. L. & Trask, J. L. (2000). Diversity at deep-sea hydrothermal vent and intertidal mussel beds. *Marine Ecology Progress Series*, 195:169–178.
- [35] Walsh, P., Metzger, D., & Higuchi, R. (1991). Chelex 100 as a medium for simple extraction of DNA for PCR-based typing from forensic material. *BioTechniques*, 10:506–513.
- [36] Warén, A. & Bouchet, P. (1989). New gastropods from East Pacific hydrothermal vents. *Zoologica Scripta*, 18:67–102.
- [37] Warén, A. & Bouchet, P. (1993). New records, species, genera, and a new family of gastropods from hydrothermal vents and hydrocarbon seeps. *Zoologica Scripta*, 22(1):1–90.
- [38] Warén, A. & Bouchet, P. (2001). Gastropoda and Monoplacophora from hydrothermal vents and seeps; new taxa and records. *Veliger*, 44(2):116–231.

2.5 Supplemental Material

	[1]				[50]
Egg Capusles	ATATGCTTGT	CTCAAAGATT	AAGCCATGCA	TGTCTAAGTT	CACACCCTTG
<i>Gymnobela</i> sp. A	-----	-----	-----	-----	-----
<i>Phymorhynchus major</i>	-----	-----	-----	-----	-----
Egg Capusles	TACGGTGAAA	CCGCGAATGG	CTCATTAAAT	CAGTCGAGGT	TCCTTAGATG
<i>Gymnobela</i> sp. A	-----	-----	-----	-----	-----
<i>Phymorhynchus major</i>	-----	-----	-----	-----	-----
Egg Capusles	ATCCAAATTT	ACTTGGATAA	CTGTGGTAAT	TCTAGAGCTA	ATACATGCCG
<i>Gymnobela</i> sp. A	-----	-----	-----	-----	-----
<i>Phymorhynchus major</i>	-----	-----	-----	-----	-----T
Egg Capusles	AACAGCTCCG	ACCCCTCGGG	GAAAGAGCGC	TTTTATTAGT	TCAAAACCAG
<i>Gymnobela</i> sp. A	-----	-----	-----	-----	-----
<i>Phymorhynchus major</i>	-----	-----	-----	-----	-----
Egg Capusles	TCGGGTCTG	CCCGTCCTTT	GGTGA CTCTG	GATAACTTTG	TGCCGATCGC
<i>Gymnobela</i> sp. A	-----	-----	-----	-----	-----
<i>Phymorhynchus major</i>	-----	-----	-----	-----	-----
Egg Capusles	ATGGCCTCGA	GCCGGCGACG	CATCTTTCAA	ATGTCTGCCC	TATCAAATGA
<i>Gymnobela</i> sp. A	-----	-----	-----	-----	-----
<i>Phymorhynchus major</i>	-----	-----	-----	-----	-----
Egg Capusles	CGATGGTACG	TGATCTGCCT	ACCATGTTAG	CAACGGGTAG	CGGGGAATCA
<i>Gymnobela</i> sp. A	-----	-----	-----	-----	-----
<i>Phymorhynchus major</i>	-----	-----	-----	-----	-----
Egg Capusles	GGGTTCGATT	CCGGAGAGGG	AGCATGAGAA	ACGGCTACCA	CATCCAAGGA
<i>Gymnobela</i> sp. A	-----	-----	-----	-----	-----
<i>Phymorhynchus major</i>	-----	-----	-----	-----	-----
Egg Capusles	AGGCAGCAGG	CGCGCAACTT	ACCCACTCCT	GGCACGGGGA	GGTAGTGACG
<i>Gymnobela</i> sp. A	-----	-----	-----	-----	-----
<i>Phymorhynchus major</i>	-----	-----	-----	-----	-----
Egg Capusles	AAAAATAACA	ATACGGA ACT	CTTTTGAGGC	TCCGTAATTG	GAATGAGTAC
<i>Gymnobela</i> sp. A	-----	-----	-----	-----	-----
<i>Phymorhynchus major</i>	-----	-----	-----	-----	-----
Egg Capusles	ACTTTAAACC	CTTTAACGAG	GATCTATTGG	[530]	
<i>Gymnobela</i> sp. A	-----	-----	-----		
<i>Phymorhynchus major</i>	??????????	??????????	??????????		

Figure 2-9: Alignment of partial 18S sequences from unknown lenticular egg capsules compared to *Gymnobela* sp. A and *Phymorhynchus major*. Dashes indicate no change from reference. The last 30 bp of *Phymorhynchus major* were not sequenced and are thus represented as question marks. Note the one base pair difference between the sequences.

	[1]				[50]
<i>L. pustulosus</i>	ACATGGCTCT	TTGCTGGTTC	TAAAGAATAA	GAATAGAGAG	TCTGACCTGC
<i>L. cristatus</i>	-----	----A---A	--G-A,-G-	-----	-----
<i>L. elevatus</i>	-----	C---A---A	---A,-G-	-----	-----
<i>L. ovalis</i>	-----	---A---T	G---A----	-----	-----
<i>L. pustulosus</i>	CCGGTGATGT	AGGAGTTAAA	CGGCCGCAGT	ACCCTGACTG	TGCAAAGGTA
<i>L. cristatus</i>	-----	---A----	-----	-----	-----
<i>L. elevatus</i>	-----	---A----	-----	-----	-----
<i>L. ovalis</i>	-----	---A----	-----	-----	-----
<i>L. pustulosus</i>	GCATAATCAT	TTGCCTTTTA	ATTGAGGGCT	AGTATGAAAG	GTTTGACGTG
<i>L. cristatus</i>	-----	-----	-----	G-----	-----
<i>L. elevatus</i>	-----	-----	-----	-----	-----
<i>L. ovalis</i>	-----	-----	-----	-----	-----
<i>L. pustulosus</i>	GACTAAGCTG	TCTCCTGAGG	ATTATATAGA	AATTAATTTT	TAGGTGAAAA
<i>L. cristatus</i>	-----	-----	---G----	-G---C---	-----
<i>L. elevatus</i>	-----	-----A	-----	-----	-----
<i>L. ovalis</i>	-----	-----	-----	-----	-----
<i>L. pustulosus</i>	AGCCTGAATT	TAACTGTGGG	ACGAGAAGAC	CCCGTTGAGC	TTTAGTTAAA
<i>L. cristatus</i>	<u>G---A----</u>	-GGT-A----	-----	-----	---AC---
<i>L. elevatus</i>	-----	--GT-A----	-----	-----	---AC---T
<i>L. ovalis</i>	-----	---A----	-----	---A----	---A----
<i>L. pustulosus</i>	<u>C</u> <u>TTTAAA</u> ATA	GGGAAAACAG	TGGC.TGTAT	TGAACTAATT	TCTAAGGTAT
<i>L. cristatus</i>	-----	-----	--AT.----	-----	-T-----G-
<i>L. elevatus</i>	---G-G----	-----A	-AAAG----	-----	-T-----G-
<i>L. ovalis</i>	---G-----	--A-----A	-ATG-----	-----	-----
<i>L. pustulosus</i>	TTTTAGTGGG	GGAAAACGGA	GGAATAGTTA	AAGCTTCCTC	TTTTTAAGA.
<i>L. cristatus</i>	-----	-----	---C-AA--	-----	---A-T
<i>L. elevatus</i>	-----	-----	---C-AA-G	-----	---TART
<i>L. ovalis</i>	-----	-----	---TAAG	-----	---GC-T
<i>L. pustulosus</i>	AGATTRAGTT	ATTTGTATCT	GTAGAGATAT	AATAAAGGAA	TTTGATAAAT
<i>L. cristatus</i>	-A---A-A--	--A.....	AA-T---AG-	-T-G-GTAG-	---TA-T--.
<i>L. elevatus</i>	-A---A---A	-CA.....	TA-A--G-G-	...G--TAT-	G--.AGA--A
<i>L. ovalis</i>	G---G----	-----T-	-A-A-T-A--	--A-.....	..AT---GT-
<i>L. pustulosus</i>	TAAATTAAAG	CTGGTGTGTA	ATGGTTTAGT	AAAAGGATCC	GTTGAAAGTA
<i>L. cristatus</i>	-----GA	-----	-A-----A	-----	-----T-G
<i>L. elevatus</i>	---GG-----	---A---C-	GA-----A	-----	---T--T--.
<i>L. ovalis</i>	-TTGG-----	---CA---G	-----GA-	-G-----	-----RTA-
<i>L. pustulosus</i>	A.GTAGATGA	TTAAGGGAGA	GAGTTACCAC	GGGGATAACA	GCGTAATTTT
<i>L. cristatus</i>	-T-A---C--	-----	A-----	-----	-----
<i>L. elevatus</i>	-TAA-A-C--	-----	-----	-----	-----
<i>L. ovalis</i>	-TT--.-----	-----A-	----- <u>T</u>	-----	-----
<i>L. pustulosus</i>	TTCTGGAGAG	TTCATATTGA	AGGAGGGGTT	TGCGACCTCG	ATGTTGGATT
<i>L. cristatus</i>	-----	-----	-----	-----	-----
<i>L. elevatus</i>	-----	-----	-----	-----	-----
<i>L. ovalis</i>	-----	-----	-----	-----	-----
<i>L. pustulosus</i>	AAGACATCCT	AAGGGTGTAG	CAGCTTTTAA	GGGTTGGTCT	GTTTCGACCAT
<i>L. cristatus</i>	-----	GG-----	---CCCG-	-----	-----
<i>L. elevatus</i>	-----	G-----	---T---C-	-----	-----
<i>L. ovalis</i>	-----	G-----	---C----	-----	-----
<i>L. pustulosus</i>	TAAAGTCTTA	CGTGATCT			
<i>L. cristatus</i>	A-----	-----			
<i>L. elevatus</i>	A-----	-----			
<i>L. ovalis</i>	A-----	-----			

[618]

Figure 2-10: Alignment of partial 16S sequences from *Lepetodrilus* spp. Box denotes the Dra I recognition site. Underline denotes the Stu I recognition site. Double underline denotes the Sty I recognition site.

[1] [50]

<i>E. fistulosa</i>	ACATGGCTCT	TTGTTTTTCA	TAGA.TAAAG	AGTCGGACCT	CCCCAGTGAA
<i>H. hirta</i>	-----C	---G-GA-G	-A-A.T---	-----G	-----G
<i>N. heminoda</i>	-----	---AA	A---.G---	-----G	-----G
<i>N. rigneae</i>	-----	---AA	C---.G---	-----G	-----G
<i>N. subnoda</i>	-----	---AA	G---.G---	-----G	-----G
<i>P. delicata</i>	-----	---GGAA-A	GA-AA--G-	-----G	-----G
<i>P. operculata</i>	-----	---AGAAA-	--AGA-GG-	-----G	-----G
<i>E. fistulosa</i>	TTA....TT	TTAACGGCCG	CGGTACCCTG	ACCGTGCAAA	GGTAGCATAA
<i>H. hirta</i>	-G-AA....	-----	-----	-----	-----
<i>N. heminoda</i>	-A-TGA.T--	-----	-----	-----	-----
<i>N. rigneae</i>	-A-TGA..--	-----	-----	-----	-----
<i>N. subnoda</i>	-AGTGA.T--	-----	-----	-----	-----
<i>P. delicata</i>	-.GGAAG.C-	-----	-----	-----	-----
<i>P. operculata</i>	--TTAAGAC-	-----	-----	-----	-----
<i>E. fistulosa</i>	TCATTTGCCT	TTTAATTGGA	GGCTAGTATG	AATGGTTTGA	CGAAAGCGAA
<i>H. hirta</i>	-----	---A	---A	---	---A-A-T
<i>N. heminoda</i>	-----	---AA	---G	---C	---A-A-
<i>N. rigneae</i>	-----	---AA	---G	---	---A-G
<i>N. subnoda</i>	-----	---AA	---G	---	---A-
<i>P. delicata</i>	-----	---A	---G	---	---A-GG
<i>P. operculata</i>	-----	---	---G	---	---A-A-
<i>E. fistulosa</i>	ACTGTCTCTT	ATTTGCTTCC	TAAAAATTAA	TTTTGATGTG	AAGAAGCATT
<i>H. hirta</i>	-----	---AT-ATT	---	---	---
<i>N. heminoda</i>	-----	---C-AT-ATT	---	---	---
<i>N. rigneae</i>	-----	---CC-AA-ATT	---	---	---
<i>N. subnoda</i>	G-----	---C-AT-ATT	---	---	---
<i>P. delicata</i>	-----	---C-AY-ATT	---	---	---
<i>P. operculata</i>	G-----	TC--AT-AGT	--G-	---	---
<i>E. fistulosa</i>	AATATTTCTA	AAAGACAAGA	AGACCCTGTT	GAGCTTAAAT	AATGAAAAAA
<i>H. hirta</i>	<u>G--TA</u> -----	-----	---A--	---T--	--ATGT--G
<i>N. heminoda</i>	---TA-----	-----	-----	---T-GC	G-AATG----
<i>N. rigneae</i>	---A-----	-----	-----	---T-C	G-AAT----
<i>N. subnoda</i>	---TA-----	-----	-----	---T-GC	G-GAT--G--
<i>P. delicata</i>	---G-----	-----	---A-	---	--GAG--T--
<i>P. operculata</i>	---GGC----	-----	---	---T--	-GAG--G--
<i>E. fistulosa</i>	ACAAAATTAT	ATAAGTAGAA	AATTATT <u>TT</u>	<u>TAAAA</u> AATTAT	TTTAGTTGGG
<i>H. hirta</i>	TGTACAGGTA	TAG-T--A--	GG-----A--	-T-T--A--	-----
<i>N. heminoda</i>	-GT--T--TA	TG--TC-A--	--A--C--	-TTTT--CT-	-----
<i>N. rigneae</i>	-AT--T--TA	TG--TC-A--	--A--	-TT-T--CT-	-----
<i>N. subnoda</i>	-AT--T--TA	TG-GTC-A--	--A--C--	-TT-T--CT-	-----
<i>P. delicata</i>	-AT-G-G-TA	TG--TC-A--	C-A-R--	-T-GT--	-----
<i>P. operculata</i>	G--GTA-.A	TG--TC-A--	T-A-G--	-TTGT-A--	-----
<i>E. fistulosa</i>	GCGACTGAGG	AACAAAA.TA	GCTTCCTTTC	ATTGTTTTAG	CACAC....
<i>H. hirta</i>	-----	-----	A-----A	-G-TAAGAAA	...ATAATTA
<i>N. heminoda</i>	-----	---G	-----A	TGAAAAAAGA	TTAATTTTAT
<i>N. rigneae</i>	-----A---	---TA	-----T	-A-AAAAGA	TTTATTGGTA
<i>N. subnoda</i>	-----	---G	-----T	T-ATAAGAGATTTAT
<i>P. delicata</i>	-----	---G	-----A	T-AAAAG-ATATA
<i>P. operculata</i>	-----	---T-AA-	---A	-A-SAAG-GAT	ATA-GATATA
<i>E. fistulosa</i>	.TTGCAAAGA	TCCAGCCAAA	TGCTGATCAA	AGAAAATAGT	TACCACAGGG
<i>H. hirta</i>	T--TT-TT--	C---AA.-TG	-TT---T--	-AG--T---	---T---
<i>N. heminoda</i>	T-....T--	---G.-T-	-C---T-G	-AG--T---	---T---
<i>N. rigneae</i>	T-....T--	---G.-	-C---T-G	-AGT-T---	---T---
<i>N. subnoda</i>	T-ATTT-T--	---G.-T-	-T---T-G	-AG--T---	---T---
<i>P. delicata</i>	T-ATTT--	---AAA-	-TT---T--	-AG--T---	---T---
<i>P. operculata</i>	T--ATGGT--	---AAA..T	-TTT--T--	-AG--T---	---T---
<i>E. fistulosa</i>	ATAACAGCGT	AATCTTCTTT	TAGAGCTCCC	ATCGAAAAAA	
<i>H. hirta</i>	-----	---T---	G---T--AT	-----	
<i>N. heminoda</i>	-----	---C-T---	---T-T---	-----	
<i>N. rigneae</i>	-----	---C-T---	---T-TT---	-----	
<i>N. subnoda</i>	-----	---C-T---	---T-TT---	-----	
<i>P. delicata</i>	-----	---C-T---	---T-TT---	-----	
<i>P. operculata</i>	-----	---C-T---	---T-TT---	-----	

[420]

Figure 2-11: Alignment of partial 16S sequences from *Echinopelta fistulosa*, *Hirtapelta hirta*, *Nodopelta heminoda*, *N. rigneae*, *N. subnoda*, *Peltopspira delicata* and *P. operculata*. Box denotes the Dra I recognition site. Underline denotes the Ssp I recognition site. Double underline denotes the EcoR V recognition site.

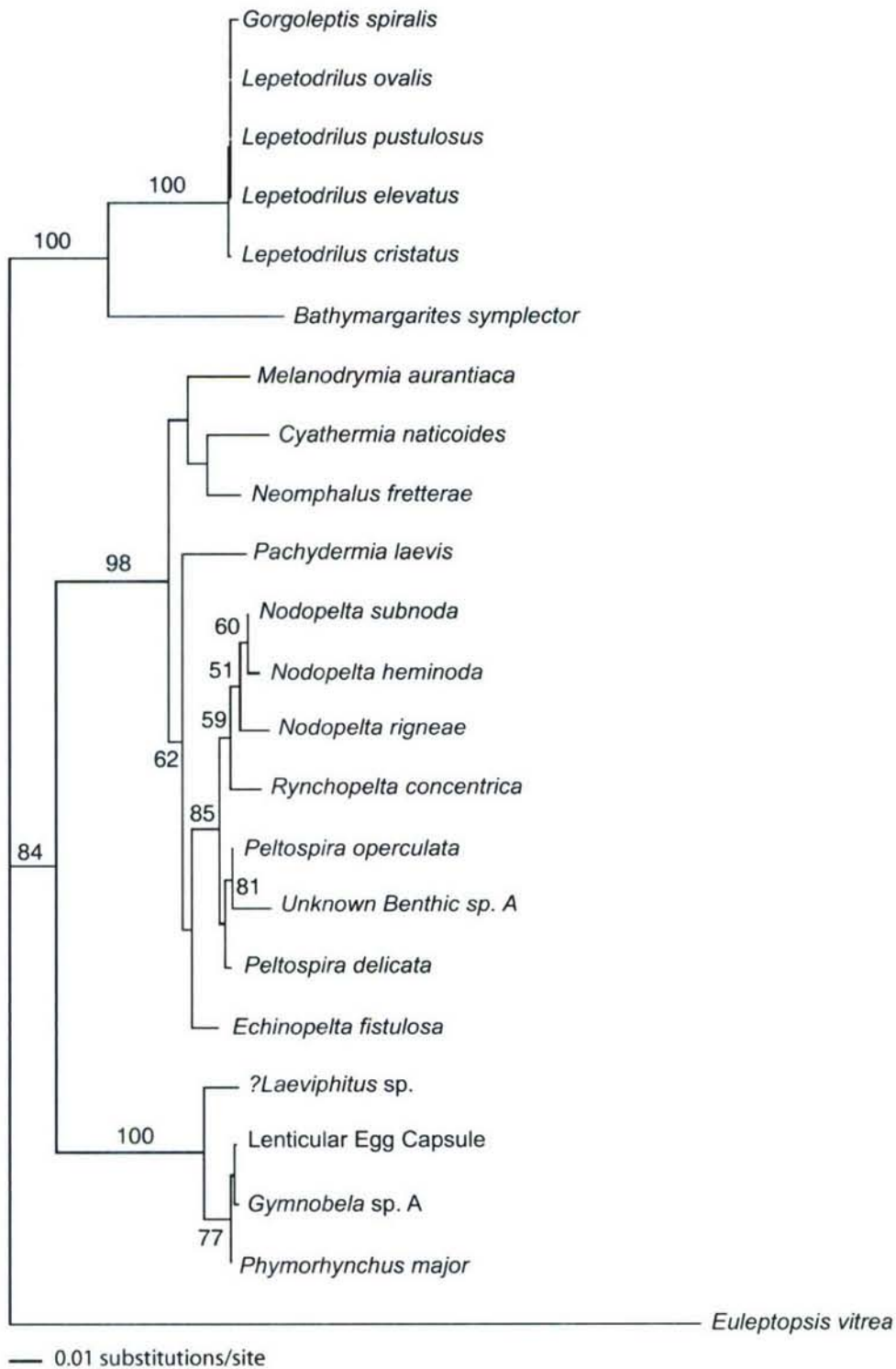


Figure 2-12: Relationship between vent gastropods found near 9° N based on partial 18S sequences. Bootstrap values (> 50%) are shown on branches. Note the inclusion of Unknown Benthic sp. A within Peltospiridae.

Chapter 3

Gastropod larval flux to hydrothermal vents influenced by spatial and temporal variability in currents on small scales

3.1 Abstract

Examination of the scales at which larval supply varies spatially and temporally and correlation with concurrent physical observations has provided insights into larval transport and delivery mechanisms. Daily variability in larval supply at two hydrothermal vents, East Wall and Choo Choo, near $9^{\circ} 50' \text{ N}$, East Pacific Rise was quantified concurrently with hydrodynamic observations at both sites. The magnitude and temporal variation in larval supply differed between the two vent sites despite their close proximity, 1.6 km. Larval supply was relatively high and uninterrupted at East Wall compared to low and episodic at Choo Choo. Observed variation in larval flux was compared to predictions based on advective transport by measured currents from a continuous and discrete larval source. Variation in larval supply at Choo Choo was correlated with along-axis southward currents, consistent with larval transport from a northern larval source. Larval supply to East Wall appeared to be independent of current velocities, suggesting that larvae came from multiple sources north and south of, and possibly including, East Wall. The results indicate that transport of larvae from discrete local sources can explain differences in larval supply

to vent communities, even on small spatial scales (km).

3.2 Introduction

Understanding the biological and physical transport mechanisms involved in the dispersal, retention, and delivery of larvae is essential to the study of marine benthic population dynamics and structure, gene flow, and connectivity. Larval supply contributes to shaping population and community structure and dynamics, and the strength of post-settlement benthic interactions: competition, facilitation, and predation [14, 29, 28, 53].

The timing and spatial extent of larval supply to benthic habitats can be governed by physical processes. Recent research has focused on larval delivery on tidal scales [9, 20, 36, 40], especially in regards to bay-ocean exchange. However, larval delivery has also been correlated with wind-driven and mesoscale events, such as wind reversals [3, 11], storms [12, 37], upwelling relaxation [42, 45], and eddies [39, 48, 49]. These events often provide short (daily) pulses of larvae to a site, but can act over large spatial scales (tens to hundreds of kilometers). Local topography and topographically generated flows can disrupt the impact of large-scale processes and create a locally mediated larval supply [41, 46, 47]. Correlation between the temporal and spatial scales of variation in larval supply varies and concurrent physical observations have provided insights into larval transport and delivery mechanisms.

Disturbed and dynamic communities, such as hydrothermal vents, may be particularly sensitive to variation in larval supply. Hydrothermal vents along the East Pacific Rise (EPR) undergo successional processes [44] reset by eruptive and/or tectonic events on a decadal time-scale [13, 51]. Initial colonization of nascent vents after a disruptive event will be determined, in part, by the availability and delivery of larvae. Environment, benthic interactions, and larval supply combine to determine the successional sequence and community composition over time. The dominant megafauna change in concert with the temperature and chemistry of the vent fluids over time [25, 44]. Colonization studies have shown that post-settlement benthic interactions, such as facilitation, competition and interference, affect recruitment success [34]. The role of larval supply in the succession of vent communities remains largely unknown due to infrequent larval collections and a poor understanding of larval dispersal and delivery along the EPR.

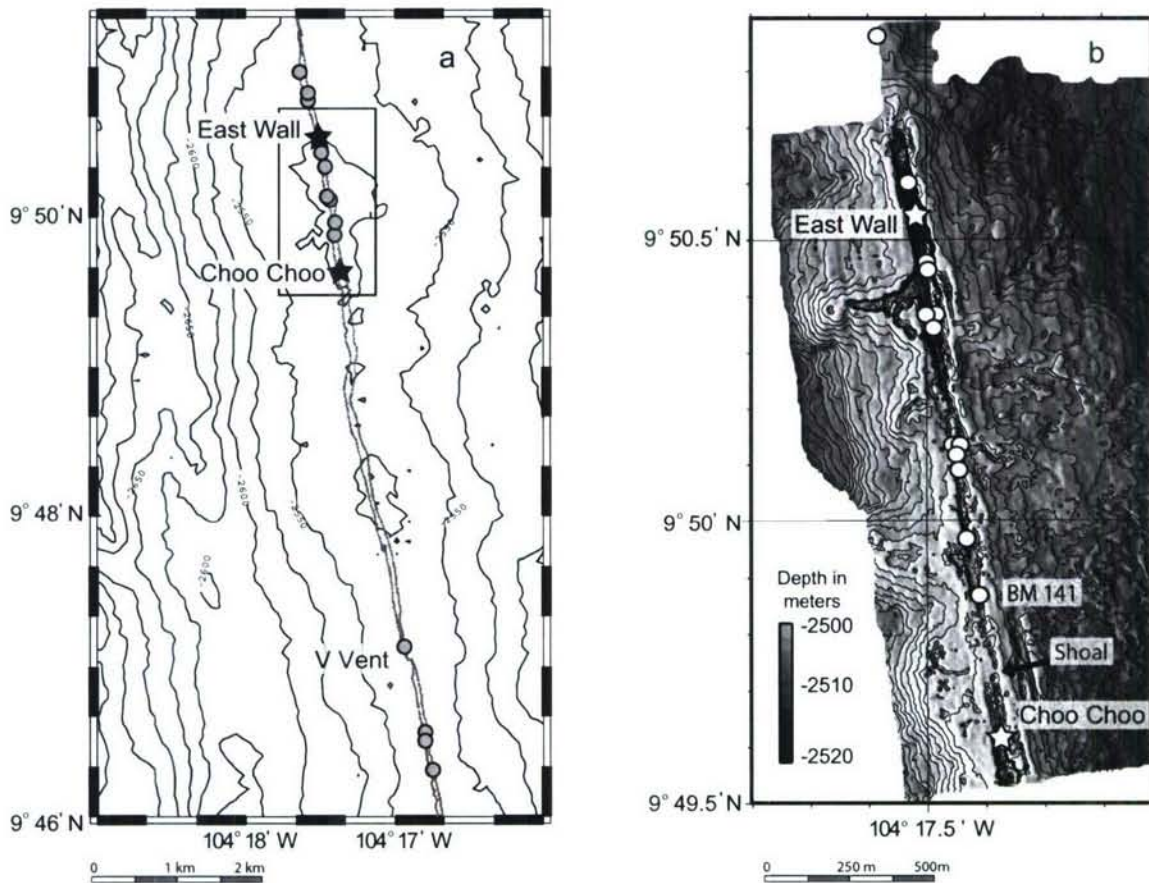


Figure 3-1: The 9° 50' N area of the East Pacific Rise. Collection sites (stars) at East Wall and Choo Choo and the known vent communities (circles) are identified. a) Distribution of known vent sites between 9° 46' N to 9° 51' N along the axial summit collapse trough (bordered by gray region). Contour lines are 25 m; the ridge axis depth near 9° 50' N is 2500 m. b) Expanded view of area in black box in (a) to show detail in axial summit trough topography; contours are 1 m. The strike of the axis is approximately 8° counterclockwise from North. Figure adapted from [43].

Temporal and spatial variation in larval transport and recruitment processes at vents along the EPR have been based on few physical and biological studies compared to shallow water. Vertical and lateral larval distributions have been inferred from snap-shots of larval abundances in net and pump sampling; however, temporal information was often complicated by time-space interactions and the potential for aliasing due to long intervals between sampling [30, 33]. Continuous time-series observations of larval supply are rare in the deep-sea. Physical observations suggest that passive advective transport in currents would carry larvae tens to hundreds of kilometers within a 30 day larval life-span [6, 27]. Population genetic studies also suggest extensive dispersal over hundreds to thousands of kilometers in many vent species [7, 19, 21, 54, 55].

Smaller-scale (meters to kilometers) buoyancy-driven flows and topography may disrupt passive transport within mean currents and create temporal and spatial heterogeneity in larval supply. Hydrothermal plumes have been hypothesized to enhance the transport of vent larvae through entrainment into the rising plume [31]. Current velocities at the height of the neutrally-buoyant plume are faster than current velocities near bottom [6, 23]. Larvae also could be transported within detached hydrothermal plume vortices [31]. However, modeling [23] suggests that entrainment into the rising plume is infrequent due to relatively strong horizontal current velocities and limited to larvae in close proximity (< 10 m) of the plume source. Larval collections [33] also suggest that relatively few larvae are dispersed at plume height. Larval abundances were highest near bottom (1 m above bottom) near vents, and decreased exponentially with increasing height above bottom [33]. Larvae near the bottom may experience hydrodynamic conditions influenced by the complex topography of the axial summit trough (AST), a narrow valley running along the crest of the ridge. Vent communities along the EPR lie predominantly within the AST [16]. The AST has been proposed to retain buoyancy-driven flows, and thus to retain larvae near hydrothermal vents along the Juan de Fuca Ridge [50]. However, the EPR has a much shallower AST (3 - 15 m depth) with numerous discontinuities suggesting that proposed larval dispersal scenarios for other biogeographic regions of hydrothermal vents are not applicable to the EPR.

I investigate variability of larval supply to hydrothermal vent communities near $9^{\circ} 50'$ N, EPR on small temporal (days) and spatial (kilometers) scales. My objectives are to 1) characterize the daily variation in larval supply and determine its correlation

with currents; and 2) investigate the effects of local larval sources on larval supply by comparing the magnitude and variation in larval supply between two nearby sites.

Field observations of currents and of daily gastropod larval supply to two hydrothermal vents are compared to predictions based on advective transport from different larval sources. My intent is to characterize whether larval supply in the field correlates with physical transport near bottom and/or at height of the neutrally-buoyant plume. Implications of variation in larval supply are discussed for population connectivity, colonization, and community succession at vents.

3.3 Methods

3.3.1 Study Sites

The study was done at two mussel dominated vent sites, East Wall and Choo Choo, in the $9^{\circ}50'$ N area on the EPR, in November 2004. At the time of sampling, the diffuse flow hydrothermal community at East Wall was located within the northern portion of an active section of the AST on the ridge axis (Fig 3-1), draping the ~ 13 m relief of the east wall of the AST. Numerous other high-temperature and diffuse-flow vent sites were located within a few hundred meters to the north and south of East Wall within a continuous section of the AST (Fig 3-1). The northern-most vent sites known on the 9° N segment lie just to the north (< 1 km) of East Wall. Choo Choo was 1.6 km south of East Wall along the ridge axis in a small section of the AST encompassing no other vent communities. The AST at Choo Choo was shallower (~ 5 m) than East Wall and was separated from the northern section by a shoal 200 m to the north (Fig 3-1b). The closest larval source to Choo Choo was the Biomarker 141 community, approximately 400 m to the north (Fig 3-1). Tubeworm Pillar and Y vent were the closest vents to Choo Choo, tens of meters south, but shut down between 2002 and 2004 (T. Shank, K. Von Damm, personal comm.) and thus were not considered a source of larvae for this study. The closest known active larval source to the south of Choo Choo was the V vent community in the $9^{\circ}47'$ N area, approximately 4.5 km away (Fig 3-1a).

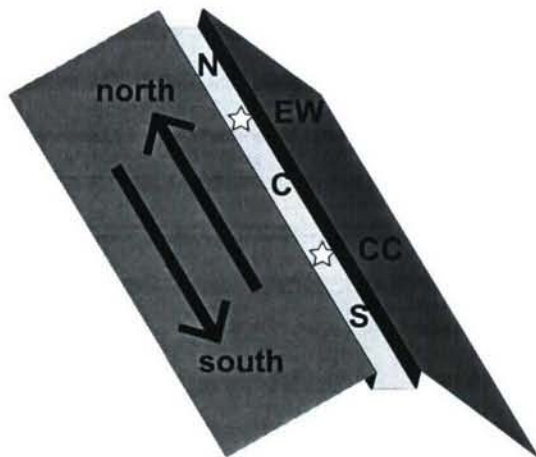


Figure 3-2: Diagram showing the position of larval sampling and current measurement sites (stars) relative to an idealized ridge axis and possible larval sources. Arrows are along-axis larval transport scenarios used in the conceptual model to describe advection northward or southward from larval sources to the north (N), south (S), in between (C) and at East Wall (EW) and Choo Choo (CC) (stars).

3.3.2 Sample Collection

Experimental Design

Moorings were deployed from November 12 - 22, 2004, one each near East Wall and Choo Choo, to collect time-series samples of larvae and to measure current velocities. The Choo Choo mooring was deployed a day after the East Wall mooring due to ship time constraints, and thus, the Choo Choo records are a day shorter. Each mooring was equipped with a McLane PARFLUX Mark 78H-21 time-series sediment trap with the opening positioned at 4 meters above bottom (mab) to collect larvae. Each trap had a sampling area of 0.5 m^2 and sampled vertical particle flux continuously on daily (24 hour) intervals until day 8 (November 19, 2004). The last two days were sampled in 4-hour intervals in an attempt to capture diurnal and semidiurnal tidal variability. Larval fluxes in each 4 h interval were too low for statistical analyses and were subsequently pooled into daily intervals.

Each mooring was also equipped with two current meters positioned near bottom (at 10 mab) and within the level of the neutrally buoyant vent plume (at 170 mab) [2]. Aanderaa RCM11 acoustic current meters were used except for the instrument at 170 mab on the Choo Choo mooring, which was a vane and rotor RCM8 model. The current meters on the Choo Choo mooring recorded at 10 minute intervals and the current meters on the East Wall mooring recorded at coincident 30 minute intervals due to lower battery capacities.

Moorings were positioned within 10 meters of the center of each of the venting areas. Exact positioning was accomplished by lowering the mooring from the ship's hydrowire and navigating it into an acoustic network on the seafloor [18] using the

ship's dynamic positioning capabilities. A transponder on the wire communicated acoustically with the long baseline navigational network used by *DSV Alvin* and allowed positioning directly above the target drop site. After placement on the seafloor, the positions of the moorings at East Wall, 9° 50.54' N, 104° 17.53' W and at Choo Choo, 9° 49.60' N, 104° 17.37' W, were verified using slant range surveys and visual observation from *DSV Alvin*.

Larval Sample Processing

Larvae were preserved in the sediment traps *in situ* and processed in the laboratory after trap recovery. I used a saturated salt - 20% dimethyl-sulfoxide (DMSO) solution [22] to preserve sediment trap samples for morphological identification and to preserve DNA for future studies. The fraction retained on a 63 μm sieve was sorted for larvae (gastropods, bivalves, polychaetes, crustaceans) under a dissecting microscope at 25x. Gastropod larvae were further identified to the lowest possible taxonomic level under dissecting and compound microscopes, often to the species level, based on shape, size and sculpture of the larval shells (Protoconch I and II) (see Chapter 2, [32, 33]). Larval identifications, groupings and nomenclature were based on Mullineaux et al. (2005) [33]. Gastropod larvae unequivocally identified as of vent origin were grouped as Vent Gastropod larvae for subsequent analyses. Gastropod larval morphotypes in high abundance and that have been found in past larval collections [33], but could not be definitively identified as of vent origin, were grouped and treated separately as Probable Vent Gastropods.

Larval Spatial and Temporal Variability

Sampling was designed to characterize spatial and temporal variability of vertical larval flux at two sites. Time-series of grouped and species-specific larval flux were not autocorrelated ($p > 0.05$) (SYSTAT v.10, Systat Software Inc., Richmond, California, USA), therefore, larval flux data were treated as independent for spatial comparisons. Differences in larval flux between the two sites were tested using Bonferroni corrected paired t-tests in SYSTAT v.10. Temporal variability in gastropod larval flux was assessed using a 95% confidence interval (CI) to identify anomalous flux compared to the mean.

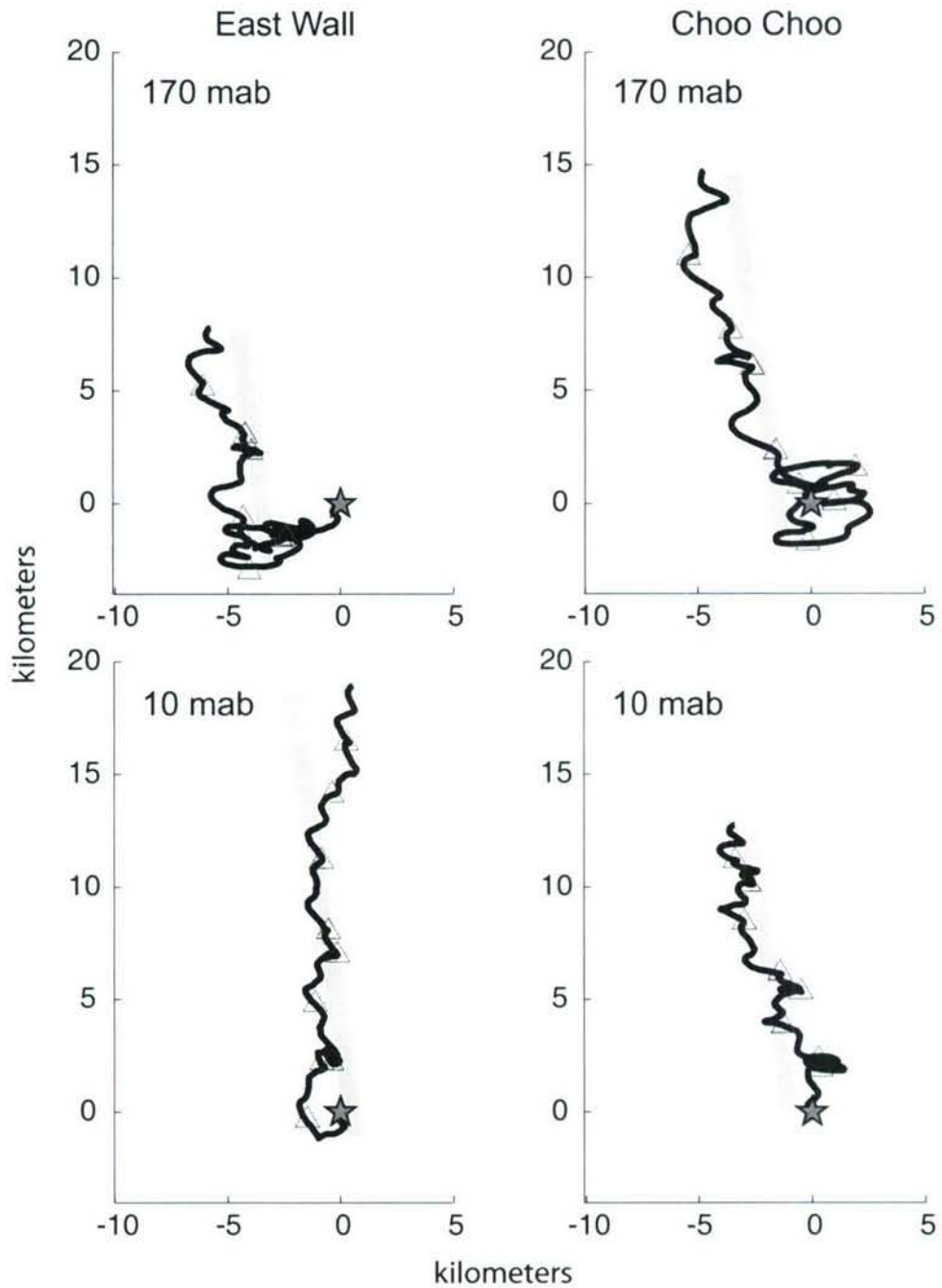


Figure 3-3: Progressive vector diagrams from current velocities measured at East Wall and Choo Choo at 170 mab (upper) and 10 mab (lower). The orientation of the ridge axis is shown in gray. The stars indicate initial start date and the triangles designate subsequent 24-hour intervals.

	Between Sites		Between Heights	
	170 mab	10 mab	East Wall	Choo Choo
Along Axis	0.8296	0.7472	0.5770	0.5954
Cross Axis	0.9326	0.7417	0.6140	0.8117

Table 3.1: Correlation coefficients of along-axis (v) and cross-axis (u) current velocities between sites at the same height, and between heights within a site. All correlations were significant at $p < 0.001$.

Current Meter Records

Currents velocities were transformed on to a coordinate system oriented along the strike of the axis (8° counterclockwise from true north and 13° from magnetic north), such that v is along-axis flow and u is cross-axis flow. Tidal analyses were performed in Matlab v.7.1 (The MathWorks, Inc., Natick, Massachusetts, USA) using `t_tide` [35]. Current records from Choo Choo were low-pass filtered [1] with a cut off of 50 minutes (5 data points) and then subsampled every 3rd record to make records of equal sampling intervals from both sites for correlations of current velocities between sites. Pearson correlations were determined for the cross-axis and along-axis components of the current velocities between heights and between sites using Matlab v.7.1.

3.3.3 Correlation between Larval Flux and Transport

Advective Transport

Larval fluxes were compared to predictions of temporal variation in larval supply at the collection sites based on horizontal advective transport from a continuous discrete larval source (Fig 3.3.1). Larval flux into the sediment traps was treated as a proxy for larval supply to the benthos, assuming a constant rate of passive downward vertical flux (sinking out) that delivered larvae from the plankton to the benthos. The observed larval flux serves only as an approximation of larval supply since little information exists on when vent larvae are competent to settle. Many vent gastropod larvae may be competent upon release or shortly thereafter because the majority are non-feeding and have no detectable development stages [26, 32], but times to competency are unknown. Based on these assumptions, delivery of larvae by horizontal advective transport will determine larval supply at a given site. Analyses were restricted to transport along the axis and ignored the cross-axis component because hydrothermal vent communities were found exclusively along the north-south

trending ridge axis [16] (Fig 3-1). The source of larvae may have been north of, south of, in between, or directly at the two collection sites, East Wall and Choo Choo. Current velocity records were used to predict the horizontal advective transport at 10 mab and 170 mab. The along-axis component of velocity determined the transport of larvae from a given source to each collection site. For example, when currents became northward, transport to East Wall was expected to increase if the larval source was at a more southern site (Central, Choo Choo, or South) and to decrease if the source was a more northern site (North). In contrast, when currents became southward, transport to East Wall should have decreased if the larval source was to the south, but increased if the source was to the north. If the larval source was directly at East Wall, larval transport was not expected to vary with current direction. The predictions for transport to Choo Choo followed the same reasoning, and depended on the direction of currents and location of source sites of larvae. These predictions assume that larvae were lost from the system when currents reverse directions, such that the only larvae available for transport during each interval of sustained transport were produced during that interval at a source site with continuous reproduction. Predictions based on advective transport were compared to the observed patterns of larval supply.

Correlation Analyses

A measure of advective transport, derived from measured current velocities, was needed for correlation with larval fluxes, integrated over 24-hour periods. Total or net transport during each 24 hour period was not adequate because the flows were not unidirectional. Changes in the direction of flow could have caused sustained transport in one direction to be obscured by transport in the opposite direction. As an alternative, sustained transport in a single direction during each 24 hour period was calculated as follows to yield estimates of along-axis northward and southward transport. This simplification allows for larval flux and current velocity observations to be compared to the predictions described in section 3.3.3. Intervals of continuous (sustained) unidirectional along-axis transport during each day were identified by filtering out high frequency variation (cut off 6 h) [1]. Daily transport was calculated from the unfiltered data by integrating v over each interval of identified sustained unidirectional transport. If multiple periods of, for example, northward flow (interrupted by an interval of southward flow) occurred in one day, the period of furthest transport

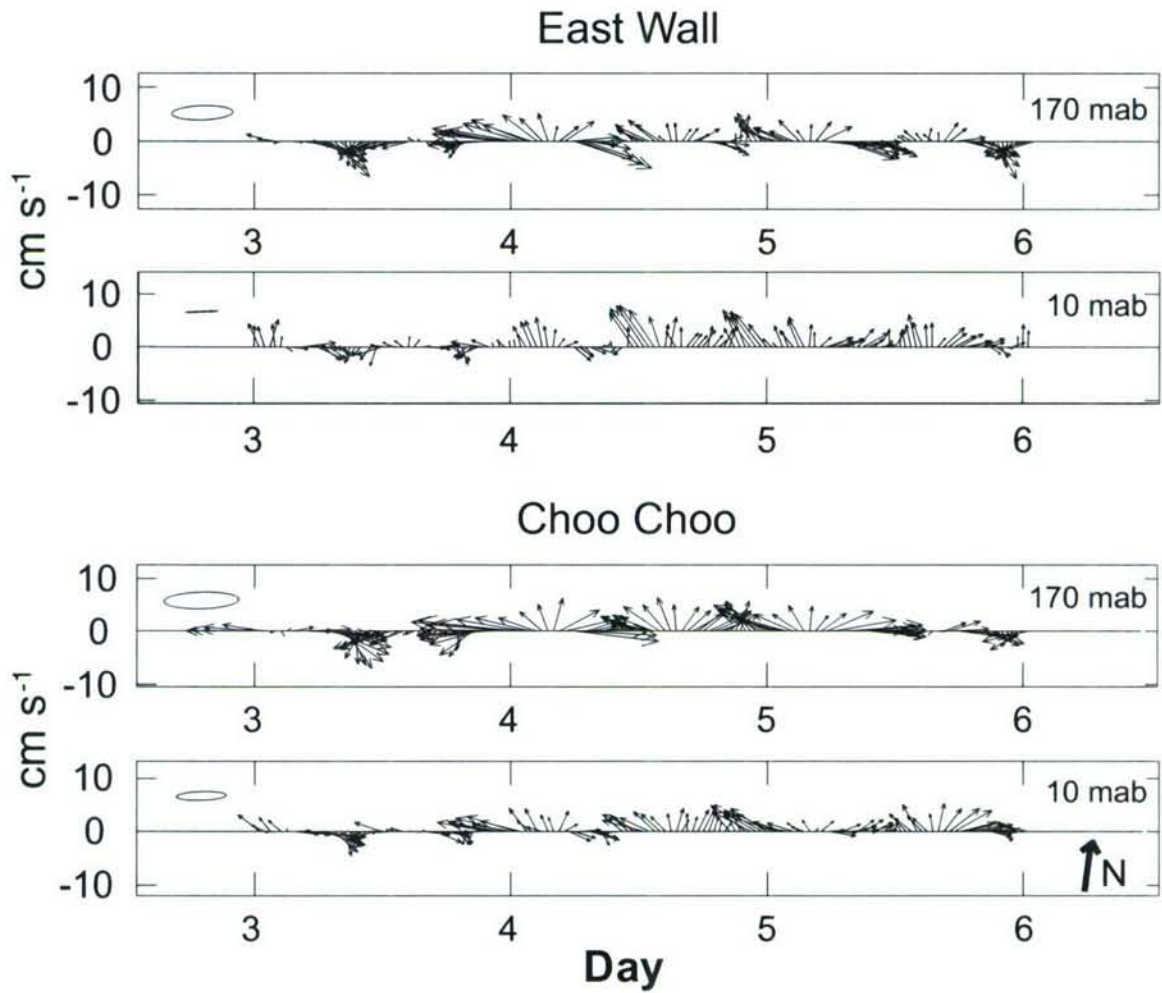


Figure 3-4: Representative current velocities from days 3 to 6 of the 10-day time-series. Current velocities are transformed onto a coordinate system oriented along the ridge axis (strike $+8^\circ$). This subset allows visualization of the predominantly cross-axis diurnal and semidiurnal tidal fluctuations. Tidal ellipses of the dominant tidal frequency, M2, are presented in the upper left corner of each time-series on the same scale as the vectors.

was used as the daily along-axis northward transport. Only northward and southward transport greater than 100 m was included. This distance represents sufficient transport to exchange material between vents - the average distance between vents clustered near 9° 50' N was 138 m. Daily larval fluxes for pooled groups and selected species were cross-correlated with daily along-axis northward, southward and net transport using Matlab v.7.1. Cross-correlations showed no evidence of lagged correlations (data not shown), therefore, Pearson correlation coefficients (cross-correlation at 0 lag) were presented. Since current velocities were likely to be autocorrelated, tests for the significance of the cross-correlations used a corrected sample distribution to account for autocorrelation of both physical variable and larval fluxes (see Section 3.6.1). The significance was corrected for autocorrelation of larval fluxes (though not significant at $p = 0.05$) as well to present a more conservative estimate.

Evaluating Trap Collection Efficiency

Collection efficiency of a sediment trap can change if eddies form within the trap at high Reynolds numbers [24]. Eddies may lead to under- or over-collection of falling particles, including larvae. Current speeds less than 10 cm s⁻¹ are thought not to induce collection bias [5, 17, 24, 56]. Therefore, periods with current speeds greater than 10 cm s⁻¹ were reviewed qualitatively for coincidences with peaks and deficits (> 95% CI) in larval flux. The daily mean and maximum current speeds at 10 mab, near the trap opening, were also cross-correlated with larval flux to determine if temporal variations in larval flux were caused by changes in Reynolds number due to current speed variation.

3.4 Results

3.4.1 Larval Fluxes

Gastropod, bivalve, polychaete, and crustacean larvae were collected over 10 days at East Wall and over 9 days at Choo Choo (Table 3.2). I identified 19 gastropod taxa, 5 polychaete taxa, 1 bivalve taxon, and 1 crustacean taxon (*Bythograea thermydron*) of probable vent origin. Of these, the crustacean and 12 gastropod taxa were unequivocally of vent origin. The bivalve and crustacean taxa were collected in small numbers and thus were not included in subsequent analyses.

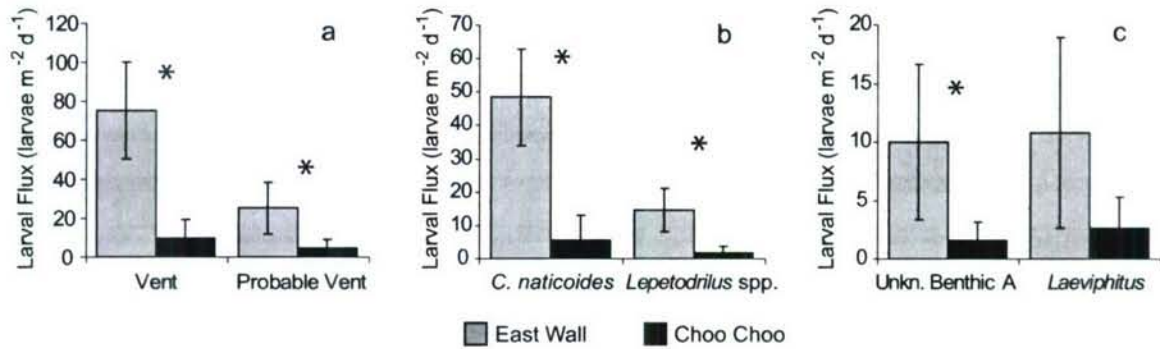


Figure 3-5: Mean daily flux of gastropod larvae at East Wall and Choo Choo for the pooled groups (a), individual vent taxa (b) and individual probable vent taxa (c) for the nine days of concurrent collection. Asterisk: significant differences between sites detected by paired t-tests after Bonferroni correction ($p < 0.05$). Error bars are one standard deviation.

I focused analyses and discussion on gastropod larvae, which were relatively well preserved and abundant in the samples. Some taxa were not identifiable to species but could be assigned to genus or a familial group and thus could be assigned as having a vent, probable vent, or non-vent origin. Taxa considered of probable vent origin had morphological characteristics common to families known to occur at vents. Analyses focused on pooled Vent Gastropods, pooled Probable Vent Gastropods, two vent gastropod taxa, *Cyathermia naticoides* and *Lepetodrilus* spp., and two gastropod taxa of probable vent origin, *Laeviphitus* sp. and Unknown Benthic sp. A, which were relatively abundant.

Spatial and Temporal Variability

All gastropod taxa had greater mean vertical flux at East Wall than at Choo Choo. (Fig 3-5, Table 3.2). Fluxes at East Wall were 2 to 18 times higher than at Choo Choo for individual taxa. Fluxes were significantly greater at East Wall than at Choo Choo ($p < 0.05$) for both pooled groups (Fig 3-5a) and the dominant gastropod taxa (Fig 3-5b, c), except for *Laeviphitus* sp. which was not significant after Bonferroni correction.

Temporal patterns of daily gastropod larval flux differed between East Wall and Choo Choo. East Wall received an uninterrupted, yet variable, flux of larvae (Fig 3-6, 3-7). Daily fluxes varied from the mean, exceeding the 95% CI. Vent gastropod flux at East Wall surpassed the upper 95% CI on days 2, 3 and 7, and fell below the 95% CI on days 5 and 10. Flux of probable vent gastropod larvae exceeded the

Taxa	Origin	East Wall	Choo Choo
GASTROPODA			
<i>Bathymargarites symplector</i>	V	5	3
<i>Clypeosectus delectus</i>	V	2	1
<i>Cyathermia naticoides</i>	V	242	25
<i>Echinopelta fistulosa</i>	V	1	0
<i>Eulepetopsis vitrea</i>	V	12	0
<i>Gorgolettis spiralis</i>	V	11	1
<i>Gorgolettis emarginatus</i>	V	15	2
<i>Laeviphitus</i> sp.	PV	54	12
<i>Lepetodrilus</i> spp.	V	73	9
<i>Neomphalus fretterae</i>	V	4	0
<i>Pachydermia laevis</i>	V	2	0
Peltospirid 240 μ m	V	5	1
Peltospirid 215 μ m	V	2	1
<i>Planorbidella planispira</i> (Unkn W)	V	1	0
Unknown Benthic sp. A	PV	50	7
Unknown slit limpet	PV	2	1
Unknown neomphalid 5	PV	18	1
Unknown neomphalid 290 μ m	PV	1	0
Vent Gastropods		375	43
Probable Vent Gastropods		126	21
POLYCHAETA			
<i>Ophryotrocha</i>	PV	28	1
chaetosphaera	?	24	1
polynoid	?	2	0
nectochaete larvae	?	1	1
unknown polychaetes	?	9	3
CRUSTACEA			
megalopae	PV	2	2

Table 3.2: Total number of larvae of benthic species collected over 10 days at East Wall and 9 days at Choo Choo on the East Pacific Rise. V: species endemic to vents; PV: probable vent species; ?: not determined or unknown.

upper 95% CI only on day 7 and fell below the 95% CI on days 1 and 2. Individual taxa generally followed the same patterns as the groups to which they were assigned (Fig 3-7). *Cyathermia naticoides*, *Lepetodrilus spp.* and Unknown Benthic sp. A had larval fluxes higher than the 95% CI on day 3 at East Wall. *Cyathermia naticoides* also had higher flux on days 2 and 7 at East Wall. *Lepetodrilus spp.* had high flux on days 2, 6 and 7. *Laeviphitus sp.* flux peaked only on day 7. On the other hand, Choo Choo received comparatively low larval flux with only one episode of elevated larval flux (Fig 3-8, 3-9). Vent gastropod flux at Choo Choo deviated from the 95% CI only on day 3, with a peak in larval flux ($34 \text{ larvae } m^{-2}d^{-1}$) coincident with the peak at East Wall (Fig 3-8). Fluxes of *C. naticoides*, *Lepetodrilus spp.*, Unknown Benthic sp. A, and *Laeviphitus sp.* also exceeded the 95% CI only on day 3 (Fig 3-9). Flux of *Lepetodrilus spp.*, Unknown Benthic sp. A and *Laeviphitus sp.* was intermittent with few or no larvae collected many days.

3.4.2 Currents

Current velocities at both sites and both heights generally trended north-northwest, nearly aligned along the ridge axis (Fig 3-3). Near-bottom currents at East Wall were an exception, and trended approximately due north (heading 002°) rather than along the general strike of the axis (heading 352°) (Fig 3-3), possibly due to local topographic steering. Diurnal and semidiurnal tides were the dominant frequencies (analyses not shown). Tidal currents were aligned cross-axis (east-west) as shown by M2 tidal ellipses (Fig 3-4). Tidally-driven cross-axis current velocities were apparent in the 170 mab current records (Fig 3-4) but were less pronounced near bottom. Some of the along-axis current reversals observed at 170 mab were also less pronounced or not observed at 10 mab (Fig 3-4).

Along-axis and cross-axis current velocities were significantly correlated ($p < 0.001$) between heights at a site and at the same height between sites (Table 3.1), but the correlation between heights was lower near bottom where the currents were likely influenced by bottom friction and the topography of the AST. The correlation between the heights was higher at Choo Choo than at East Wall possibly because the AST was shallower at Choo Choo.

Current speeds varied with height above bottom and between sites. Mean current speeds were 5.20 cm s^{-1} (max 14.4 cm s^{-1}) at 170 mab and 3.93 cm s^{-1} (max 9.7 cm s^{-1}) at 10 mab at East Wall. Mean current speeds were 6.41 cm s^{-1} (max 11.4 cm s^{-1}) at 170 mab at Choo Choo.

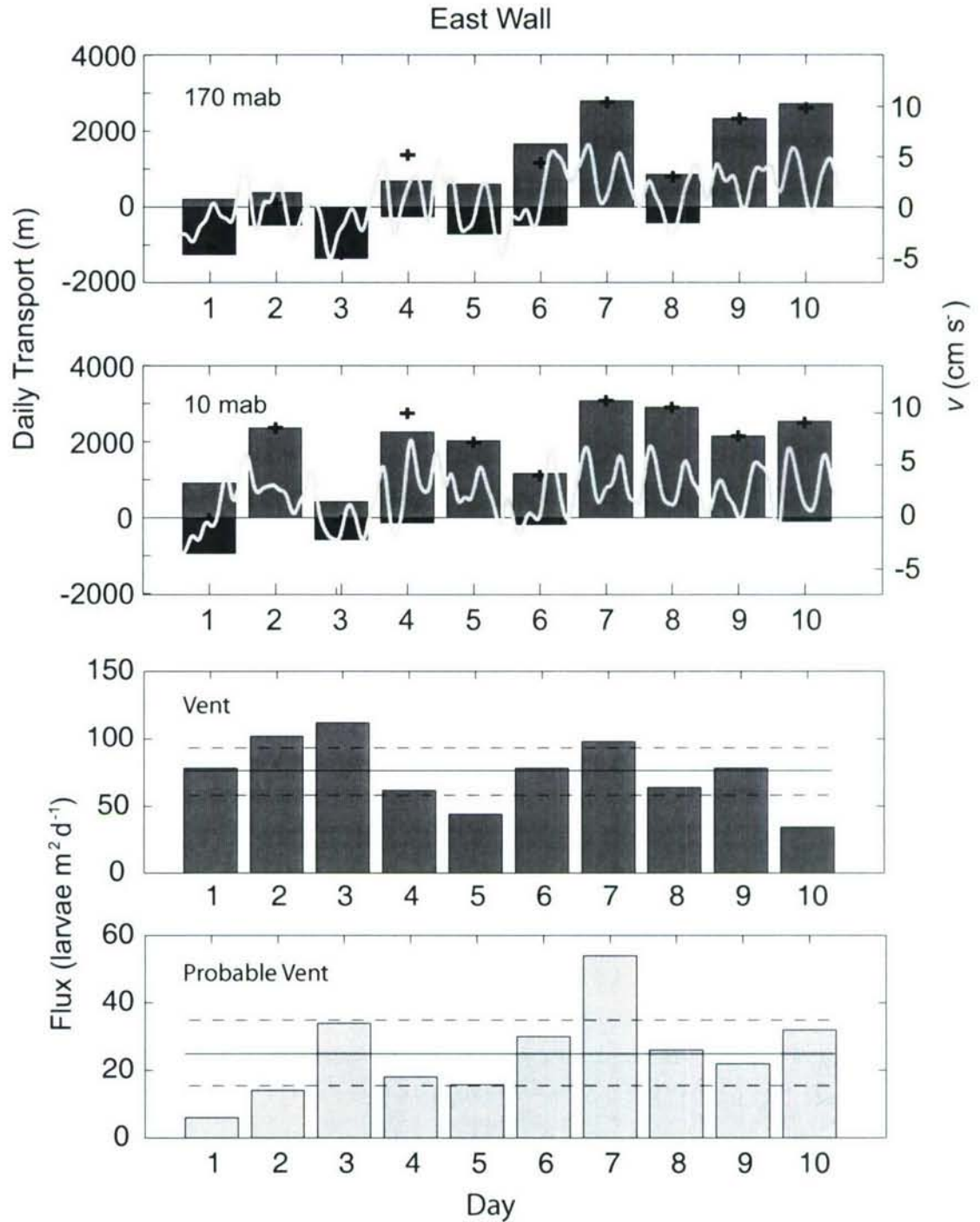


Figure 3-6: Along-axis current velocities and transport compared to flux of gastropod larvae at East Wall. Bars in the top two panels denote the northward (medium gray) and southward (dark gray) transport over each 24 h period of larval collection. Crosses denote the daily net along-axis transport. The light gray line is the smoothed along-axis (v) current velocity (low-pass filtered 6 h); tidal variation was preserved. Fluxes of Pooled Vent and Probable Vent gastropod larvae at East Wall are presented with a solid line denoting mean flux and dashed lines denoting the 95% confidence interval.

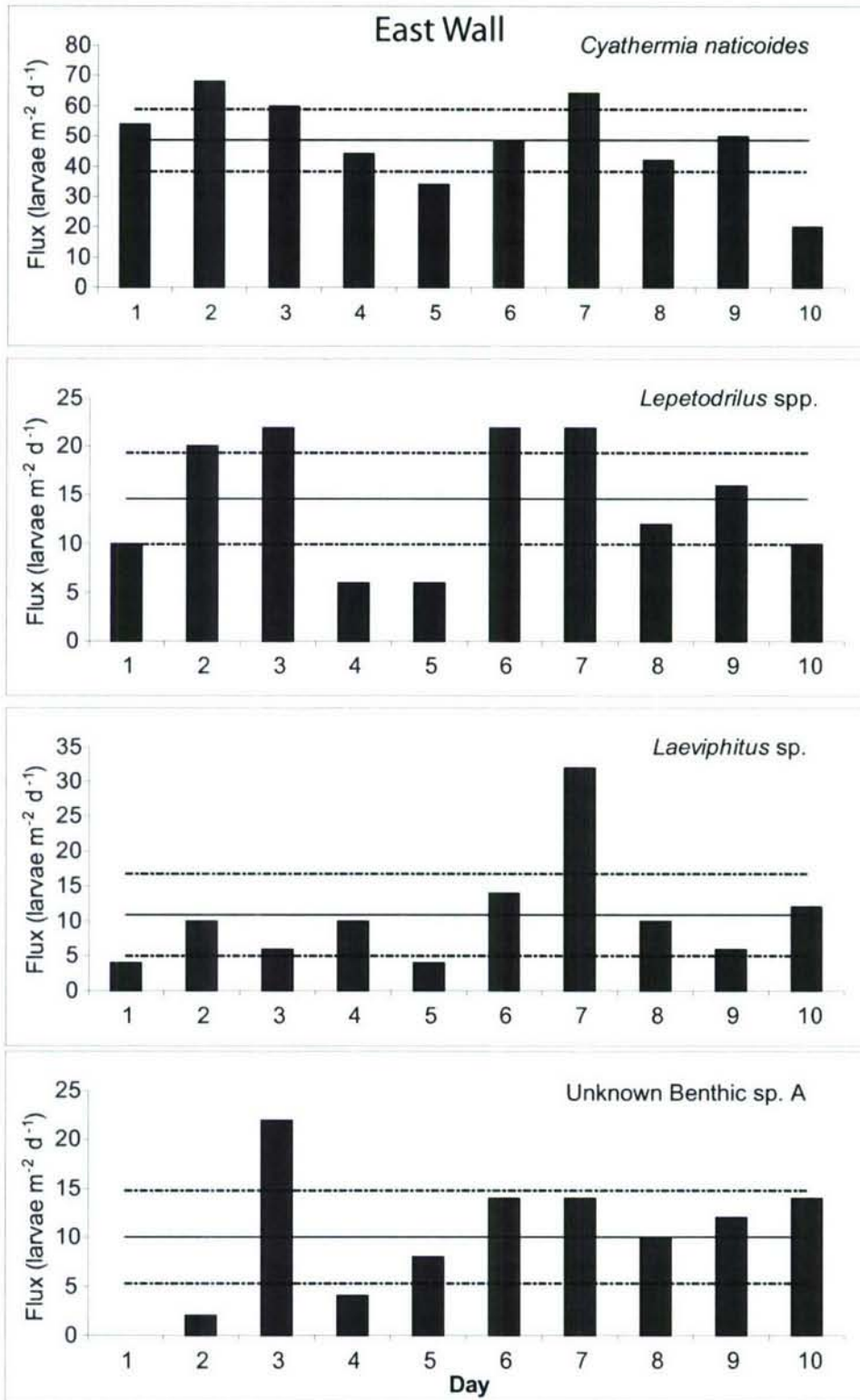


Figure 3-7: Daily larval flux of vent, *C. naticoides* and *Lepetodrilus* spp., and probable vent gastropod taxa, *Laeviphitus* sp. and Unknown Benthic sp. A, at East Wall. The solid line denotes the mean flux and dashed lines denote the 95% confidence interval.

East Wall			
170 mab	Net Transport	North Transport	South Transport
Pooled Vent	-0.293	-0.252	0.349
Pooled Probable Vent	0.550	0.628	-0.396
<i>Cyathermia naticoides</i>	-0.279	-0.282	0.282
<i>Lepetodrilus</i> spp.	0.060	0.183	0.282
<i>Laeviphitus</i> sp.	0.628	0.634	-0.534
Unknown Benthic sp. A	0.207	0.360	-0.040

10 mab	Net Transport	North Transport	South Transport
Pooled Vent	-0.356	-0.341	0.266
Pooled Probable Vent	0.313	0.317	-0.334
<i>Cyathermia naticoides</i>	-0.228	-0.197	0.201
<i>Lepetodrilus</i> spp.	-0.197	-0.193	-0.022
<i>Laeviphitus</i> sp.	0.495	0.524	-0.368
Unknown Benthic sp. A	-0.130	-0.177	-0.114

Table 3.3: Correlation between daily advective transport and larval fluxes at East Wall. Pearson correlation coefficients are shown comparing measured larval flux and predicted along-axis advective transport during 24-hour periods at East Wall. Larval values were from pooled groups and individual taxa; transport was calculated as net, northward, and southward advection at heights of 10 and 170 m above bottom. **Bold** indicates significance at the $p < 0.05$ level after correction for autocorrelation.

s^{-1}) at 170 mab and 4.31 cm s^{-1} (max 18.2 cm s^{-1}) at 10 mab at Choo Choo.

3.4.3 Larval Flux and Hydrodynamics

Larval Supply

Daily along-axis transport during the study was sufficient to advect particles, including larvae, between the vent sites in the $9^{\circ} 50'$ area. Mean net transport at both sites was 1.4 and 1.9 kilometers per day at 10 mab and 170 mab, respectively. Advective transport to the north was greater and more frequent than transport to the south (Figs 3-3, 3-6 and 3-8).

Flux of gastropod larvae at East Wall was not significantly correlated at the $p < 0.05$ level with advective transport at either height (Table 3.3). Pearson correlation coefficients for both groups and all taxa analyzed were generally low ($r < 0.5$). The only relationship was the positive association of the Probable Vent group (not significant, $p > 0.05$) and *Laeviphitus* sp. ($p < 0.05$) with northward along-axis transport at 170 mab.

Flux of gastropod larvae was significantly correlated with along-axis southward transport at Choo Choo at the $p < 0.05$ level (Table 3.4). Pooled Vent gastropods, Probable Vent gastropods, and *Cyathermia naticoides* were significantly correlated with southward transport at 10 mab and at 170 mab ($p < 0.05$). Analyses for *Lepetodrilus* spp., Unknown Benthic sp.A and *Laeviphitus* sp. were not performed due to the low magnitude of larval flux for most days. Both the Vent and Probable Vent groups and *C. naticoides* showed the same trends of negative correlation with net along-axis transport (where positive was northward) and with northward transport, and positive correlation with southward transport. A qualitative comparison (Fig 3-8) of along-axis flow to pooled larval fluxes shows the peak flux of both Vent and Probable Vent larvae occurred on day 3 when currents were predominantly southward at 10 mab and 170 mab.

Trap Collection Efficiency

If trapping efficiency changed with current velocity, then one might expect to see a correlation between larval flux and current speed. Speeds directly above the trap openings did not exceed 10 cm s^{-1} at East Wall and rarely exceeded 10 cm s^{-1} at Choo Choo (only seven 10-minute intervals). These high-speed intervals occurred at Choo

Choo on days 3, 4, and 5, during periods of relatively high and low larval flux. Higher current speeds could have been due to the shorter recording interval at Choo Choo (averaged over 10 min) compared to East Wall (averaged over 30 min). However, when the Choo Choo record was averaged over 30 min intervals, speeds still peaked on days 3, 4, and 5 at greater than 9.5 cm s^{-1} . Only one instance of currents greater than 9.0 cm s^{-1} occurred at East Wall, on day 4 when larval supply was within the 95% CI. Additionally, observed daily larval flux was not correlated with both mean and maximum current speed during each 24 hour collection at 10 mab ($p > 0.5$) (Table 3.5). Therefore, I conclude that observed spatial and temporal variability in larval flux reflected changes in larval supply to the vents, and not changes in collection efficiency of the traps caused by hydrodynamic bias.

3.5 Discussion

3.5.1 Transport from a Larval Source

Variations in larval flux conformed to predictions based on advective transport from a realistic distribution of discrete sources, because East Wall and Choo Choo differed in their proximity to local sources and in larval supply. Variation in vent gastropod larval flux at East Wall did not correlate with along-axis transport at either height and thus did not appear to result from immigration from a single larval source. Instead, East Wall and/or multiple sources to the north and south may have contributed to an uninterrupted flux of larvae, independent of the currents. Multiple sources were likely to have contributed to the larval flux at East Wall given the close proximity of numerous vent communities during the study (Fig 3-1). The positive correlation between gastropod larval flux and southward transport at Choo Choo was consistent with a larval source north of the vent site. Again, this result is consistent with the distribution of vent communities: many vents to the north within 1 km of Choo Choo and few vents to the south of Choo Choo that were further away ($> 4.5 \text{ km}$). It seems that advection of vent larvae between irregularly spaced sources created spatial variability in larval flux between two vent communities less than 1 km apart.

Diffusion, cross-axis advection, and topographic barriers could have contributed to the decreased abundance of larvae transported over larger distances. Assuming lateral homogeneity of flow, northward advection over a couple of days (for example days 7 & 8 at 170 mab or any three of days 4 to 10 at 10 mab) would have been

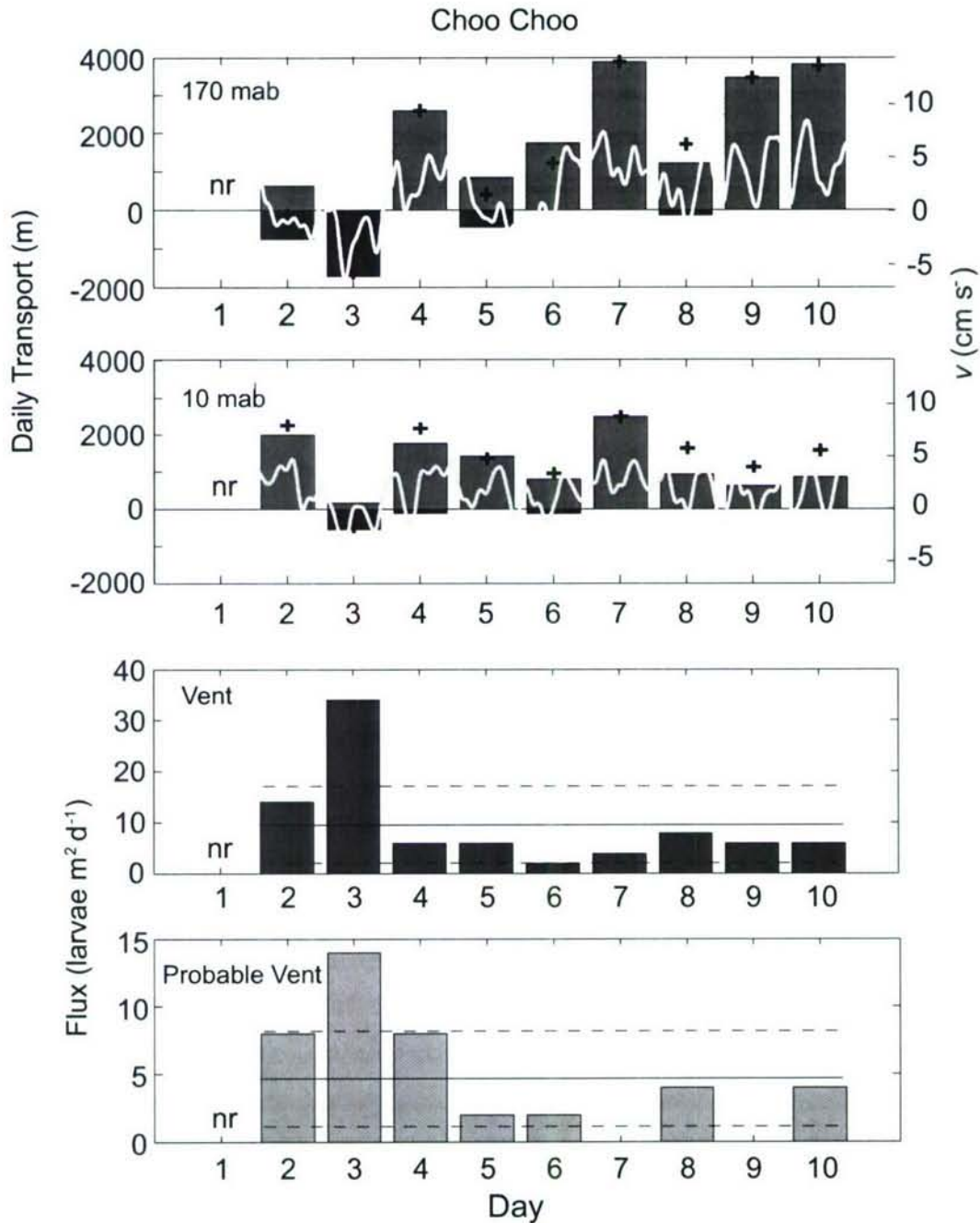


Figure 3-8: Along-axis current velocities and transport compared to flux of gastropod larvae at Choo Choo. Bars in the top two panels denote the northward (medium gray) and southward (dark gray) transport over each 24 h period of larval collection. Crosses denote the daily net along-axis transport. Light gray line is the smoothed along-axis (v) current velocity (low-pass filtered 6 h); tidal variation was still evident. Fluxes of pooled vent and probable vent gastropod larvae at Choo Choo are presented with a solid line denoting mean flux and dashed lines denoting the 95% confidence interval. Larval flux and transport was not recorded (nr) on day 1.

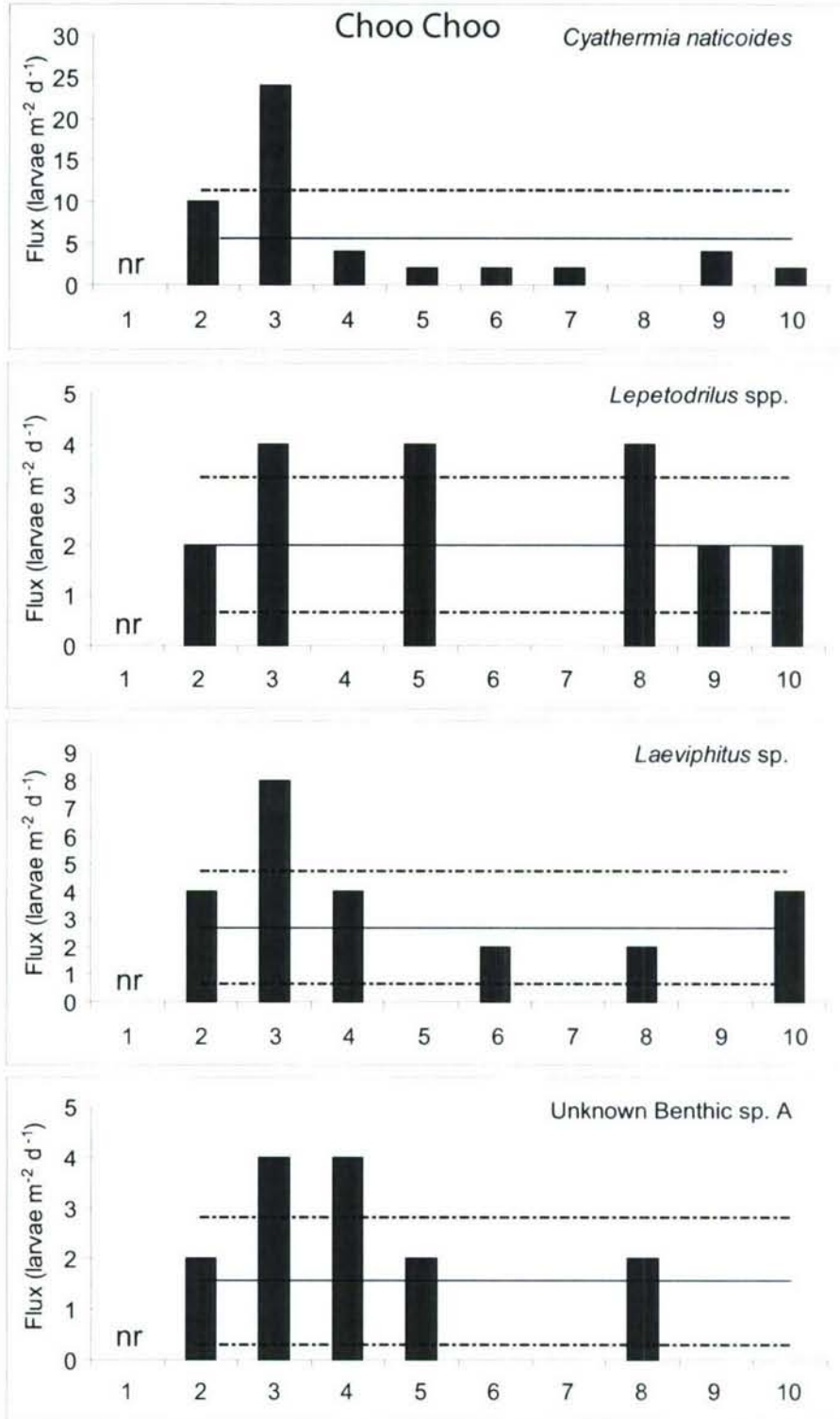


Figure 3-9: Daily larval flux of vent, *C. naticoides* and *Lepetodrilus* spp., and probable vent gastropod taxa, *Laeviphitus* sp. and Unknown Benthic sp. A, at Choo Choo. The solid line denotes the mean flux and dashed lines denote the 95% confidence interval. Larval flux and transport was not recorded (nr) on day 1.

Choo Choo			
170 mab	Net Transport	North Transport	South Transport
Pooled Vent	-0.739	-0.631	0.962
Pooled Probable Vent	-0.700	-0.628	0.811
<i>Cyathernia naticoides</i>	-0.721	-0.571	0.941

10 mab			
	Net Transport	North Transport	South Transport
Pooled Vent	-0.678	-0.432	0.863
Pooled Probable Vent	-0.451	-0.278	0.785
<i>Cyathernia naticoides</i>	-0.665	-0.378	0.884

Table 3.4: Correlation between daily advective transport and larval fluxes at Choo Choo. Pearson correlation coefficients are shown comparing measured larval flux and predicted along-axis advective transport during 24-hour periods at Choo Choo. Larval values were from pooled groups and *Cyathernia naticoides*; transport was calculated as net, northward, and southward advection at heights of 10 and 170 m above bottom. **Bold** indicates significance at the $p < 0.05$ level after correction for autocorrelation.

sufficient to transport larvae from V Vent to Choo Choo. The very low larval flux, < 10 larvae $\text{m}^{-2} \text{d}^{-1}$ during northward flows, suggests that larvae from a southern source did not reach Choo Choo, at least not in high abundances, during the study period. The well-defined AST near East Wall may have facilitated transport between vents by providing a connecting conduit, whereas larvae may have been more easily lost due to diffusion and cross-axis transport south of Choo Choo where the AST was discontinuous and shallower. Topographic breaks in the AST may have directly impeded transport from V Vent to Choo Choo. Any retention mechanisms would also reduce long-distance transport of larvae. Separation by a few kilometers (< 10 km) appears to substantially reduce larval exchange between vent sites, such that larval flux was primarily from neighboring vent communities (within ~ 1 -2 km). This does not preclude occasional exchange of a few individuals that could maintain high gene flow. Based on these observations, larval flux would be intermittent and correlated with along-axis currents at sites isolated from other communities by as little as 5 km, whereas sites within the center of a vent cluster would receive uninterrupted larval flux.

Larval settlement behavior also could account for the spatial variability in larval flux. East Wall was a more expansive and active vent community than Choo Choo.

	East Wall		Choo Choo	
	Mean	Maximum	Mean	Maximum
Pooled Vent	-0.445	0.039	0.366	0.424
Pooled Probable Vent	0.248	0.114	0.573	0.433
<i>Cyathermia naticoides</i>	-0.347	0.188	0.310	0.371
<i>Lepetodrilus</i> spp.	-0.466	-0.049	0.099	0.250
<i>Laeviphitus</i> sp.	0.374	0.522	0.407	0.320
Unknown Benthic sp. A	-0.187	-0.429	0.731	0.624

Table 3.5: Correlation between larval flux and current speeds. Pearson correlation coefficients comparing larval flux and current speeds during 24-hour periods at East Wall and Choo Choo. Larval values are presented as pooled groups and individual taxa; speeds are presented as means and maxima at heights of 10 and 170 m above bottom. Correlations were not significant at the $p < 0.05$ level after correction for autocorrelation.

Therefore, East Wall was more likely than Choo Choo to have possible settlement cues [38] such as redox potential, chemical constituents, or conspecifics. Larvae responding to these cues would thus preferentially settle out of the plankton at and near East Wall, resulting in higher larval flux. However, behavioral responses to settlement cues were not likely to be the primary process driving variation in larval flux because chemical cues are greatly diluted within the water column at the sediment trap height and distance from main vent site ([52], Luther pers. comm.).

Spatial variation in larval production also could have contributed to the observed spatial variation in larval fluxes. Since East Wall and its neighbors had a larger total population of metazoans than the isolated Choo Choo site, more larvae could have been produced and thus collected at or near East Wall. It is possible that an abrupt spawning event at Choo Choo caused the 1-day peak in larval flux recorded there. Given a lack of reproductive data and the significant correlation between southward transport and larval flux, I propose that advection of larvae from nearby sources is a more plausible explanation for the temporal variability of larval flux observed at Choo Choo.

3.5.2 Implications for Larval Sampling

Larval flux into sediment traps is potentially a useful proxy for measuring larval supply to the benthos [30, 57]. While the correlation between measured vertical larval flux and the actual larval supply remains unknown, the results of this study show that this is a reasonable and feasible proxy for studying changes in larval supply and

a valuable tool for obtaining continuous time-series in the deep-sea. However, analysis of sediment trap collections should carefully consider the biases associated with larval collection. While there was no evidence for changes in trapping efficiency in the current study, current velocities in other locations and environments may induce changes in trapping efficiency over time and the bias should always be tested if possible. Sediment traps also bias particles of different sizes and weights. Larvae with slower fall velocities (small larvae or positive and/or neutrally buoyant larvae), may be under-collected relative to larvae with faster fall velocities (larger, sinking or downward swimming larvae) ([5], reviewed in [24]). Therefore, sediment trap collections of larvae do not represent absolute abundance and the bias will differ between species. Bias based on particle fall velocity should not affect temporal or spatial comparisons of changes in relative abundance of a single species or a defined species group. Additionally, patterns of relative temporal or spatial change of different taxa can be compared, for example at East Wall Unknown Benthic sp. A peaked in abundance on day 3 while *Laeviphitus* sp. peaked in abundance on day 7. Other sampling methods should be used for quantification of abundance and for comparison of abundances of different species. However, observations of surprisingly high daily variation in larval supply compared to seasonal and annual variability in previous ‘snap-shot’ (e.g. pumps and nets [23, 33]) samples suggests that discontinuous ‘snap-shot’ samples may not be a good indicator of longer-term means and patterns.

3.5.3 Ecological Implications of Variable Supply

The inferred spatial and temporal variability in larval flux has important implications for community maintenance and succession, if it indeed represents larval supply to the benthos. Habitable space for vent endemic species is restricted to areas with a suitable mix of hydrothermal fluid and seawater [8, 15, 25, 44]. Space is a limited resource for which organisms may compete and on which organisms interact. If larval supply is consistently high at East Wall, benthic interactions such as competition may be strong [29, 28, 42, 53]. Initial settlers of mobile species, including vent gastropods, have been shown to inhibit subsequent colonization through interference and competition [34]. In areas like East Wall where larval supply was high and continuous, direct and indirect competition for space are likely to affect recruits and shape the community. The first species to successfully recruit could become the dominant species through facilitation of conspecifics and interference with the successful recruitment of other

species. The dominant macrofauna may be different at individual vents based on the “lottery winners” and may be an alternative explanation for the observations of dominance by different macrofaunal species in mussel communities [10]. In contrast, relatively low larval supply to Choo Choo and other isolated vent communities may decrease the strength of benthic interactions during initial colonization due to lower densities of organisms. Larval supply and settlement may have a greater influence on shaping the initial community structure at Choo Choo than post-settlement processes.

3.6 Supplemental Material

3.6.1 Correction for Autocorrelation

While the time-series did not show any significant autocorrelation, one would expect that current velocities would be autocorrelated (non-random). Therefore, the variance of the sample cross-correlation function must be corrected to account for autocorrelation. The variance of two independent time-series, X and Y , with no autocorrelation and length n is given as

$$\text{Var}\hat{\rho}_{XY}(h) = \frac{1}{n} \sum_{h=-\infty}^{\infty} \rho_X(h)\rho_Y(h) \quad (3.1)$$

in terms of the autocorrelation functions ρ_X of each series at a given lag, h [4].

To correct for autocorrelation or serial dependence, I assume that the time-series follows a first order autoregressive model,

$$X_t - \mu_X = \beta(X_{t-1} - \mu_X) + \epsilon_t, \quad (3.2)$$

where μ_X is the mean of X , β is the autoregressive parameter at lag 1 that, for stationarity, must lie between -1 and 1, and ϵ is the error with mean 0 and variance σ^2 . While the first order autoregressive model may not fit the data perfectly, it is a good approximation (Fig 3.6.1) and a simple method for correcting for autocorrelation. The autocorrelation function ρ_X for the first order autoregressive model is

$$\rho_X(h) = \beta^{|h|}. \quad (3.3)$$

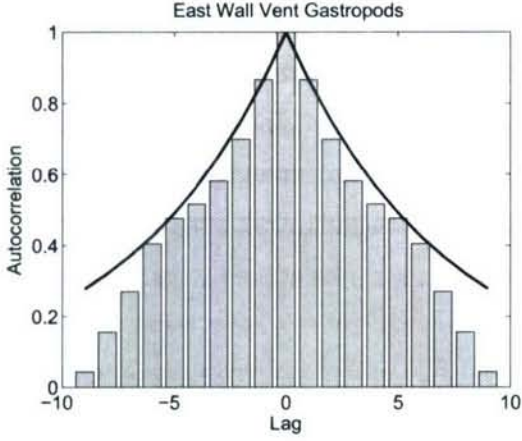


Figure 3-10: Autocorrelation of East Wall pooled vent gastropods (bars) are presented in comparison to the predicted autocorrelation (line) at each lag based on the autocorrelation function (Eq. 3.3) of the first order autoregressive model.

Through substitution of Eq. 3.3 into Eq. 3.1,

$$\text{Var} \hat{\rho}_{XY}(h) = \frac{1}{n} \sum_{h=-\infty}^{\infty} \beta^{|h|} \gamma^{|h|} \quad (3.4)$$

where γ is the autoregressive parameter for series Y. Since the autoregressive parameters are symmetrical around zero, such that $h = -1 = 1$, and by definition $\rho_x(0) = 1$, the equation simplifies as follows

$$\text{Var} \hat{\rho}_{XY}(h) = \frac{1}{n} (1 + 2 \sum_{h=1}^{\infty} (\beta\gamma)^{|h|}). \quad (3.5)$$

Eq. 3.5 includes the expansion of the geometric series

$$\frac{x_m}{1-x} = \sum_{n=m}^{\infty} x^n \quad (3.6)$$

where, $x = \beta\gamma$; and satisfies the condition $|x| < 1$, since β and γ must lie between -1 and 1. Replacement with the geometric series yields

$$\text{Var} \hat{\rho}_{XY}(h) = \frac{1}{n} (1 + 2 \frac{\beta\gamma}{1 - \beta\gamma}). \quad (3.7)$$

Sample cross-correlation can then be compared to this estimate of variance, which is estimated using the lag 1 autoregressive parameter of each time-series and the length of the time-series. At the 0.05 significance level, the sample cross-correlation is significant if greater than $2\sqrt{|\text{Var} \hat{\rho}_{XY}(h)|}$.

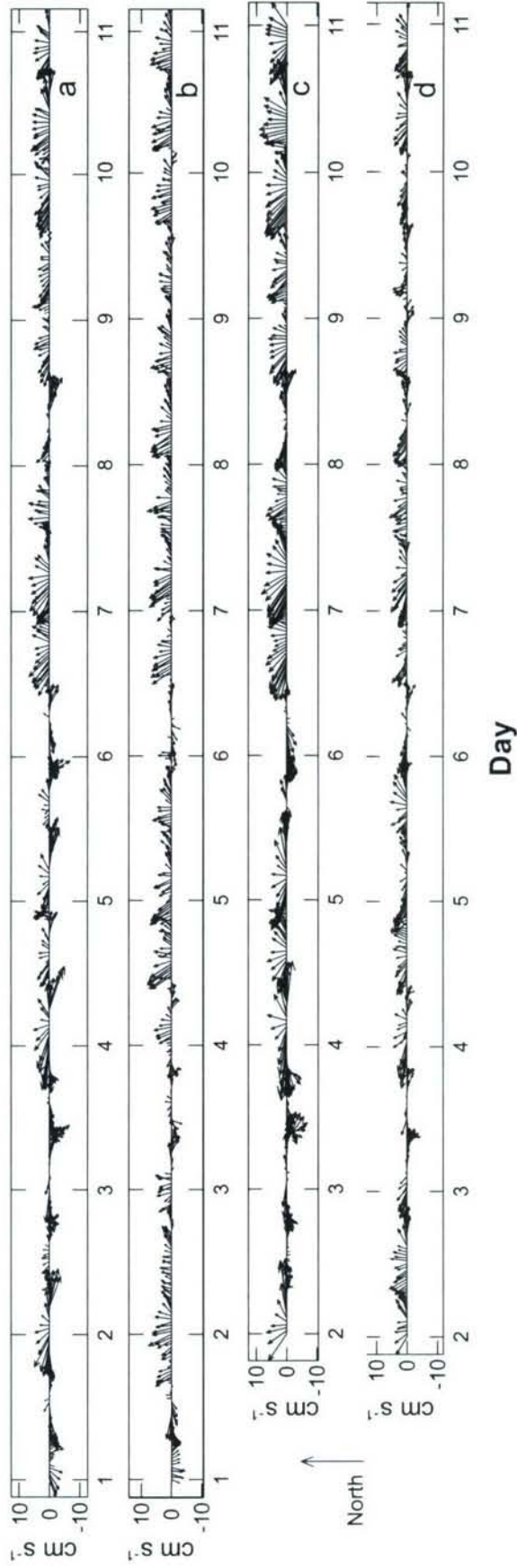


Figure 3-11: Current velocities from the 10-day time-series at East Wall at 170 mab (a) and at 10 mab (b) and from the 9-day time-series at Choo Choo at 170 mab (c) and at 10 mab (d). Current velocities are oriented along the ridge axis.

Bibliography

- [1] C.A. Alessi, R.C. Beardsley, R. Limeburner, L.K. Rosenfeld, S. J. Lentz, E. Send, C.D. Winant, J.S. Allen, G.R. Halliwell, W.S. Brown, and J.D. Irish. CODE-2: moored array and large-scale data report. Technical Report WHOI 85-35, Woods Hole Oceanographic Institution, 1985.
- [2] E. T. Baker, R. A. Feely, M. J. Mottl, F. T. Sansone, C. G. Wheat, J. A. Resing, and J. E. Lupton. Hydrothermal plumes along the east pacific rise, 8 degree 40' to 11 degree 50'n: Plume distribution and relationship to the apparent magmatic budget. *Earth and Planetary Science Letters*, 128(1-2):1–17, 1994.
- [3] M. D. Bertness, S. D. Gaines, and R. A. Wahle. Wind driven settlement patterns in the acorn barnacle *Semibalanus balanoides*. *Marine Ecology Progress Series*, 137:103–110, 1996.
- [4] P.J. Brockwell and R.A. Davis. Time Series: Theory and Methods. In *Springer Series in Statistics*, pages 400–402. Springer-Verlag, 1987.
- [5] C. A. Butman. Sediment-trap experiments on the importance of hydrodynamical processes in distributing settling invertebrate larvae in near-bottom waters. *Journal of Experimental Marine Biology and Ecology*, 134(1):37–88, 1989.
- [6] P. Chevaldonné, D. Jollivet, A. Vangriesheim, and D. Desbruyeres. Hydrothermal-vent alvinellid polychaete dispersal in the Eastern Pacific. 1. Influence of vent site distribution, bottom currents, and biological patterns. *Limnology and Oceanography*, 42(1):67–80, 1997.
- [7] C. Craddock, W. R. Hoeh, R. A. Lutz, and R. C. Vrijenhoek. Extensive gene flow among mytilid (*Bathymodiolus thermophilus*) populations from hydrothermal vents of the eastern Pacific. *Marine Biology*, 124(1):137–146, 1995. Bibliogr.: 72 ref. English.
- [8] E. Dahlhoff, J. O'Brien, G. N. Somero, and R. D. Vetter. Temperature effects on mitochondria from hydrothermal vent invertebrates: Evidence for adaptation to elevated and variable habitat temperatures. *Physiological Zoology*, 64(6):1490–1508, 1991.
- [9] C. DiBacco, D. Sutton, and L. McConnico. Vertical migration behavior and horizontal distribution of brachyuran larvae in a low-inflow estuary: Implications for bay-ocean exchange. *Marine Ecology Progress Series*, 217:191–206, 2001.
- [10] J. Dreyer, K.E. Knick, W.B. Flickinger, and C.L. Van Dover. Development of macrofaunal community structure in mussel beds on the northern East Pacific Rise. *Marine Ecology Progress Series*, 302:121–134, 2005.
- [11] C. E. Epifanio. Transport of blue crab (*Callinectes sapidus*) larvae in the waters off Mid-Atlantic states. *Bulletin of Marine Science*, 57(3):713–725, 1995. Conference Blue Crab Recruitment Symp., Hilton Head, SC (USA), 16 Nov 1993.

- [12] L. L. Etherington and D. B. Eggleston. Large-scale blue crab recruitment: Linking postlarval transport, post-settlement planktonic dispersal, and multiple nursery habitats. *Marine Ecology Progress Series*, 204:179–198, 2000.
- [13] DJ Fornari and RW Embley. Tectonic and volcanic controls on hydrothermal processes at the mid-ocean ridge: an overview based on near-bottom and submersible studies. *Geophysical Monographs*, 91:1–46, 1995.
- [14] S. Gaines, S. Brown, and J. Roughgarden. Spatial variation in larval concentrations as a cause of spatial variation in settlement for the barnacle, *Balanus Glandula*. *Oecologia*, 67(2):267–272, 1985.
- [15] B. Govenar, N. Le Bris, S. Gollner, J. Glanville, A. B. Aperghis, S. Hourdez, and C. R. Fisher. Epifaunal community structure associated with *Riftia pachyptila* aggregations in chemically different hydrothermal vent habitats. *Marine Ecology Progress Series*, 305:67–77, 2005.
- [16] R. M. Haymon, D. J. Fornari, M. H. Edwards, S. Carbotte, D. Wright, and K. C. Macdonald. Hydrothermal vent distribution along the East Pacific Rise crest (9°–54' n) and its relationship to magmatic and tectonic processes on fast-spreading midocean ridges. *Earth and Planetary Science Letters*, 104(2-4):513–534, 1991.
- [17] S. Honjo and K.W. Doherty. Large aperture time-series sediment traps; design objectives, construction and application. *Deep Sea Research*, 35(1):133–149, 1988.
- [18] M.M. Hunt, M.M. William, A.M. Donald, R.P. Kenneth, K.S. Woolcott, and R.C. Spindell. An acoustic navigation system. Technical Report WHOI-74-6, Woods Hole Oceanographic Institution, 1974.
- [19] L. A. Hurtado, R. A. Lutz, and R. C. Vrijenhoek. Distinct patterns of genetic differentiation among annelids of eastern Pacific hydrothermal vents. *Molecular Ecology*, 13(9):2603–2615, 2004.
- [20] Z. Jager. Selective tidal stream transport of flounder larvae (*Platichthys flesus* L.) in the dollard (ems estuary). *Estuarine Coastal and Shelf Science*, 49(3):347–362, 1999.
- [21] S. A. Karl, S. Schutz, D. Desbruyeres, R. Lutz, and R. C. Vrijenhoek. Molecular analysis of gene flow in the hydrothermal vent clam (*Calypptogena magnifica*). *Molecular Marine Biology and Biotechnology*, 5(3):193–202, 1996.
- [22] A. Khripounoff, T. Comtet, A. Vangriesheim, and P. Crassous. Near-bottom biological and mineral particle flux in the Lucky Strike hydrothermal vent area (Mid-Atlantic Ridge). *Journal of Marine Systems*, 2:101–118, 2000.
- [23] S. L. Kim and L. S. Mullineaux. Distribution and near-bottom transport of larvae and other plankton at hydrothermal vents. *Deep Sea Research*, 45:1–3, 1998.

- [24] G Knauer and V Asper. Sediment trap technology and sampling. Technical Report 10, U.S. GOFS, August 1989.
- [25] G.W. Luther, T.F. Rozan, M. Taillefert, D.B. Nuzzio, C. Di Meo, T.M. Shank, R.A. Lutz, and S.C. Cary. Chemical speciation drives hydrothermal vent ecology. *Nature*, 410(6830):813–816, 2001.
- [26] R. A. Lutz, P. Bouchet, D. Jablonski, R. D. Turner, and A. Warén. Larval ecology of mollusks at deep-sea hydrothermal vents. *American Malacological Bulletin*, 4(1):49–54, 1986. Conference International Symposium on the Ecology of Larval Molluscs.
- [27] A.G. Marsh, L. S. Mullineaux, C. M. Young, and D. T. Manahan. Larval dispersal potential of the tubeworm *Riftia pachyptila* at deep-sea hydrothermal vents. *Nature*, 411:77–80, 2001.
- [28] B. A. Menge. Recruitment vs. postrecruitment processes as determinants of barnacle population abundance. *Ecological Monographs*, 70:265–288, 2000.
- [29] BA Menge. Relative importance of recruitment and other causes of variation in rocky intertidal community structure. *Journal of Experimental Marine Biology and Ecology*, 146:69–100, 1991.
- [30] A. Metaxas. Spatial and temporal patterns in larval supply at hydrothermal vents in the northeast Pacific Ocean. *Limnology and Oceanography*, 49(6):1949–1956, 2004.
- [31] L. S. Mullineaux and S. C. France. Dispersal mechanisms of deep-sea hydrothermal vent fauna. In S. E. Humphris, R.A. Zierenberg, L. S. Mullineaux, and G. Thomson, editors, *Seafloor Hydrothermal Systems: Physical, Chemical, Biological, and Geological Interactions*, pages 408–424. AGU Monographs, 1995.
- [32] L. S. Mullineaux, S. L. Kim, A. Pooley, and R. A. Lutz. Identification of archaeogastropod larvae from a hydrothermal vent community. *Marine Biology*, 124(4):551–560, 1996.
- [33] L. S. Mullineaux, S. W. Mills, A. K. Sweetman, A. H. Beaudreau, A. Metaxas, and H. L. Hunt. Vertical, lateral and temporal structure in larval distributions at hydrothermal vents. *Marine Ecology Progress Series*, 293:1–16, 2005.
- [34] L. S. Mullineaux, C. H. Peterson, F. Micheli, and S.W. Mills. Successional mechanism varies along a gradient in hydrothermal fluid flux at deep-sea vents. *Ecological Monographs*, 73(4):523–542, 2003.
- [35] R Pawlowicz, R.C. Beardsley, and S. J. Lentz. Classical tidal harmonic analysis including error estimates in MATLAB using t_tide. *Computers and Geosciences*, 2002.

- [36] J. Pineda. Predictable upwelling and the shoreward transport of planktonic larvae by internal tidal bores. *Science*, 253(5019):548–551, 1991.
- [37] D.C. Reed, D.R. Laur, and A.W. Ebeling. Variation in algal dispersal and recruitment - the importance of episodic events. *Ecological Monographs*, 58:321–335, 1988.
- [38] D. Rittschof, Jr. Forward, R. B., G. Cannon, J. M. Welch, Jr. McClary, M., E. R. Holm, A. S. Clare, S. Conova, L. M. McKelvey, P. Bryan, and C. L. Van Dover. Cues and context: Larval responses to physical and chemical cues. *Biofouling*, 12:31–44, 1998.
- [39] J. M. Rodriguez, E. D. Barton, S. Hernandez-Leon, and J. Aristegui. The influence of mesoscale physical processes on the larval fish community in the Canaries CTZ, in summer. *Progress in Oceanography*, 62:171–188, 2004.
- [40] G. C. Roegner. Transport of molluscan larvae through a shallow estuary. *Journal of Plankton Research*, 22(9):1779–1800, 2000.
- [41] M. Roughan, A. J. Mace, J. L. Largier, S. G. Morgan, J. L. Fisher, and M. L. Carter. Subsurface recirculation and larval retention in the lee of a small headland: A variation on the upwelling shadow theme. *Journal of Geophysical Research. C. Oceans*, 110(C10):doi:10.1029/2005JC002898, 2005.
- [42] J. Roughgarden, S. Gaines, and H. Possingham. Recruitment dynamics in complex life cycles. *Science*, 241(4872):1460–1466, 1988.
- [43] H. Schouten, M. Tivey, D. Fornari, D. R. Yoerger, and A. Bradley. ABE Imagenex microbathymetry for the East Pacific Rise. *Ridge 2000 Events: A Newsletter of Ridge 2000 Program*, 1(1):1, 2003.
- [44] T. M. Shank, D. J. Fornari, K. L. Von Damm, M. D. Lilley, R. M. Haymon, and R. A. Lutz. Temporal and spatial patterns of biological community development at nascent deep-sea hydrothermal vents (9° 50' N, East Pacific Rise). *Deep-Sea Research (Part 2, Topical Studies in Oceanography)*, 45:465–515, 1998.
- [45] A. L. Shanks and L. Brink. Upwelling, downwelling, and cross-shelf transport of bivalve larvae: test of a hypothesis. *Marine Ecology Progress Series*, 302:1–12, 2005.
- [46] A. L. Shanks, A. McCulloch, and J. Miller. Topographically generated fronts, very nearshore oceanography and the distribution of larval invertebrates and holoplankters. *Journal of Plankton Research*, 25(10):1251–1277, 2003.
- [47] S. Sponaugle, R. K. Cowen, A. Shanks, S. G. Morgan, J. M. Leis, J. Pineda, G. W. Boehlert, M. J. Kingsford, K. C. Lindeman, C. Grimes, and J. L. Munro. Predicting self-recruitment in marine populations: Biophysical correlates and mechanisms. *Bulletin of Marine Science*, 70(1):S341–375, 2002.

- [48] S. Sponaugle, T. Lee, V. Kourafalou, and D. Pinkard. Florida current frontal eddies and the settlement of coral reef fishes. *Limnology and Oceanography*, 50(4):1033–1048, 2005.
- [49] G. E. Swaters and L. A. Mysak. Topographically-induced baroclinic eddies near a coastline, with application to the Northeast Pacific. *Journal of Physical Oceanography*, 15(11):1470–1485, 1985.
- [50] R.E. Thomson, S.F. Mihaly, A.B. Rabinovich, R.E. McDuff, S.R. Viers, and F.R. Stahr. Constrained circulation at endeavor ridge facilitates colonization by vent larvae. *Nature*, 424:545–549, 2003.
- [51] M. Tolstoy, J.P. Cowen, E.T. Baker, D.J. Fornari, K.H. Rubin, T.M. Shank, F. Waldhauser, D.R. Bohnenstiel, D.W. Forsyth, R.C. Holmes, B. Love, M.R. Perfit, R.T. Weekly, S.A. Soule, and B. Glazer. A sea-floor spreading event captured by seismometers. *Science*, 314(5807):1920–1922, 2006.
- [52] D.A. Trivett. Effluent from diffuse hydrothermal venting 1. a simple model of plumes from diffuse hydrothermal sources. *Journal of Geophysical Research*, 99(C9):18,403–18,415, 1994.
- [53] A.J. Underwood and M. J. Keough. *Marine Community Ecology*, chapter Supply-Side Ecology: The Nature and Consequences of Variations in Recruitment of Intertidal Organisms, pages 183–200. Sinauer Associates, Inc, Sunderland, 2001.
- [54] R. C. Vrijenhoek, T. M. Shank, and R. Lutz. Gene flow and dispersal in deep-sea hydrothermal vent animals. *Cahier de Biologie Marine*, 39:363:366, 1998.
- [55] Y. Won, C. R. Young, R. A. Lutz, and R. C. Vrijenhoek. Dispersal barriers and isolation among deep-sea mussel populations (Mytilidae: *Bathymodiolus*) from eastern Pacific hydrothermal vents. *Molecular Ecology*, 12(1):169–184, 2003.
- [56] E.F. Yu, R. Francois, M.P. Bacon, S Honjo, A.P. Fler, S.J. Manganini, M.M.R van der Loeff, and V. Ittekkot. Trapping efficiency of bottom-tethered sediment traps estimated from the intercepted fluxes of Th²³⁰ and Pa²³¹. *Deep-Sea Research (Part I, Oceanographic Research Papers)*, 48(3):865–889, 2001.
- [57] P. O. Yund, S. D. Gaines, and M. D. Bertness. Cylindrical tube traps for larval sampling. *Limnology and Oceanography*, 36(6):1167–1177, 1991.

Chapter 4

Larval transport contributes to successful larval dispersal and larval loss

4.1 Introduction

Physical mechanisms involved in larval supply have received much attention over the past decades (e.g. [9, 16]), in part due to the suggestion that larval supply is a major factor in structuring the benthic community [18, 32, 33]. Understanding the processes that control the supply of larvae to benthic communities may provide insights into metapopulation dynamics. Since populations of many marine benthic invertebrates are aligned roughly linearly along the coastline, currents perpendicular to the coast can contribute both to increasing larval supply through delivery and to decreasing larval supply through loss. Episodes of larval supply to subtidal and intertidal populations have been correlated with on-shore transport of larvae in surface slicks generated by internal waves [29, 30], internal tidal bores [25], and wind-generated currents [2, 11, 15]. Off-shore currents can transport larvae away from suitable benthic habitats, for example during upwelling [3, 26]. Variation in along-shore currents also has the potential to impact larval supply by delivering larvae from different larval pools/sources along the coast [28].

Similar processes could be also be important in the deep-sea. Hydrothermal vent communities on the East Pacific Rise (EPR) are aligned approximately linearly along the north-south trending ridge axis (Fig 4-1). Cross-axis flow in either direction (east

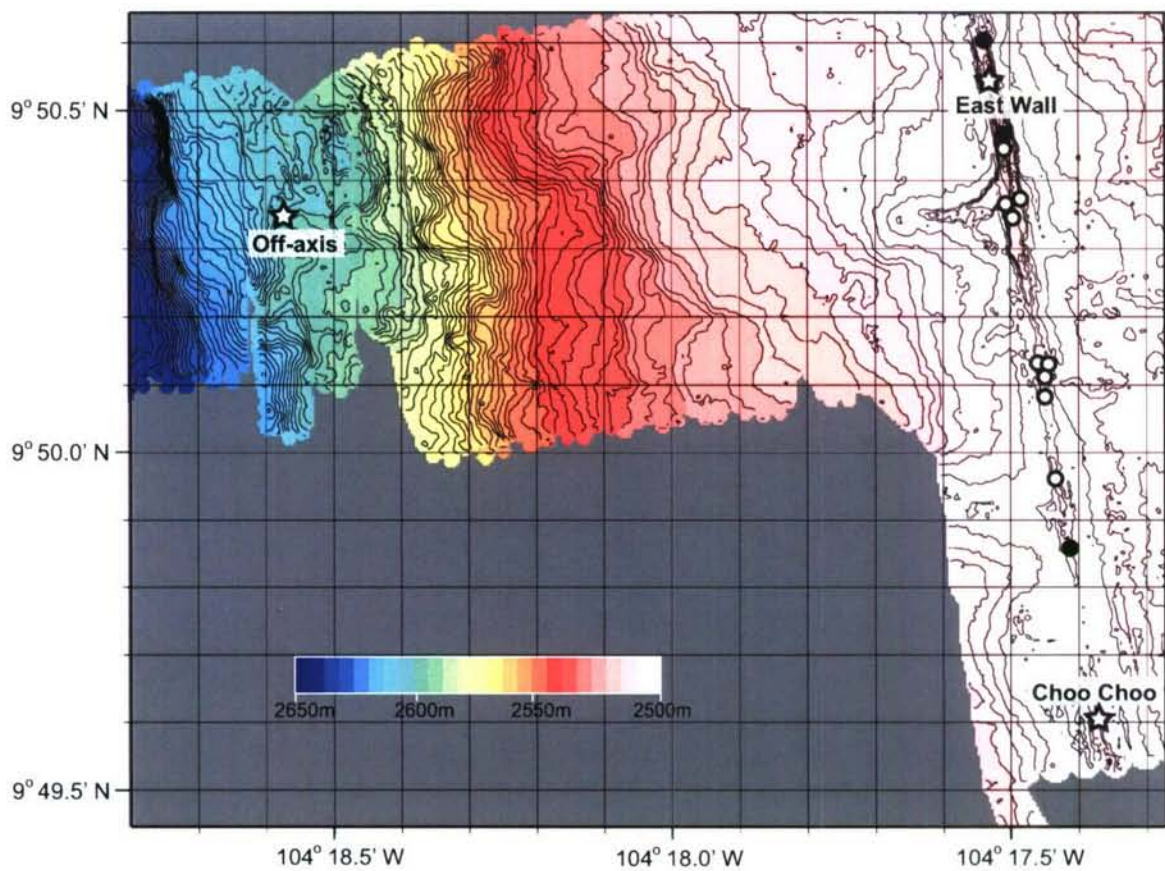


Figure 4-1: The 9° 50' N area of the East Pacific Rise. Mooring sites at East Wall, Choo Choo, and off-axis (stars) and the known vent communities (circles) are identified. The vent communities closest to the collection sites are denoted by solid circles. The closest known vent to the south of Choo Choo is not shown on this map. Contour lines are 2 m; the ridge axis depth near 9° 50' N is 2500 m. Figure adapted from [27].

or west) could transport larvae away from the vent communities on the ridge axis to unsuitable habitat, and thus, contribute to larval loss. Mean near bottom flow in the eastern tropical Pacific is to the west; thus one might expect larval loss primarily to the west of the ridge axis. Such larval losses may not be permanent. Larvae transported off-axis may be transported back on-axis during cross-axis current reversals. If westward current velocities transported larvae off-axis, episodes of eastward current velocities might be expected to transport larvae back onto the ridge.

Advective transport along the axis may also control larval supply to vents. In Chapter 3, there was a strong correlation between along-axis flow and larval supply, but the pattern was driven largely by a single event. One of the goals of the present study is to determine whether this relationship between along-axis flow and larval supply holds true on longer time scales. Based on the results of Chapter 3, I expect that additional observations should show intermittent larval flux correlated with along-axis currents at sites isolated from other communities by as little as 5 km, and uninterrupted larval flux at sites in close proximity (< 1-2 km) to other vents to the north and south.

The role of variation in cross-axis and along-axis currents in the loss and delivery of gastropod larvae to hydrothermal vent communities was investigated using concurrent vertical larval flux collections (as a proxy for larval supply) and current velocity measurements over 5 months, November 2004 - April 2005. The experimental set up was similar to that presented in Chapter 3, however this longer time-series can assess the robustness of the results from the previous chapter and provide an opportunity to investigate the role of cross-axis current velocities, which were weak during November 2004. Specifically, I assess whether cross-axis currents contribute to the loss of larvae from the ridge axis and also whether they contribute to the delivery of larvae back to vents along the ridge axis.

4.2 Methods

4.2.1 Experimental Design

Time-series of larval fluxes and current velocities were obtained concurrently from November 25, 2004 to April 21, 2005 at three study sites on the East Pacific Rise near 9° 50' N (Fig 4-1). Two vent communities, East Wall and Choo Choo, were chosen as on-axis study sites. East Wall and Choo Choo were located on the ridge

axis within the axial summit trough 1.6 km apart and differed in their proximity to neighboring vent populations. Vertical larval fluxes measured at these two on-axis sites were used as a proxy for larval supply to the two vents. A third study site located on the western ridge flank, 2 km (measured orthogonal to the strike of the axis) off-axis of East Wall, was occupied to investigate the possibility for larvae transported off-axis to return to the ridge axis.

Two subsurface moorings were deployed on the ridge axis within 10 m of East Wall and Choo Choo (also referred to as on-axis moorings). Exact positioning was accomplished by lowering the mooring from the ship's hydrowire and navigating it into an acoustic network on the seafloor [13] (as in Section 3.3.2). Due to technical difficulties with the transponder, the Choo Choo mooring landed off target and was repositioned with *DSV Alvin* to $9^{\circ} 49.61' \text{ N}$, $104^{\circ} 17.37' \text{ W}$, 10 m south of the Choo Choo vent site. The position of the East Wall mooring, $9^{\circ} 50.54' \text{ N}$, $104^{\circ} 17.52' \text{ W}$, was verified by a slant range survey. Each on-axis mooring was equipped with two current meters, one positioned near bottom (10 m above bottom (mab)) and the other within the neutrally buoyant vent plume (170 mab), and a McLane PARFLUX Mark 78H-21 time-series sediment trap with the opening positioned at 4 mab. Aanderaa RCM11 acoustic current meters were used at all positions except at 170 mab on the Choo Choo mooring, where a vane and rotor RCM8 model was employed. The current meters on the Choo Choo mooring recorded at 10 minute intervals whereas those on the East Wall mooring recorded data at coincident 30 minute intervals due to lower battery capacities. Each McLane PARFLUX Mark 78H-21 time-series sediment trap had a sampling area of 0.5 m^2 and sampled vertical particle flux continuously on weekly intervals for 21 weeks.

A third mooring was deployed at the off-axis study site on the western ridge flank 2 km away from East Wall $9^{\circ} 50.36' \text{ N}$, $104^{\circ} 18.57' \text{ W}$ (hereto referred to as the off-axis mooring) (Fig 4-1). Since the placement of the off-axis mooring did not need to be positioned precisely near a vent, the mooring was dropped anchor-first over the side of the ship without navigation and then surveyed acoustically from the ship using slant ranges. The off-axis mooring was equipped with an Aanderaa RCM11 acoustic current meter positioned at 10 m above bottom (mab) to record near-bottom current velocities that might transport larvae towards the ridge axis. A height of 10 mab was chosen because larval concentrations on and off-axis are greatest near bottom ($< 20 \text{ mab}$) [21]; thus near-bottom currents would have the highest probability of

transporting larvae onto the ridge axis. Current velocities were recorded at 30 minute intervals coincident with the on-axis current records at East Wall.

Currents velocities were transformed onto a coordinate system oriented along the strike of the axis (8° counterclockwise from true north and 13° from magnetic north) and decomposed into along-axis (v) and cross-axis (u) current velocities¹. Current records from Choo Choo were low-pass filtered [1] with a cut off of 50 minutes (5 data points) before subsampling to make records the same length as those from other sites. Pearson correlations (r) were determined for the cross-axis and along-axis components of the current velocities between heights and between sites using Matlab v.7.1 (The MathWorks, Inc., Natick, Massachusetts, USA).

Larvae were preserved in the sediment traps *in situ* and later processed in the laboratory. I used a saturated salt - 20% DMSO solution [14] to preserve sediment trap samples for morphological identification and to preserve DNA for future studies. Twenty-one time-series samples were collected at each site. Samples 15 - 21 from both sites and samples 12 - 14 from Choo Choo were sorted in whole. High particulate flux in the remaining samples made sorting too time consuming. To facilitate sorting, the remaining samples were subsampled as follows. Samples were split into ten aliquots using a McLane WSD-10 PARFLUX Wet Sample Divider. Nine of the ten aliquots were sorted for Choo Choo samples 1 and 2 to determine the number of aliquots to sort to minimize the standard error. Sorting five aliquots was found to be sufficient, as sorting more did not reduce the standard error; therefore only five aliquots were sorted for the remaining split samples. Mean standard errors for total gastropod flux were 12.1% for Choo Choo samples and 7.4% for East Wall samples. The standard errors were sufficiently small relative to the estimated variability in flux to resolve temporal patterns. Larval flux for the samples was estimated as 10 times the mean flux of the sorted aliquots.

The fraction retained on a $63 \mu\text{m}$ sieve was sorted for larvae under a dissecting microscope at 25x. Gastropod larvae were identified to the lowest possible taxonomic level under dissecting and compound microscopes, often to the species level, based on shape, size and sculpture of the larval shells (Protoconch I and II) (see Chapter 2, [20, 21]). Larval identifications, groupings and nomenclature were based on Mullineaux et al. [21] and consistent with Chapter 3. Pooled Vent Gastropods (VG) and Probable Vent Gastropods (PVG) and the three most dominant vent (*Cy-*

¹along-axis to the north was positive and cross-axis to the east was positive

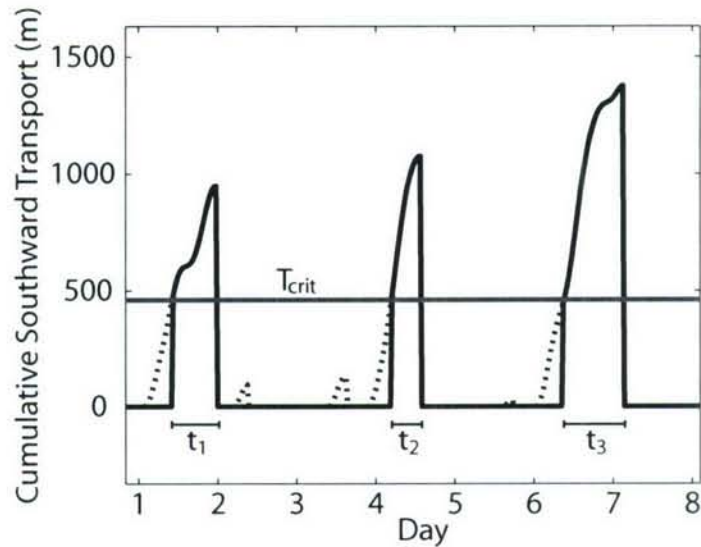


Figure 4-2: Example of how transport in each direction was calculated for each week based on the proportion of time transport exceeded a threshold value, T_{crit} , indicated by the grey line, here at 450 m. The dashed line represents the cumulative transport for each interval. Solid line represents the interval in which the cumulative transport exceeds the threshold value. The time of sustained transport during each interval, t_i , is summed and divided by the total time, one week.

athermia naticoides, *Lepetodrilus* spp., *Gorgolettis emarginatus*) and probable vent taxa (*Laeviphitus* sp., Unknown Benthic sp. A, and Unknown neomphalid 5) were used in subsequent analyses. Larval fluxes were log-transformed for subsequent cross-correlations so their distribution did not deviate from a normal distribution.

4.2.2 Along-Axis Transport

To assess whether variation in larval flux was due to along-axis transport from neighboring vents, along-axis current velocities were cross-correlated with vertical larval fluxes. Studies have suggested that mean current velocities may not capture important variations in current velocities (e.g. [4, 10, 28], Chapter 3). Thus, I used both mean along-axis current velocities (\bar{v}) and a measure to quantify sustained unidirectional along-axis transport² (assuming lateral homogeneity) between a continuous, discrete larval source and the collection site. I assume that larvae were lost when the current directions reversed, such that at the beginning of a sustained period of unidirectional transport the only larvae in the plankton originated from a neighboring

²I use the term transport to describe the advection of a particle/larva in fluid. Transport for the purposes here does not include diffusion.

vent during that period. This means that larvae would not pass a collection site more than once. For a larva to be transported from a source to the collection site, advective transport must be equal to or greater than the distance separating the source and the collection site. Therefore, I define a threshold value for sustained transport, T_{crit} , as the distance between the collection site and the nearest larval source in each along-axis direction. For instance, the nearest source (vent community) that could supply larvae to Choo Choo during southward flow was located 450 m to the north (Fig 4-1); therefore T_{crit} of 450 m would be used to define sustained southward transport to Choo Choo. During southward transport, T_{crit} for East Wall was 225 m (approximate distance to nearest northern vent). During northward flow, T_{crit} for Choo Choo was 4500 m and T_{crit} for East Wall was 100 m (approximate distance to nearest southern vent).

Since numerous current reversals were likely to occur during each week of integrated larval collections, I calculated the probability of larvae being transported from a continuous discrete source to the collection site in northward (P_n) and southward (P_s) currents. The transport statistic used in Chapter (3.3.3) was not used here because using only the maximum transport would ignore many intervals of sustained transport during each week, rather than at most one interval of sustained transport per day as in Chapter (3). Instead, I considered transport here as a probability: as the proportion of time during which transport meets or exceeds T_{crit} increases, the probability of larval transport between the source and collection site also increases. Intervals of unidirectional along-axis transport were identified from filtered v -component time-series (cut off 6 h). The time, t_i , for each successive interval $i = 1, 2, \dots$, during which cumulative transport exceeds the threshold was calculated (Fig 4-2). Cumulative transport was calculated by integrating the current velocities over each interval of unidirectional transport, t_i ; for example, to calculate cumulative northward transport, the decomposed along-axis current velocity, v , was integrated as follows

$$\begin{aligned} \int v & \text{ for } v > 0 \\ 0 & \text{ for } v < 0. \end{aligned} \tag{4.1}$$

Cumulative transport dropped off sharply (Fig 4-2) when the current direction reversed indicating that the specific interval of sustained transport, i , ends. The measure assumes that larvae were transported only during one sustained transport interval and then lost from the system, so the cumulative transport must be reset to zero at

every current reversal. The probability that a larva was transported in sustained northward (southward) currents, $P_n(P_s)$, is then

$$P_{n,s} = \frac{1}{\mathbf{t}} \sum t_i, \quad (4.2)$$

the sum of t_i from each period of sustained northward (southward) transport divided by the total time (\mathbf{t}), one week. The measure was insensitive to changes in T_{crit} if the threshold is less than 500 m, because most periods of sustained transport resulted in cumulative transport greater than or close to 1000 m.

Log-transformed larval fluxes were cross-correlated with \bar{v} , P_n and P_s . Since there was no *a priori* reason to expect a non-linear or lagged correlation, Pearson correlations were presented. Significance was determined at the $p = 0.05$ level after correction for autocorrelation (see Section 3.6.1).

4.2.3 Cross-Axis Transport

Cross-axis currents could affect larval flux to vents in two opposing ways: 1) currents at the ridge axis could advect larvae off-axis, resulting in larval loss, and 2) if currents were different on the ridge flank, off-axis currents oriented towards the ridge could return larvae back to the ridge, resulting in increased larval supply. I investigated scenarios 1 & 2 by cross-correlating larval fluxes with on-axis current velocities and off-axis current velocities, respectively. Significance for all Pearson correlations was determined at the $p = 0.05$ level after correction for autocorrelation.

Log-transformed larval fluxes were cross-correlated with the probability of being transported and ‘lost’ off-axis. Transport in tidal currents across the ridge would not necessarily lead to loss if currents are laterally homogenous because return transport would occur when the tides reversed. Diurnal tidal excursions resulted in ~ 500 -

	Between Sites			Between Heights		
	10 mab		170 mab	EW	CC	
	EW-CC	EW-Off	CC-Off	EW-CC	EW-CC	
along-axis	0.747	0.708	0.708	0.830	0.577	0.595
cross-axis	0.742	0.662	0.856	0.933	0.614	0.812

Table 4.1: Correlation coefficients of along-axis (v) and cross-axis (u) current velocities between sites at the same height, and between heights within a site. EW: East Wall; CC: Choo Choo; Off: Off-axis. All correlations were significant at $p < 0.001$.

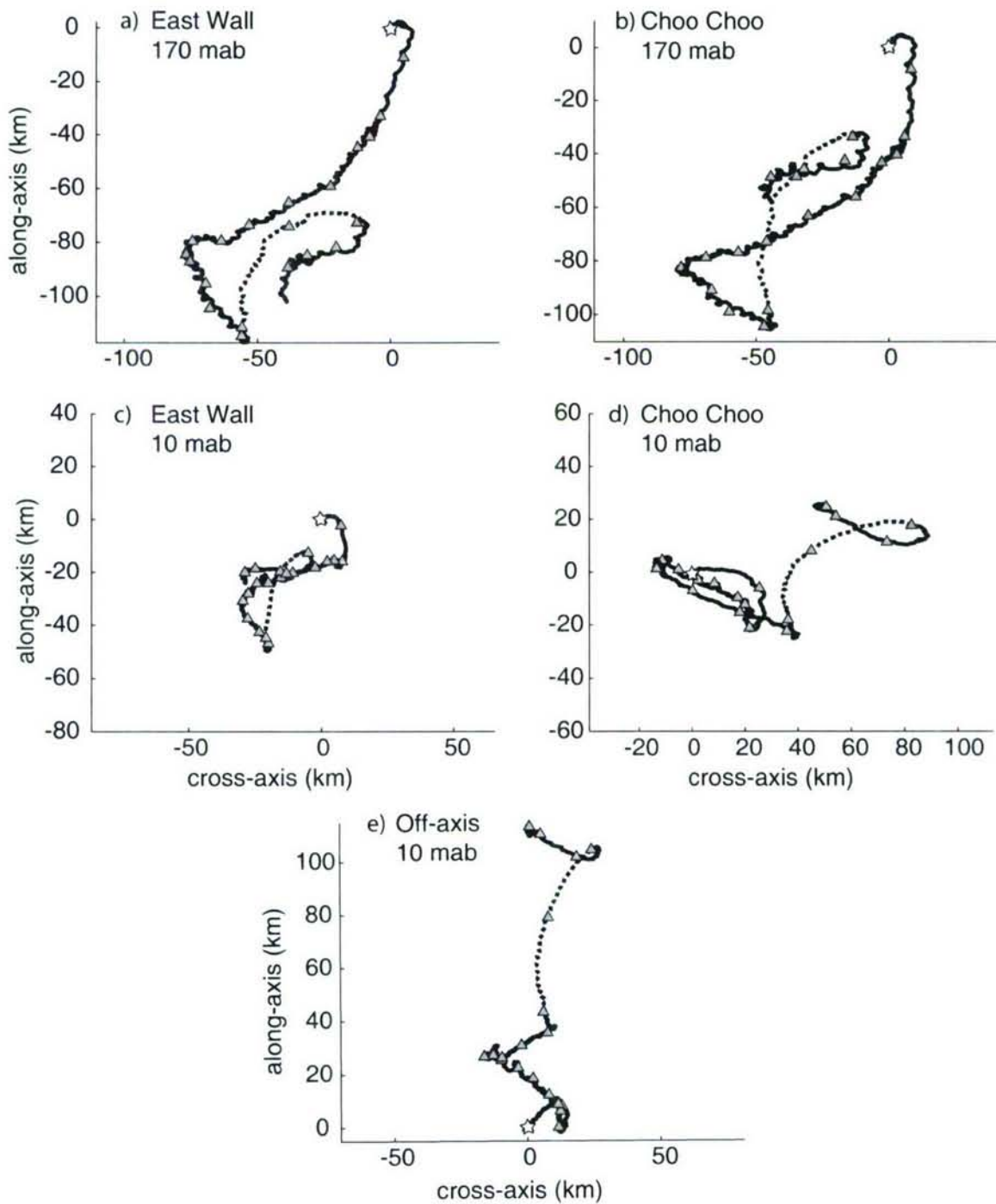


Figure 4-3: Progressive vector diagrams from current velocities measured at East Wall, Choo Choo, and off-axis at 170 mab and 10 mab. The stars indicate initial start date and the triangles designate weekly intervals. Displacement during weeks 16 and 17 are denoted by dashed lines. The scale is the same for all plots.

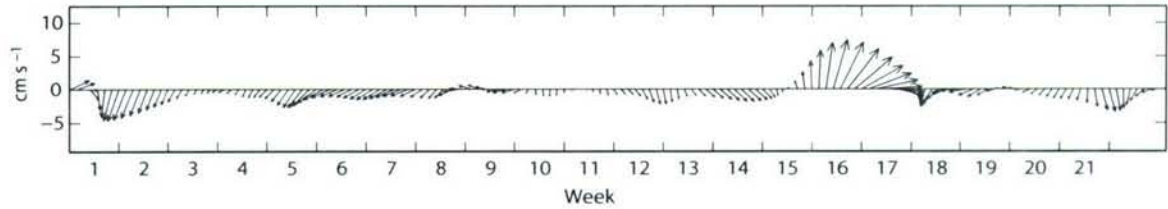


Figure 4-4: Current velocities at East Wall at 170 mab. Current velocities were transformed onto a coordinate system oriented along the ridge axis (strike $+8^\circ$) and low-pass filtered with a cut-off of 150 h to remove tidal and inertial frequencies. Note the relatively strong current velocities during weeks 16 and 17.

1000 m (based on 10 days of current velocities from November 2004, Fig 4-3) of cross-axis displacement. Transport greater than 1000 m would then represent transport greater than that of typical tidal excursions, and thus not be cyclically returned. Therefore, I used 1000 m as T_{crit} for larval loss from the ridge. The probabilities of transport off-axis to the east, P_e , and to the west, P_w , were calculated in the same manner as for transport along-axis, P_n and P_s . Since cross-axis currents in either direction could have contributed to loss of larvae, the probability of being transported off-axis, P_{off} , was the sum of the probabilities for eastward and westward off-axis transport, $P_{off} = P_e + P_w$.

To investigate whether larvae initially ‘lost’ from the ridge axis might be delivered back to the ridge axis, larval fluxes were cross-correlated with the probability of transport to the ridge axis, P_{on} , based on current velocities measured off-axis. Mean flow in the bottom layer of the eastern tropical Pacific is to the west, therefore I specifically investigated whether episodes of eastward flow, measured 2 km off-axis, could return larvae previously transported off of the ridge axis. I calculated the probability, P_{on} , for eastward intervals with T_{crit} equal to 1000 m (reasoning as for transport off of the ridge) and 2000 m (distance of current meter from ridge).

4.2.4 Sea Level Anomalies

An interval of strong northeasterly flow observed in the current record suggested that an eddy-like feature may have impacted the site during the study period (Fig 4-4). This prompted an investigation into the sea level anomalies (SLA) above the study sites that might be indicative of a passing mesoscale eddy. Mesoscale eddy that can transport a water mass within its core could displace the water mass and thus larvae on the ridge as it passes the EPR. In order for an eddy to transport a

water mass within its core, the rotating currents within the eddy must be faster than the propagation, or translation, of the eddy as a whole. Under this assumption, the displacement of the water mass, which would occur as the eddy propagates slowly past the ridge, might not be detectable in the current velocities due to the stronger current velocities associated with the eddy rotation. To determine if any eddy was impacting the study site and larval fluxes, current velocities were compared to the change in SLA and the SLA time-series was qualitatively compared to changes in larval flux, as follows.

Data from Jason, Topex/Poseidon 2, ENVIRONMENTAL SATellite (Envisat), and GEOSAT Follow-On (GFO) were downloaded from the Colorado Center for Astro-dynamics Research at http://argo.colorado.edu/~realtime/global_realtime/alongtrack.html and merged to achieve mesoscale resolution on a daily time-scale to generate a time-series of SLA. Fields of SLA were determined using objective analysis modified from Carter and Robinson [5]. The SLA approximately above the study sites (9° 50' N, 104° 20' W) was extracted from the fields of SLA for October 2004 to June 2005. The long term mean (including mean circulation and geoid) was removed from the initial sea surface level anomalies to estimate the residual sea level anomaly (as in [31]) used in subsequent calculations and comparisons.

Assuming geostrophic balance, current velocities are proportional to the pressure gradient caused by the gradient in the sea level. Since eddies propagate approximately westward [7, 22], the SLA time-series represents an estimate of an east-west cross-section. The zonal (east-west) pressure gradient is positively proportional to the meridional (north-south) surface current velocity,

$$\mathbf{v} = \frac{1}{\rho_0 f} \frac{\delta p}{\delta x}, \quad (4.3)$$

where \mathbf{v} is the meridional surface current velocity, ρ_0 is the density, f is the coriolis parameter, and $\frac{\delta p}{\delta x}$ is the zonal pressure gradient³. To determine whether the SLA gradient (ΔSLA) could have caused the observed anomalies in the near bottom current velocities, the observed meridional current velocities were cross-correlated with ΔSLA - a proxy for $\frac{\delta p}{\delta x}$. The parameters were not regressed because the relationship between the bottom current velocities and ΔSLA was unknown.

³determined primarily by the zonal gradient in sea level

	Origin	N	
		East Wall	Choo Choo
Vent Gastropods		2891	1854
Probable Vent Gastropods		2587	746
<i>Bathymargarites symplector</i>	V	78	89
<i>Clypeosectus delectus</i>	V	29	13
<i>Ctenopelta porifera</i>	V	2	0
<i>Cyathermia naticoides</i>	V	1404	1020
<i>Echinopelta fistulosa</i>	V	22	1
<i>Euleptopsis vitrea</i>	V	53	25
<i>Gorgolettis emarginatus</i>	V	230	87
<i>Gorgolettis spiralis</i>	V	94	41
<i>Lepetodrilus</i> spp.	V	729	513
<i>Lirapex</i> sp.	V	6	1
<i>Melanodrymia aurantiaca</i>	V	15	0
<i>Melanodrymia galeronae</i>	V	4	2
<i>Neomphalus fretterae</i>	V	61	27
<i>Neoleptopsis densata</i>	V	1	0
<i>Pachydermia laevis</i>	V	15	10
Peltospirid	V	98	4
<i>Phymorhynchus major?</i>	V	0	2
<i>Planorbidella planispira</i>	V	7	4
<i>Rhynchopelta concentrica</i>	V	43	15
<i>Laeviphitus</i> sp.	PV	1184	31
Unknown Benthic sp. A	PV	931	444
Unknown neomphalid 5	PV	388	266
Unknown neomphalid 260 μm	PV	10	4
Unknown neomphalid 290 μm	PV	2	1
Unknown slit limpet	PV	72	49
unknown	?	80	14

Table 4.2: Total number (N) of gastropod larvae collected over 21 weeks at East Wall and Choo Choo. V: species endemic to vents; PV: probable vent species; ?: not determined or unknown.

4.3 Results

4.3.1 Current Velocities

Current velocities were highly variable with episodes of strong along-axis and cross-axis flows (Fig 4-3). Diurnal and semidiurnal tidal frequencies and the inertial frequency were the dominant frequencies (analyses not shown). Current velocities at both on-axis sites were higher at 170 mab than at 10 mab. Near bottom, cross-axis current velocities were higher at Choo Choo than at East Wall. Current velocities were significantly correlated between heights and between sites (Table 4.1). Pearson correlation coefficients were lower between sites at 10 mab than at 170 mab, possibly due to interactions of near bottom flows with topography and bottom friction. An episode of strong along-axis northward current velocities occurred during the 16th week (10 - 17 March) followed by strong westward current velocities in the 17th week at all sites and heights (Fig 4-4, 4-3).

Abrupt changes in current direction occurred simultaneously at all sites and heights, but the resulting trajectories and mean flows differed substantially (Fig 4-3). Cross-axis flow was more prominent at Choo Choo at 10 mab compared to the other sites and heights. Mean along and cross-axis current speeds were slower at East Wall at 10 mab compared the other on-axis sites. Off-axis current velocities at 10 mab trended northward ($\bar{v} = 0.92 \text{ cm s}^{-1}$) parallel to the ridge axis with relatively small cross-axis deviations (Fig 4-3 e). The along-axis current reversals observed on-axis were also relatively small off-axis.

4.3.2 Variation in Larval Flux

The total number of gastropod larvae (VG, PVG, and unknown) collected at East Wall ($N = 5556$) was higher than at Choo Choo ($N = 2663$) during the study period (Table 4.2). This pattern was also apparent for most individual taxa and pooled groups (Tables 4.5, 4.6, 4.7, & 4.8). The pattern of temporal variation in flux of pooled Vent Gastropods (VG) was different at East Wall and Choo Choo, although both sites had low flux in the first and last few weeks and a rapid increase in flux in week 3 (Fig 4-5).

East Wall appeared to receive two levels of VG flux: ~ 150 larvae above or below the mean flux ($276 \pm 166 \text{ larvae m}^{-2} \text{ week}^{-1}$). During weeks 2 - 11, larval

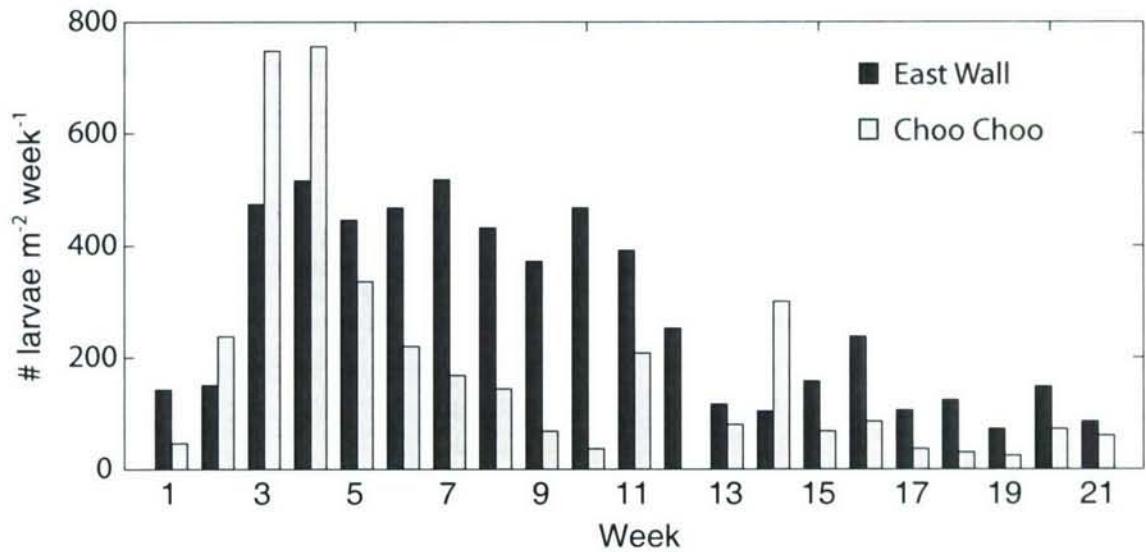


Figure 4-5: Flux of pooled Vent Gastropod (VG) larvae at East Wall (dark grey) and Choo Choo (light grey).

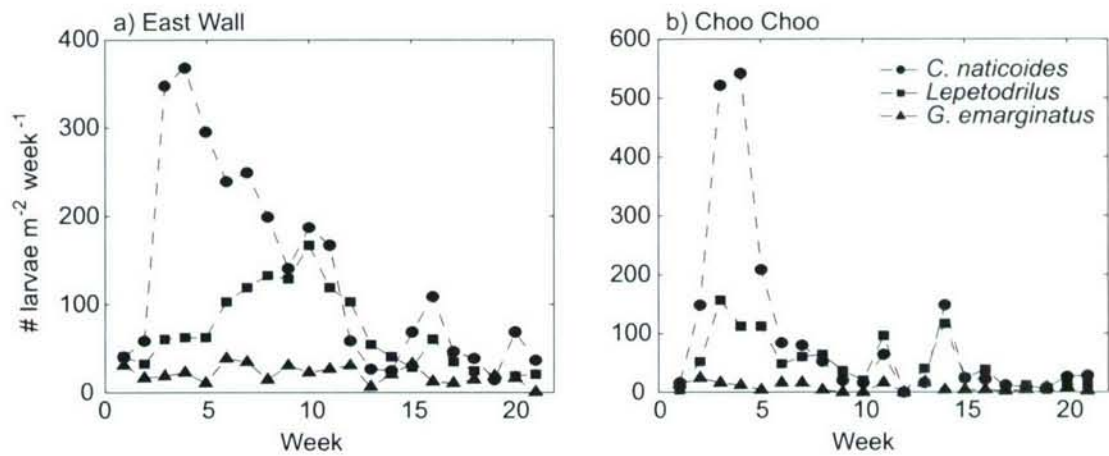


Figure 4-6: Species-specific larval flux at (a) East Wall and (b) Choo Choo for the three most abundant vent species, *Cyathernia naticoides* (circles), *Lepetodrilus* spp. (squares), and *Gorgoleptis emarginatus* (triangles).

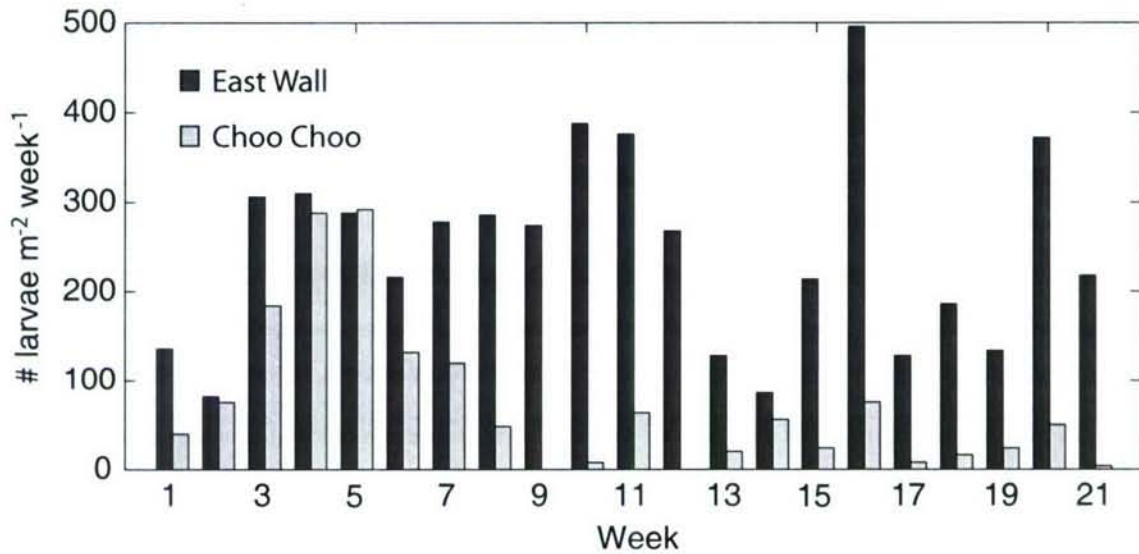


Figure 4-7: Flux of pooled Probable Vent Gastropod (PVG) larvae at East Wall (dark grey) and Choo Choo (light grey).

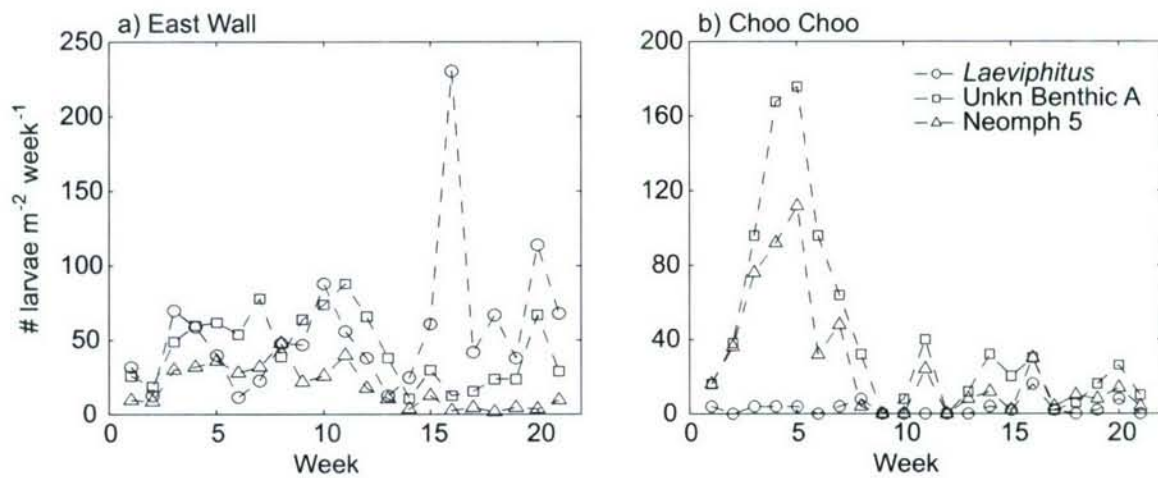


Figure 4-8: Species-specific larval flux at (a) East Wall and (b) Choo Choo for the three most abundant probable vent species, *Laeviphitus* sp. (circles), Unknown Benthic sp. A (squares), and Unknown neomphalid 5 (triangles).

flux was high with a mean VG flux of 454 ± 50 (mean \pm standard deviation⁴) larvae $\text{m}^{-2} \text{week}^{-1}$, whereas during weeks 1, 2 and 12 - 21, larval flux was lower with a mean of $142 (\pm 54)$ larvae $\text{m}^{-2} \text{week}^{-1}$. The apparent constant flux of VG from week 3-11 was primarily due to high flux of *Cyathernia naticoides* during weeks 3 - 6 followed by an increase in *Lepetodrilus* spp. flux as *C. naticoides* flux declined during weeks 6 - 11 (Fig 4-6). The period of low VG flux was not due to the loss of one or two dominant taxa; all of the dominant taxa were still present but had low fluxes.

Vent Gastropod (VG) flux was more variable at Choo Choo (mean 176 ± 212 larvae $\text{m}^{-2} \text{week}^{-1}$) than at East Wall (mean 276 ± 166 larvae $\text{m}^{-2} \text{week}^{-1}$) (Fig 4-5). VG flux peaked at Choo Choo reaching values of 748 and 752 larvae $\text{m}^{-2} \text{week}^{-1}$ during weeks 3 and 4, respectively, well above the mean VG flux at Choo Choo and even the maximum flux of VG at East Wall, 518 larvae $\text{m}^{-2} \text{week}^{-1}$ (Fig 4-5). The peak in VG flux was primarily due to concurrent peaks of *Cyathernia naticoides* and *Lepetodrilus* spp. (Fig 4-6). Fluxes of other vent gastropod species, such as *Bathymargarites symplector*, *Euleptopsis vitrea*, and *Pachydermia laevis*, were also elevated during weeks 3 and 4 (Table 4.7).

The temporal pattern of PVG flux was qualitatively similar to that of VG flux at Choo Choo, but differed from that of VG flux at East Wall, especially at the end of the time-series (Fig 4-7). Flux of PVG at East Wall had a period of relatively constant flux during weeks 3-11 and lower flux during weeks 1 and 2. However, PVG flux did not remain low at the end of the time-series (weeks 12-21). The elevated flux of PVG at the end of the time-series was primarily due to high fluxes of *Laeviphitus* sp. and Unknown Benthic sp. A (Fig 4-8). Flux of *Laeviphitus* sp. peaked sharply during week 16, accounting for 93% of the probable vent specimens collected, and remained high for the remainder of the study. At Choo Choo, flux of PVG gradually increased to a peak during weeks 4 and 5, one week behind the peak in VG flux. Flux then decreased over the next three weeks and remained low for the remainder of the study period (Fig 4-7). The peak in PVG flux at Choo Choo was primarily due to concurrent peaks of Unknown Benthic sp. A and Unknown neomphalid 5 (Fig 4-8). Flux of *Laeviphitus* sp. peaked in week 16 at Choo Choo but the abundance was low compared to flux of other probable vent taxa and thus was not apparent in the pooled PVG flux.

⁴this notation will be used throughout unless otherwise noted

	East Wall			Choo Choo		
	P_{off}	P_{on}		P_{off}	P_{on}	
	1000 m	1000 m	2000 m	1000 m	1000 m	2000 m
Vent	-0.506	-0.377	-0.263	-0.409	-0.241	-0.159
Probable Vent	-0.518	-0.435	-0.266	-0.338	-0.286	-0.242
<i>C. naticoides</i>	-0.484	-0.330	-0.171	-0.473	-0.270	-0.195
<i>Lepetodrilus</i> spp.	-0.340	-0.180	-0.153	-0.553	-0.347	-0.248
<i>G. emarginatus</i>	-0.082	-0.108	-0.152	-0.037	-0.204	-0.281
<i>Laeviphitus</i> sp.	-0.195	-0.144	-0.025	-0.204	-0.149	-0.162
Unkn Benthic sp. A	-0.446	-0.441	-0.321	-0.513	-0.453	-0.404
Unkn neomphalid 5	-0.402	-0.313	-0.230	-0.250	-0.197	-0.191

Table 4.3: Correlation between cross-axis advective transport measures and larval flux. Pearson correlation coefficients are shown comparing measured larval flux with the probability of being lost from the ridge axis (P_{off} , with $T_{crit} = 1000$ m) and the probability of being transported back onto the ridge (P_{on} with $T_{crit} = 1000$ m and 2000 m). Larval fluxes were for pooled Vent Gastropods (VG) and Probable Vent Gastropods (PVG) and the three most dominant vent (*Cyathernia naticoides*, *Lepetodrilus* spp., *Gorgolettis emarginatus*) and probable vent taxa (*Laeviphitus* sp., Unknown Benthic sp.A, and Unknown neomphalid 5.) **Bold** indicates significance at the $p < 0.05$ level after correction for autocorrelation.

4.3.3 Cross-Axis Transport

Fluxes of larvae were compared to the probability of transport off of the ridge axis, P_{off} (Table 4.3). Fluxes of VG, PVG, *Cyathernia naticoides*, and Unknown Benthic sp. A were significantly negatively correlated with P_{off} from East Wall at 10 mab. *Lepetodrilus* spp. and Unknown Benthic sp. A were significantly correlated with P_{off} from Choo Choo at 10 mab. No species or groups were significantly correlated with P_{off} at 170 mab at the $p < 0.05$ level (data not shown).

Fluxes of larvae were not correlated with eastward currents measured off-axis that could transport ‘lost’ larvae from the western flank back onto the ridge axis, P_{on} (Table 4.3). Unknown Benthic sp. A was the only taxon with a significant correlation, however the correlation was negative, suggesting that larval fluxes decreased with increasing P_{on} - opposite of the expectation.

4.3.4 Along-Axis Transport

Pearson correlation coefficients between log-transformed larval flux and \bar{v} and the probability of along-axis transport were low at both East Wall and Choo Choo (Ta-

ble 4.4). Fluxes of only two taxa were significantly correlated with along-axis flow. The vent gastropod *Gorgoleptis emarginatus* was significantly correlated with P_s at Choo Choo at 170 mab ($r = 0.479$, $p < 0.05$). *Laeviphitus* sp. was significantly correlated with \bar{v} at both heights and vent sites, P_n (Fig 4-9) at both heights and vent sites (except Choo Choo at 170 mab) and significantly negatively correlated with P_s at 170 mab at East Wall (Table 4.4). Pooled PVG at East Wall were also significantly correlated with mean along-axis current velocities at 170 mab, likely due to the dominance of *Laeviphitus* sp. in PVG at East Wall.

The observations of sustained cross-axis flows at the vent sites (Fig 4-3 & 4-4) and reduced larval fluxes during those periods (Table 4.3) raised the question of whether one would expect to see any correspondence between along-axis transport and larval flux during intervals when larval abundances were depleted due to off-axis loss. To evaluate this possibility, I repeated the comparison of along-axis transport and larval flux, but examined only the times when cross-axis flows were weak. Intervals of weak cross-axis transport were defined as times when both the cumulative eastward and westward transport was *less than* the T_{crit} for sustained cross-axis transport, 1000 m. The majority of the current velocity records had weak cross-axis transport; 73.4% and 81.5% of East Wall current records, at 170 mab and 10 mab respectively, were during periods of weak cross-axis transport. 68.6% and 64.9% of Choo Choo current records, at 170 mab and 10 mab respectively, were during periods of weak cross-axis transport. P_n and P_s were adjusted such that only periods of sustained northward and southward transport during weak cross-axis transport intervals were considered. The adjusted P_n and P_s were not significantly correlated to larval fluxes, except for *Laeviphitus* sp. and PV (data not shown). The adjusted P_n and P_s correlations showed the same patterns as the non-adjusted along-axis results above. Larval fluxes were poorly correlated with all of the adjusted measures. The only exception was the previously noted positive relationship between the flux of *Laeviphitus* sp. and northward transport and negative relationship between *Laeviphitus* sp. and southward transport.

Qualitative comparisons also do not support the hypothesized relationship between along-axis transport and larval fluxes. Qualitative inspection the current velocity records (Figs 4-3 & 4-4) showed numerous periods of sustained southward transport, especially at 170 mab, except during weeks 16 and 17. The strongest and longest continuous intervals of southward transport occurred during weeks 2 and 18

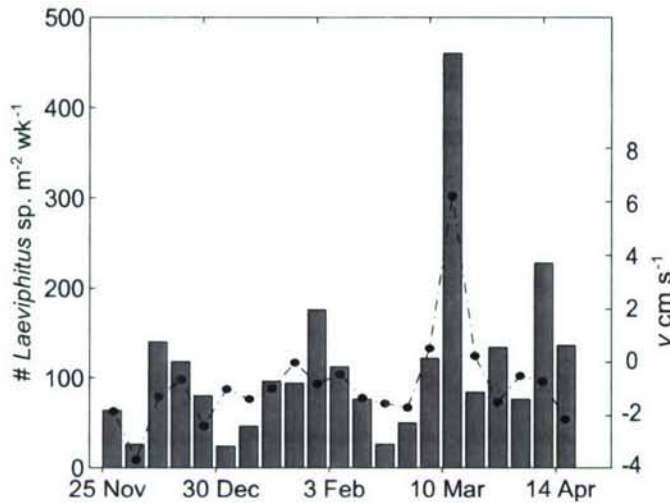


Figure 4-9: Mean along-axis current velocity, \bar{v} , at 170 mab (dashed line) compared to flux of *Laeviphitus* sp. (grey bars) at East Wall.

when larval fluxes of vent gastropods were low.

4.3.5 Sea Level Anomalies

The sea level anomaly above the study site varied over the course of the study period (Fig 4-10). Δ SLA, a proxy for meridional geostrophic current velocities (Equation 4.3), and the observed meridional current velocities on the bottom had an inverse relationship (Fig 4-11). The weekly mean Δ SLA were significantly negatively correlated with \bar{v} at East Wall ($r = -0.596$ at 170 mab and $r = -0.693$ at 10 mab), Choo Choo ($r = -0.625$ at 170 mab and $r = -0.712$ at 10 mab), and off-axis ($r = -0.696$) at $p < 0.05$. VG larval fluxes at both on-axis sites were low during weeks 12-21 when the sea level was changing dramatically (> 10 mm). While the sea level was relatively constant, VG larval flux was also relatively constant at East Wall, except during weeks 1 and 2.

4.4 Discussion

Larval dispersal in the plankton may have many ecological and evolutionary advantages, including gene flow and colonization of new habitat, but dispersal can also lead to larval loss by transport to unsuitable habitat. The negative correlations between larval fluxes and sustained off-axis transport suggests that larval loss due to off-axis transport was occurring during this study (Table 4.3). Larval flux decreased during episodes of strong (> 1 km,) near bottom cross-axis transport. P_{off} at 170 mab

East Wall	10 mab			170 mab		
	\bar{v}	P_n	P_s	\bar{v}	P_n	P_s
Vent	0.041	-0.094	-0.004	0.067	-0.084	0.046
Probable Vent	0.424	0.237	-0.317	0.495	0.398	-0.401
<i>C. naticoides</i>	0.113	0.016	-0.113	0.087	-0.049	0.034
<i>Lepetodrilus</i> spp.	0.005	-0.109	0.123	0.094	-0.061	-0.039
<i>G. emarginatus</i>	-0.029	-0.127	0.026	0.078	0.058	-0.158
<i>Laeviphitus</i> sp.	0.593	0.522	-0.441	0.636	0.646	-0.624
Unkn Benthic sp. A	-0.300	-0.424	0.198	-0.240	-0.324	0.192
Unkn neomphalid 5	-0.241	-0.309	0.192	-0.271	-0.441	0.290

Choo Choo	10 mab			170 mab		
	\bar{v}	P_n	P_s	\bar{v}	P_n	P_s
Vent	0.099	-0.122	-0.240	-0.127	-0.111	0.340
Probable Vent	0.186	-0.003	-0.321	-0.064	-0.052	0.408
<i>C. naticoides</i>	0.017	-0.207	-0.204	-0.228	-0.192	0.409
<i>Lepetodrilus</i> spp.	0.063	-0.112	-0.129	-0.067	-0.103	0.236
<i>G. emarginatus</i>	-0.210	-0.233	0.096	-0.325	-0.285	0.479
<i>Laeviphitus</i> sp.	0.525	0.467	-0.401	0.514	0.396	-0.218
Unkn Benthic sp. A	0.133	-0.136	-0.303	-0.145	-0.205	0.413
Unkn neomphalid 5	0.105	0.031	-0.234	-0.101	-0.011	0.462

Table 4.4: Correlation between along-axis advective transport measures and larval flux at East Wall and Choo Choo. Pearson correlation coefficients are shown comparing measured larval flux with the mean along-axis velocity \bar{v} and with the probability of transport from a larval source in northward (P_n) and southward (P_s) currents. Larval fluxes were for pooled Vent Gastropods (VG) and Probable Vent Gastropods (PVG) and the three most dominant vent (*Cyathernia naticoides*, *Lepetodrilus* spp., *Gorgoleptis emarginatus*) and probable vent taxa (*Laeviphitus* sp., Unknown Benthic sp. A, and Unknown neomphalid 5.) **Bold** indicates significance at the $p < 0.05$ level after correction for autocorrelation.

was not significantly correlated with larval flux, which is consistent with previous observations of lower larval abundances away from bottom [21].

Once transported sufficiently far off-axis the larvae may be lost from the system. Eastward currents on the western ridge flank were episodically sufficient to transport larvae 1 - 2 km to the ridge axis. However, there was no evidence for increased larval supply during periods of transport towards the ridge axis from the western flank (Table 4.3). (Transport from the eastern flank was not assessed.)

Despite the suggested larval loss, larvae were present and being supplied (i.e. sinking) to the benthos during the study. The mechanism for increased larval supply proposed in Chapter 3 was not apparent during this study. In the previous study, correlations between daily larval flux and along-axis currents suggested that along-axis current velocities transported larvae from neighboring vent communities (within ~ 1 -2 km) to East Wall and Choo Choo (Chapter 3). These results suggested that larval flux to East Wall would be uninterrupted and independent of the current direction based on the close proximity of vents to the north and south, while larval flux to Choo Choo would be correlated with southward along-axis transport of larvae from the relatively close vent communities (sources) to the north compared to distant vents to the south. Larval fluxes during this study did not generally confirm these expectations. Only *Gorgolettis emarginatus* conformed to the expectations of a positive correlation with the probability of southward transport, P_s , at Choo Choo (at 170 mab) and no significant correlation at East Wall. All other vent taxa and VG (except *Laeviphitus* sp.) were not significantly correlated with mean along-axis current velocities nor the probability of northward or southward transport (P_n or P_s). *Laeviphitus* sp. was significantly positively correlated with \bar{v} and P_n , and negatively correlated with P_s . These patterns suggest that *Laeviphitus* sp. was primarily transported in northward currents from a source(s) to the south of East Wall and Choo Choo. Since adult *Laeviphitus* sp. have not been observed on the benthos, the actual source remains uncertain.

Numerous factors could have caused the deviation from the expected correlations between larval flux and along-axis currents. Strong cross-axis current velocities, spatial heterogeneity in current velocities, larval production, and larger scale flows will be discussed as possible factors confounding the expected relationship between along-axis currents and larval fluxes developed from daily in Chapter 3.

While along-axis current velocities dominated at all heights and sites during daily

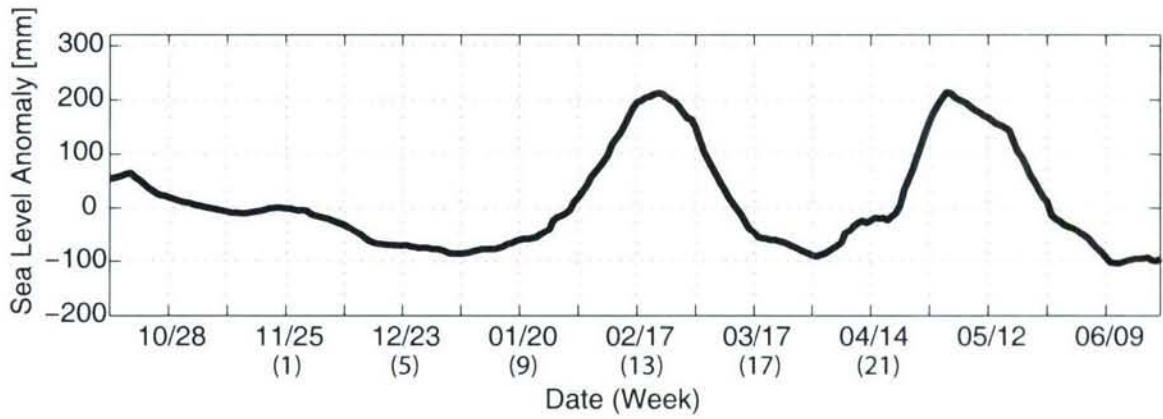


Figure 4-10: Sea level anomaly (SLA) at $9^{\circ} 50' N$, $104^{\circ} 20' W$ during the study period. Note that (Week) corresponds to larval and bottom current measurement intervals.

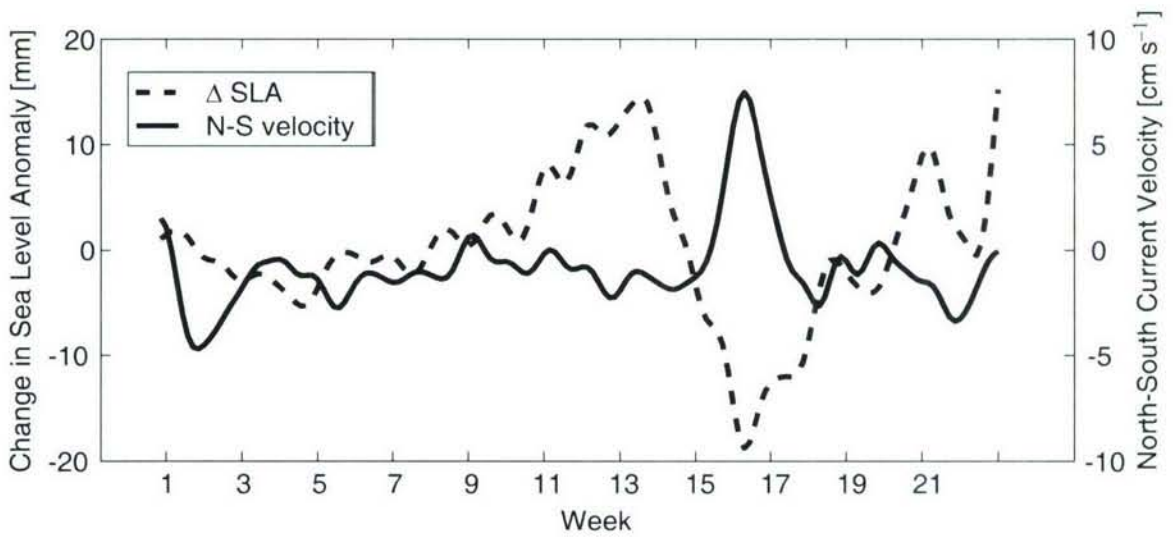


Figure 4-11: Comparison between observed meridional current velocities near bottom (solid line), low-pass filtered (cut off 100 hours), compared to smoothed ΔSLA , sea level gradient (dashed line). ΔSLA is presented offset 6 days. Geostrophic balance would predict a positive correlation between the two variables.

observations and larval collections in November 2004 (Fig 3-3), current velocities during this study were highly variable with strong cross-axis flows and spatial heterogeneity observed in the current velocities. Loss due to cross-axis currents could have masked supply due to along-axis transport. However, removal of periods with high cross-axis transport did not greatly alter the along-axis correlations or produce the expected correlations. Trying to assess along-axis transport during intervals of strong cross-axis flow and spatial heterogeneity was difficult with currents from only three locations. The cumulative transport calculations would likely be more powerful if the spatial heterogeneity in current velocities was incorporated. Larvae swept off-axis may enter a completely different advective environment than that on-axis. Numerical modeling by Bill Lavelle (NOAA PMEL) predicts jets parallel to the ridge axis on both ridge flanks, one on the west flank going northward and one on the east flank going southward. The off-axis current observations presented in this study lend the first support towards the existence of northward and southward 'jets' on the ridge flanks that could enhance long distance larval dispersal.

Variation in larval production could have also confounded the relationship between larval flux and along-axis transport. Correlations between larval supply and current measures assume that larval production was continuous. Episodic or seasonal reproduction could have accounted for the observed variation in larval supply. However, reproduction of vent gastropod species on the East Pacific Rise is largely believed to be continuous based on asynchronous oocyte development (all stages of development observed) [8] and continuous gametogenesis [24]. Limited temporal sampling for reproductive studies due to weather and ship constraints could have missed seasonal or episodic pulses of reproduction. The continuous larval collections from this study provide additional evidence for continuous reproduction. Of the 32 taxa collected during the study, 30 taxa showed no evidence of a restricted temporal presence/absence (see examples in Fig 4-6, 4-8 and Tables 4.5, 4.6, 4.7, & 4.8). The other two taxa, *Ctenopelta porifera* and *Neolepetopsis densata*, were only collected in one sample each in low numbers (1 and 2 individuals, respectively).

Large sea level anomalies and current anomalies suggest that mesoscale flows also may have impacted larval flux during the study. The large anomalies in current velocities observed during weeks 15-17 corresponded to a large SLA (Fig 4-10), consistent with the passage of an anticyclonic mesoscale eddy. Mesoscale eddies develop in the Gulfs of Tehuantepec and Papagayo on the west coast of Central America during the

winter and spring, and then propagate across the EPR (e.g. [12, 17, 23]). An eddy crossing the ridge could have displaced the water mass on the ridge which contained larvae - consistent with the observation of low larval flux at both East Wall and Choo Choo at the end of the study period. Water displacement due to the eddy would change the larval flux at the collection sites independent of the direction of the current velocities. However, the connection between the peak in SLA and strong current velocities is tentative. The direction of observed near bottom flow lagged and was opposite to the predicted geostrophic flows based on the SLA gradient (Fig 4-11). Observations of eddy-induced current velocities at depth (below 1500 m) are rare but the few measurements reported velocities in phase with the surface flows (e.g. [6, 19, 34]).

The discrepancy between the results of this chapter and Chapter 3 may be due to the different temporal scales analyzed. The weekly temporal scale of sampling may not have been sufficient to detect variation in larval fluxes due to smaller temporal scale mechanisms, such as daily or diurnal. This does not preclude the previous hypothesis of larval transport primarily between local vent communities on small temporal and spatial scales. Local transport may be important on daily timescales and supply the majority of larvae to a vent site, but, on a longer weekly timescale, losses due to cross-axis flows and mesoscale eddies may have a larger impact on temporal variation in larval supply.

Bibliography

- [1] Alessi, C., Beardsley, R., Limeburner, R., Rosenfeld, L., Lentz, S. J., Send, E., Winant, C., Allen, J., Halliwell, G., Brown, W., & Irish, J. (1985). CODE-2: moored array and large-scale data report. Technical Report WHOI 85-35, Woods Hole Oceanographic Institution.
- [2] Bertness, M. D., Gaines, S. D., & Wahle, R. A. (1996). Wind driven settlement patterns in the acorn barnacle *Semibalanus balanoides*. *Marine Ecology Progress Series*, 137:103–110.
- [3] Botsford, L. W. (2001). Physical influences on recruitment to California Current invertebrate populations on multiple scales. *ICES Journal of Marine Science*, 58(5):1081–1091.
- [4] Byers, J. & Pringle, J. (2006). Going against the flow: retention, range limits and invasions in advective environments. *Marine Ecology Progress Series*, 313:27–41.

- [5] Carter, E. & Robinson, A. (1987). Analysis models for the estimation of oceanic fields. *Journal of Atmospheric and Oceanic Technology*, 4:49–74.
- [6] Clement, A. & Gordon, A. (1995). The absolute velocity field structure of Agulhas eddies and the Benguela Current. *Journal of Geophysical Research*, 100:22591–22601.
- [7] Cushman-Roisin, B., Chassignet, E., & Tang, B. (1990). Westward motion of mesoscale eddies. *Journal of Physical Oceanography*, 20:758–768.
- [8] Eckelbarger & Young, C. (2001). Gonad ultrastructure, gametogenesis and observations on reproduction of hydrothermal vent enteropneusts, polychaetes and gastropods. In: *LARVE Results Symposium*.
- [9] Epifanio, C. E. & Garvine, R. W. (2001). Larval transport on the Atlantic continental shelf of North America: a review. *Estuarine, Coastal and Shelf Science*, 52(1):51–77.
- [10] Gaines, S., Gaylord, B., & Largier, J. (2003). Avoiding current oversights in marine reserve design. *Ecological Applications*, 13:S32–S46.
- [11] Garland, E. D., Zimmer, C. A., & Lentz, S. J. (2002). Larval distributions in inner-shelf waters: the roles of wind-driven cross-shelf currents and diel vertical migrations. *Limnology and Oceanography [Limnol. Oceanogr.]*, 47(3):803–817.
- [12] Gonzalez-Silvera, A., Santamaria-del Angel, E., Millán-Nunez, R., & Manzo-Monroy, H. (2004). Satellite observations of mesoscale eddies in the Gulfs of Tehuantepec and Papagayo (Eastern Tropical Pacific). *Deep-Sea Research II*, 51:587–600.
- [13] Hunt, M., William, M., Donald, A., Kenneth, R., Woolcott, K., & Spindell, R. (1974). An acoustic navigation system. Technical Report WHOI-74-6, Woods Hole Oceanographic Institution.
- [14] Khrifounoff, A., Comtet, T., Vangriesheim, A., & Crassous, P. (2000). Near-bottom biological and mineral particle flux in the Lucky Strike hydrothermal vent area (Mid-Atlantic Ridge). *Journal of Marine Systems*, 2:101–118.
- [15] Lagos, N. A., Navarrete, S. A., Veliz, F., Masuero, A., & Castilla, J. C. (2005). Mesoscale spatial variation in settlement and recruitment of intertidal barnacles along the coast of central Chile. *Marine Ecology Progress Series*, 290:165–178.
- [16] Levin, L. (2006). Recent progress in understanding larval dispersal: new directions and digressions. *Integrative and Comparative Biology*, 46:282–297.
- [17] McCreary, J., Hyong, S., & Enfield, D. (1989). The response of the coastal ocean to strong offshore winds: with application to circulations in the Gulfs of Tehuantepec and Papagayo. *Journal of Marine Research*, 47:81–109.

- [18] Menge, B. A. (2000). Recruitment vs. postrecruitment processes as determinants of barnacle population abundance. *Ecological Monographs*, 70:265–288.
- [19] Mulhearn, P., Filloux, J., Lilley, F., Bindoff, N., & Ferguson, I. (1986). Abyssal currents during the formation and passage of a warm-core ring in the East Australian Current. *Deep-Sea Research*, 33:1563–1576.
- [20] Mullineaux, L. S., Kim, S. L., Pooley, A., & Lutz, R. A. (1996). Identification of archaeogastropod larvae from a hydrothermal vent community. *Marine Biology*, 124(4):551–560.
- [21] Mullineaux, L. S., Mills, S. W., Sweetman, A. K., Beaudreau, A. H., Metaxas, A., & Hunt, H. L. (2005). Vertical, lateral and temporal structure in larval distributions at hydrothermal vents. *Marine Ecology Progress Series*, 293:1–16.
- [22] Nof, D. (1981). On the β -induced movement of isolated baroclinic eddies. *Journal of Physical Oceanography*, 11:1662–1672.
- [23] Palacios, D. & Bograd, S. (2005). A census of Tehuantepec and Papagayo eddies in the northeastern tropical Pacific. *Geophysical Research Letters*, 32:doi:10.1029/2005GL024324.
- [24] Pendlebury, S., Tyler, P., Young, C., & Mullineaux, L. (2001). Gametogenesis and population analysis of the hydrothermal vent limpets genus *Lepetodrilus*. In: *LARVE Symposium Results*.
- [25] Pineda, J. (1991). Predictable upwelling and the shoreward transport of planktonic larvae by internal tidal bores. *Science*, 253(5019):548–551.
- [26] Roughgarden, J., Gaines, S., & Possingham, H. (1988). Recruitment dynamics in complex life cycles. *Science*, 241(4872):1460–1466.
- [27] Schouten, H., Tivey, M., Fornari, D., Yoerger, D. R., & Bradley, A. (2003). ABE Imagenex microbathymetry for the East Pacific Rise. *Ridge 2000 Events: A Newsletter of Ridge 2000 Program*, 1(1):1.
- [28] Selkoe, K., Gaines, S., Caselle, J., & Warner, R. (2006). Current shifts and kin aggregation explain genetic patchiness in fish recruits. *Ecology*, 87:3082–3094.
- [29] Shanks, A. (1983). Surface slicks associated with tidally forced internal waves may transport pelagic larvae of benthic invertebrates and fishes shoreward. *Marine Ecology Progress Series*, 13:311–315.
- [30] Shanks, A. L. (2006). Mechanisms of cross-shelf transport of crab megalopae inferred from a time series of daily abundance. *Marine Biology*, 148(6):1383–1398.
- [31] Siegel, D., McGillicuddy, D., & Fields, E. (1999). Mesoscale eddies, satellite altimetry, and new production in the Sargasso Sea. *Journal of Geophysical Research*, 104:13,359–13,379.

- [32] Underwood, A. & Fairweather, P. (1989). Supply-side ecology and benthic marine assemblages. *Trends in Ecology and Evolution*, 4:16–20.
- [33] Underwood, A. & Keough, M. J. (2001). *Marine Community Ecology*, chapter Supply-Side Ecology: The Nature and Consequences of Variations in Recruitment of Intertidal Organisms, pages 183–200. Sinauer Associates, Inc.
- [34] van Aken, H., van Veldhoven, A., Veth, C., de Ruijter, W., van Leeuwen, P., Drijfhout, S., Whittle, C., & Rouault, M. (2003). Observations of a young Agulhas ring, Astrid, during MARE in March 2000. *Deep-Sea Research II*, 50:167–195.

4.5 Supplemental Material

Taxa	11/25	12/02	12/09	12/16	12/23	12/30	01/06	01/13	01/20	01/27	02/03
	1	2	3	4	5	6	7	8	9	10	11
<i>Bathymargarites symplector</i>	1	3	4	6	2	2	4	4		4	4
<i>Clypeosectus delectus</i>	2	3	2	2		2	4			2	
<i>Ctenopelta porifera</i>						2					
<i>Cyathermia naticoides</i>	21	30	174	184	148	120	125	100	71	94	84
<i>Echinopelta fistulosa</i>		1	2		4		3	3	4	4	
<i>Euleptopsis vitrea</i>	2	1	5	8	4	2	5	10	4	6	2
<i>Gorgolettis emarginatus</i>	16	9	10	12	6	20	18	8	16	12	14
<i>Gorgolettis spiralis</i>	3	2	2	8	8	16	10	4	8	8	12
<i>Lepetodrilus</i> spp.	21	17	31	32	32	52	60	67	65	84	60
<i>Lirapez</i> sp.								2			
<i>Melanodrymia aurantiaca</i>					2	2		4			
<i>Melanodrymia galeronae</i>										2	
<i>Neomphalus fretterae</i>	2	3			4	6	11	2	2	4	8
<i>Neoleptopsis densata?</i>											
<i>Pachydermia laevis</i>			2		3			2	2	2	2
<i>Peltopirid</i>	1	4	5	6	6	6	10	10	10	6	4
<i>Planorbidella planispira</i>	1								2		1
<i>Rhynchopelta concentrica</i>	1	2			4	4	9		2	6	6
<i>Laeviphitus</i> sp.	32	13	70	59	40	12	23	48	47	88	56
Unknown Benthic sp. A	26	19	49	60	62	54	78	39	64	74	88
Unknown neomphalid 5	10	9	30	32	36	28	32	48	22	26	40
Unknown neomphalid 260 μ m							2		2	2	2
Unknown neomphalid 290 μ m							2				
Unknown slit limpet			4	4	6	14	4	8	2	4	2
unknown	5	7				2		6	10	10	6
Vent Gastropods	71	75	237	258	223	234	259	216	186	234	197
Probable Vent Gastropods	68	41	153	155	144	108	141	143	137	194	188
TOTAL gastropods	144	123	390	413	367	344	400	365	333	438	391
Std Error Total gastropods			9.6%	8.3%	4.8%	10.4%	4.9%	6.3%	8.5%	4.6%	10.2%

Table 4.5: Continued on Next Page.

Week of	02/10	01/17	02/24	03/03	03/10	03/17	03/24	03/31	04/07	04/14	TOTAL
Taxa	12	13	14	15	16	17	18	19	20	21	
<i>Bathymargarites symplector</i>	6	4		2	6		7	4	9	6	78
<i>Clypeosectus delectus</i>	2		2		1		1	2	4		29
<i>Ctenopelta porifera</i>											2
<i>Cyathermia naticoides</i>	30	14	13	35	55	24	20	8	35	19	1404
<i>Echinopelta fistulosa</i>				1	1						22
<i>Euleptopsis vitrea</i>				1			2	1			53
<i>Gorgoleptis emarginatus</i>	16	4	11	17	7	6	8	10	9	1	230
<i>Gorgoleptis spiralis</i>	4	2	2	1	1				2	1	94
<i>Lepetodrilus</i> spp.	52	28	21	15	31	18	13	9	10	11	729
<i>Lirapex</i> sp.		1			1		1		1		6
<i>Melanodrymia aurantiaca</i>	2	1			1		1	1			15
<i>Melanodrymia galeronae</i>	2										4
<i>Neomphalus fretterae</i>	10	2	1		2		1			3	61
<i>Neoleptopsis densata?</i>										1	1
<i>Pachydermia laevis</i>						1	1				15
<i>Peltospirid</i>	2	2	1	4	8	3	6	1	2	1	98
<i>Planorbidella planispira</i>			1		1		1				7
<i>Rhynchopelta concentrica</i>			1	2	4	1			1		43
<i>Laeviphitus</i> sp.	38	13	25	61	230	42	67	38	114	68	1184
Unknown Benthic sp. A	66	38	11	30	13	16	24	24	67	29	931
Unknown neomphalid 5	18	11	4	13	3	5	2	5	4	10	388
Unknown neomphalid 260 μm						1				1	10
Unknown neomphalid 290 μm	12	2	3	3	2				1	1	2
Unknown slit limpet		8	2	7	9		1	1	1	3	72
unknown							1	1	1	3	78
Vent Gastropods	126	58	53	77	119	53	62	36	74	43	2891
Probable Vent Gastropods	134	64	43	107	248	64	93	67	186	109	2587
TOTAL gastropods	260	130	98	191	376	117	156	104	261	155	5556
Std Error Total gastropods	6.1%										

Table 4.6: Weekly larval flux (larvae $0.5 \text{ m}^{-2} \text{ week}^{-1}$) for each taxa at East Wall.

Week of	11/25	12/02	12/09	12/16	12/23	12/30	01/06	01/13	01/20	01/27	02/03
Taxa	1	2	3	4	5	6	7	8	9	10	11
<i>Bathymargarites symplector</i>	3	2	10	12	16	16	6	1			
<i>Clypeosectus delectus</i>			2	2	2	2					2
<i>Cyathermia naticoides</i>	8	74	260	270	104	42	40	26	10	8	32
<i>Echinopelta fistulosa</i>											
<i>Euleptopsis vitrea</i>	1	1	4	8	2	2	2	2	2		2
<i>Gorgoleptis emarginatus</i>	7	12	8	6	2	8	8	2			8
<i>Gorgoleptis spiralis</i>	2		6	8	6	4		2			6
<i>Lepetodrilus</i> spp.	2	26	78	56	56	24	30	32	18	10	48
<i>Lirapex</i> sp.		1									
<i>Melanodrymia galeronae</i>											
<i>Neomphalus fretterae</i>				8			4	4	2		2
<i>Pachydermia laevis</i>		1	2	4							
Peltospirid											2
<i>Phymorhynchus major?</i>					2						
<i>Planorbidella planispira</i>			2								2
<i>Rhynchopelta concentrica</i>		1	2	2		4					
<i>Laeviphitus</i> sp.	2		2	2	2		2	4			
Unknown Benthic sp. A	8	19	48	84	88	48	32	16		4	20
Unknown neomphalid 5	8	18	38	46	56	16	24	2			12
Unknown neomphalid 260 μ m				2		2					
Unknown neomphalid 290 μ m											
Unknown slit limpet	2	2	4	14		10	2	6	2		
unknown	1	1	2			2					2
<i>B. symplector juvenile</i>								1			
Vent Gastropod	23	118	374	376	170	102	88	69	32	18	104
Probable Vent Gastropod	18	37	88	134	146	66	58	22		4	32
TOTAL gastropod	44	158	468	524	316	180	148	97	34	22	138
Std Error Total gastropod	17.1%	6.7%	9.3%	4.9%	6.5%	12.1%	12.7%	16.8%	19.9%	26.5%	8.7%

Table 4.7: Continued on Next Page.

Week of	02/10	01/17	02/24	03/03	03/10	03/17	03/24	03/31	04/07	04/14	TOTAL
Taxa	12	13	14	15	16	17	18	19	20	21	
<i>Bathymargarites symplector</i>			6	6	7	2	1	1	10	6	89
<i>Clypeosectus delectus</i>		2	2		1						13
<i>Cyathermia naticoides</i>		8	74	12	11	6	4	4	13	14	1020
<i>Echinopelta fistulosa</i>										1	1
<i>Euleptopsis vitrea</i>				1	1	1					25
<i>Gorgolettis emarginatus</i>		8	2	2	2	1	2	4	4	1	87
<i>Gorgolettis spiralis</i>			2	1		3			1		41
<i>Lepetodrilus</i> spp.		20	58	12	19	4	6	2	6	6	513
<i>Lirapex</i> sp.											1
<i>Melanodrymia galeronae</i>			2								2
<i>Neomphalus fretterae</i>			3	1				2	1		27
<i>Pachydermia laevis</i>							2	1		1	10
<i>Peltospirid</i>					1						4
<i>Phymorhynchus major?</i>											2
<i>Planorbidella planispira</i>											4
<i>Rhynchopelta concentrica</i>			4			2					15
<i>Laeviphitus</i> sp.			2	1	8	1		1	4		31
Unknown Benthic sp. A		6	16	10	15	1	3	8	13	5	444
Unknown neomphalid 5		4	6	1	15	2	5	4	7	2	266
Unknown neomphalid 260 μm											4
Unknown neomphalid 290 μm									1		1
Unknown slit limpet		2	4		1						49
unknown				3	1		1		1		14
<i>B. symplector juvenile</i>							3		2	1	7
Vent Gastropod	0	38	153	35	42	19	15	12	36	30	1854
Probable Vent Gastropod	0	10	24	12	38	4	8	13	25	7	746
TOTAL gastropod	0	50	181	50	82	23	24	25	62	37	2663
Std Error Total gastropod	0.0%	12.6%	14.3%								

Table 4.8: Weekly larval flux (larvae $0.5 \text{ m}^{-2} \text{ week}^{-1}$) for each taxa at Choo Choo.

Chapter 5

Mesoscale eddies extend into the deep-sea: implications for larval dispersal

5.1 Introduction

Mesoscale eddies have been suggested to influence the dispersal of marine benthic invertebrate larvae. Research efforts have largely focused on mesoscale eddies as possible retention mechanisms. Stationary eddies, for example those formed in the wake of an island [5, 6, 31, 42], could keep larvae near the natal site during planktonic development. However, if the eddies were shed or if larvae were entrained in open ocean eddies, larvae could be transported away from the natal site [30, 35]. As for all modes of larval transport, transport in eddies could result in loss or successful dispersal to other populations.

Dispersal in eddies, even if infrequent, could play a significant role in determining the connectivity of benthic populations with patchy distributions (e.g. reef and island fauna). Eddies have the potential to propagate for weeks to months [23, 37, 43] potentially transporting water and larvae hundreds to thousands of kilometers between populations. During this mass transport, high productivity caused by upwelling [2] and residual ‘island mass effects’ [15, 26] in many eddies may enhance growth and survival of larvae [16, 35]. Since the larvae would be transported as an aggregate within the eddy core, high numbers of larvae could be delivered in pulses as an eddy passed a suitable recruitment site [49].

If eddies observed at the surface extend into the deep-sea, they also have the potential to affect dispersal between deep benthic populations in patchy habitats like hydrothermal vents. Eddies interact with the mid-ocean ridge globally (e.g. Walvis Ridge and Mid-Atlantic Ridge [23, 46], Southeast Indian Ridge [13], East Pacific Rise [37]). Multiple eddies generated by wind jets [3, 32, 34] and baroclinic instabilities [3, 17, 25, 55] off of the coast of Central America (Fig 5-1) propagate¹ westward across the East Pacific Rise each year [37]. Most eddies propagate to the west due to the latitudinal variation in the Coriolis parameter, called the β -effect [12, 36]. However, hydrothermal vents are primarily aligned north-south along a ridge axis (e.g. Juan de Fuca, East Pacific Rise, Mid-Atlantic Ridge), so transport between vents due to mean eddy propagation may be unlikely. Transport between vents could still be enhanced by eddies through another mechanism. Should an eddy encompass two or more vent fields at the same time, the swirl² of the eddy could transport larvae between the vent sites if the eddy residence time over the vents is long enough. The Tehuantepec and Papagayo eddies often reached diameters of 100 - 450 km at the surface. If the extent of the eddies were similar at depth, the size would be sufficient to encompass multiple vent fields along the EPR.

However, eddies expressed at the surface are generally considered to be weak at depth. Eddy kinetic energy decreases rapidly with increasing depth (e.g. [45, 50]). Observed current velocities at depth are generally at least an order of magnitude less than those at the surface [33, 40, 51], order 10 cm s^{-1} at 4000 m compared to 100 cm s^{-1} at the surface. Still, these relatively slow current velocities could represent a means for increased dispersal potential in the deep-sea where mean current velocities are typically slow, less than 10 cm s^{-1} .

Recent current observations on the East Pacific Rise (EPR) ridge axis have suggested that the influence of eddies in the eastern tropical Pacific may indeed extend to at least the depth of hydrothermal vents (see Section 4.3.5). An episode of strong current velocities measured on the ridge axis (2500 m depth) was coincident with the observation of a large ($> 200 \text{ mm}$) positive sea level anomaly (SLA). However, the connection between the surface and near-bottom observations was tentative because of the vertical distance separating the observations, and because the near-bottom current velocities suggested a cyclonic eddy while the SLA suggested an anticyclonic

¹Propagate refers to movement of the eddy as a whole.

²Swirl refers to the tangential current velocity associated with the clockwise or counterclockwise rotation of the eddy.

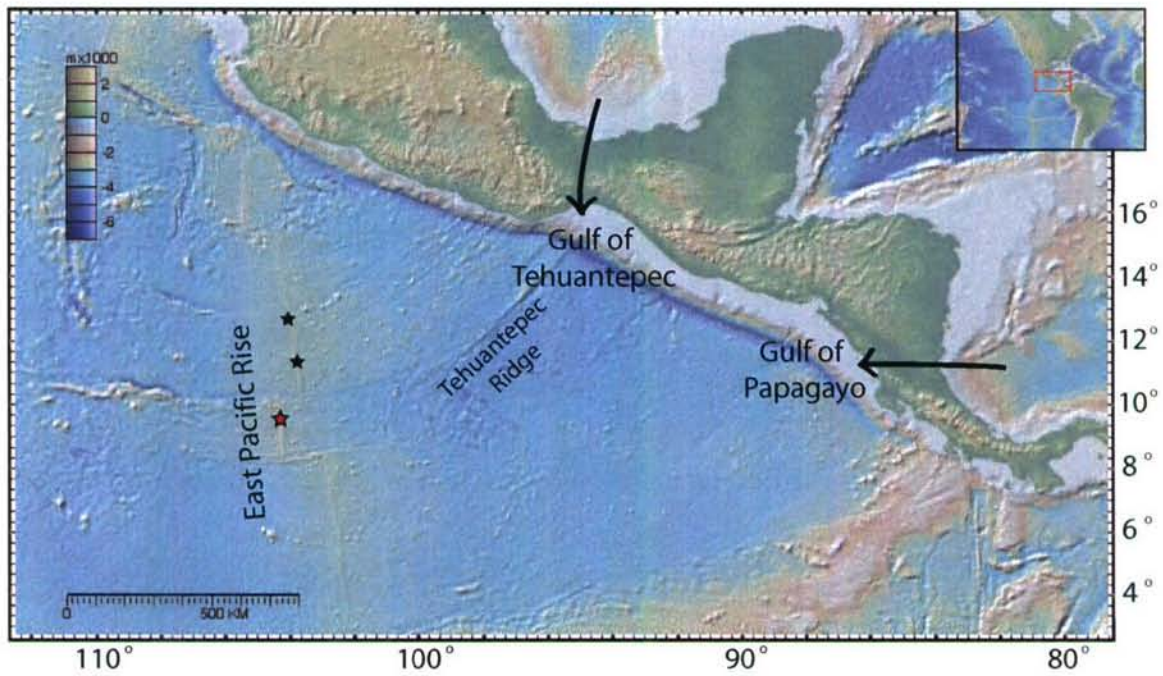


Figure 5-1: Topography of Central America and bathymetry of the East Pacific. Arrows indicate the location of two mountain-pass jets near the Gulfs of Tehuantepec and Papagayo. Wind jets are formed when high pressure develops over the Gulf of Mexico causing air to flow rapidly through the passes down the pressure gradient. The bathymetry shows the Tehuantepec Ridge and East Pacific Rise. The 9° N, 11° N and 13° N vent fields are noted as stars. The location of near-bottom observations on the ridge is denoted by the red star. Map created in GeoMapApp.

eddy. Observations of eddy-induced current velocities at depth (below 1500 m) are rare but the few reported field observations have shown that eddies formed from current meanders maintained the same sign throughout the water column [11, 33, 52] (e.g. an anticyclonic eddy at the surface was anticyclonic at depth). However, experimental and theoretical studies have shown that an eddy consisting of a vertical dipole (cyclonic in one layer and anticyclonic in another layer, also known as a heton) can be stable as an isolated vortex [27, 28]. Despite the extensive theory and experimental evidence, only a few field observations have confirmed the presence of vertical dipole pairs [41].

The main goal of this study was to investigate the potential for mesoscale eddies to influence the dispersal/retention of hydrothermal vent species. Building upon the near-bottom observations presented in Chapter 4, this chapter considered the interaction between Tehuantepec and Papagayo eddies and the East Pacific Rise (EPR). First, the surface eddy field was characterized with satellite altimetry observations to place the near-bottom observations and subsequent modeling in context. Then, a two layer quasi-geostrophic model of an isolated vortex was employed to investigate the flow in the deep layer and potential for larval transport in these flows. The general dynamics of Tehuantepec and Papagayo eddies in the surface and deep flows were considered with a flat bottom and with actual ridge topography. Model results also were qualitatively compared to near-bottom current observations to determine whether the near-bottom and surface observations were consistent with expected deep flows in the eddy. A tracer was introduced into the model to investigate the potential for particle transport.

5.2 Methods

5.2.1 Observations

The generation and propagation of the surface expression of Tehuantepec and Papagayo eddies were characterized from satellite observation of sea level anomalies (SLA). A time-series of daily SLA was generated for October 2004 to May 2005 using objective analysis of data from four satellites. This period corresponds to the expected period of eddy generation by strong winds blowing through mountain gaps [3, 32, 34] (Fig 5-1). Coastally trapped waves [55] and instabilities in the North Equatorial Current [17, 39] may also contribute to the generation and strengthen-

Abbreviation	Source	Propagation		Radius [km]	Swirl [cm s ⁻¹]	Date of Formation	Date Cross EPR
		Direction	Speed [cm s ⁻¹]				
Teh1	N Tehuantepec	257°	11.2	90	–	10-Nov-04	9-Dec-04
Teh2	Tehuantepec	254°	9.3	175	65	before obs	14-Feb-05
Teh3	Tehuantepec	243°	7.9	140	–	24-Dec-04	see Mixed
Pap (pre-split)	Papagayo	285°	6.9	110	–	21-Dec-04	see Mixed
Pap (post-split)	Papagayo	262°	20.8	195	–	20-Feb-05	see Mixed
Pap + Teh3	Mixed	252°	13.7	250	95	17-Apr-05	3-May-05

Table 5.1: Characteristics of anticyclonic Tehuantepec and Papagayo eddies observed by satellite altimetry concurrent with the period of near-bottom observations, November 2004 - April 2005. Swirl speed estimates were from HYCOM simulations from February 11, 2005 [personal comm. Zamudio, NRL]. Propagation direction is degrees from north.

ing of the eddies. Data from Jason, Topex/Poseidon 2, ENVironmental SATellite (Envisat), and GEOSAT Follow-On (GFO) were merged to achieve mesoscale resolution on a daily time scale. Jason and Topex/Poseidon2 achieve global coverage in 10 days with between-track spacing of 325 km at the equator. Envisat achieves exact track sampling in 35 days providing higher resolution coverage but over a longer time. Data were obtained from the Colorado Center for Astrodynamic Research at http://argo.colorado.edu/~realtime/global_realtime/alongtrack.html for the region between 18° - 6° N and 80° - 110° W. The domain of influence used each day included a mean of 52 (± 5 , standard deviation) satellite tracks, providing sufficient data for characterizing mesoscale variability with confidence. Sea level anomalies were estimated by removing the long term mean (including mean circulation and geoid) from the initial sea surface height (as in [48]). Fields of SLA were determined using objective analysis modified from Carter and Robinson [9] assuming a phase speed of -10 cm s^{-1} . SLA fields were used to characterize the anticyclonic eddies. Cyclonic eddies were weaker, non-coherent features (consistent with previous observations [3, 22, 24, 37]) and thus were not considered in this study. Propagation trajectory and speed were determined by tracking the center (maximum SLA) of each anticyclonic eddy every five days. The radius was estimated as the maximum distance between the center and the largest change in SLA.

Near-bottom observations used in this study for comparison to the satellite observations and the modeled deep flows are described in detail in Chapter 4. Briefly, moorings deployed from November 25, 2004 to April 30, 2005 at two vent sites along the ridge axis at 2500 m depth supported instruments that collected time-series samples of vertical larval flux and measured current velocities at 10 m above bottom (mab) and 170 mab. For the present study, only currents measured at 170 mab

were analyzed because bottom friction and topographic effects may have obscured mesoscale variability in the 10 mab current meters. The distance between the two vent sites, 1.6 km apart, was small relative to the size of an eddy, and the current records from 170 mab were highly coherent between sites (see Section 4.3.1). Thus, only the Aanderaa RCM11 current record at 170 mab from East Wall was considered here. Current records were low-pass filtered [1] over 150 hours to remove diurnal and semidiurnal tidal components and the inertial frequency³ so that mesoscale variability was isolated.

5.2.2 Quasi-Geostrophic Model

A rigid-lid, two-layer quasi-geostrophic model was employed to investigate the effects of an isolated vortex on the currents and transport in the deep-sea. The quasi-geostrophic approximation assumes that the dominant forces, the Coriolis force and the pressure gradient force, balance (geostrophic balance) but accounts for ageostrophic corrections such as the inclusion of topographic effects and non-linear forces associated with the rotation of the vortex. To ensure that non-linear forces are relatively small compared to the Coriolis force and pressure gradient, the Rossby number must be small ($R_o \ll 1$). When the Rossby number is small, the Coriolis force is strong relative to advection. Additionally, topographic elevation must be small compared to the depth of the lower layer, and the depression of the pycnocline must be small compared to the depth of the upper layer. The Coriolis parameter is approximated by $f = f_0 + \beta y$, which assumes that the northward gradient of the Coriolis parameter, β , over the meridional (north-south) length scale, L , is small compared to the Coriolis parameter itself ($\frac{\beta_0 L}{f_0} \ll 1$). Based on these conditions/assumptions, the dimensional quasi-geostrophic equations for two layers were used in the following form, (as in [38] eq. 3.2.34 & 3.2.36)

$$\begin{aligned} q_1 &= \nabla^2 \psi_1 + F_1(\psi_2 - \psi_1) + \beta y, \text{ and} \\ q_2 &= \nabla^2 \psi_2 + F_2(\psi_1 - \psi_2) + \beta y + \frac{f_0}{H_2} b, \end{aligned} \tag{5.1}$$

$$\text{for } F_i = \frac{f_0^2}{g' H_i}, \tag{5.2}$$

³The inertial frequency is equal to $\frac{f}{2\pi}$, where f is the Coriolis parameter; 4.0×10^{-6} Hz (~ 70 h period) at $9^\circ 50' \text{ N}$

where q_i is the potential vorticity, ψ_i is the stream function in each layer i , b is the topographic elevation, H_i is the mean depth of layer i , and g' is the reduced gravity. The stream function gives the direction of flow (along the contours) and the speed (inverse to the spacing between contours). When the flow is geostrophic, ψ is related to pressure as $\psi = \frac{p'}{\rho_0 f_0}$, where p' is the pressure and ρ_0 is the density. The reduced gravity was not an explicit parameter, but was calculated based on the Rossby radius of deformation, R_D , and the relationship $F_1 + F_2 = \frac{1}{R_D}$. The Rossby radius of deformation is the length scale at which buoyancy and rotation effects are comparable. The first term in each of equations 5.1 is the relative vorticity, due to the local currents. The second term takes into account a modified contribution of vertical stretching due to variations in layer-thickness and stratification. The third term represents the planetary vorticity due to variation in the Coriolis force, β , along the meridional length, y . The last term for the lower layer ($i=2$) represents the effect of topography.

From these equations, the zonal (east-west, u_i) and meridional (v_i) velocities in each layer i are given by

$$\mathbf{u}_i = (u_i, v_i) = \left(-\frac{\partial}{\partial y}\psi_i, \frac{\partial}{\partial x}\psi_i\right) \quad (5.3)$$

where \mathbf{u}_i is the velocity.

The two-layer equations were originally programmed in Fortran-77 by Bill Dewar [14] and modified by G.R. Flierl [20]. Friction was not explicitly modeled (and no bottom friction was included), but an exponential wavenumber cutoff filter [7] was employed to dampen variability at small spatial scales, similar to the effects of frictional viscosity. All simulations were done on an IBM ThinkCentre running UNIX, part of MIT's academic computing system Athena. The vortices were modeled on a 1536 km by 1536 km domain, with periodic boundary conditions and a 3 km grid size.

I set the range of model parameters to generally represent that of Tehuantepec and Papagayo eddies as

$$\begin{aligned} H_1 &= 655 \text{ m}, & H_2 &= 2625 \text{ m} \\ f_0 &= 2.48 \times 10^{-5} \text{ s}^{-1}, & \beta &= 2.20 \times 10^{-8} \text{ km}^{-1} \text{ s}^{-1} \\ R_D &= 90 \text{ km}, & l &\in [50 : 25 : 200] \text{ km} \\ V_1 &\in [-150 : 25 : -50] \text{ cm s}^{-1} \end{aligned}$$

where f_0 is the Coriolis parameter at the center of the domain ($9^\circ 50'$ N), β is the northward gradient of the Coriolis parameter, and l is the e -folding radius (distance at which the amplitude (SLA) has decreased by e^{-1}). $R_D = 90$ km was chosen for this study to represent conditions near the vents at 10° N [10]. The qualitative results were not sensitive to the small difference in R_D between the Gulfs of Tehuantepec and Papagayo, $R_D = 70$ km and 90 km [10], respectively (data not shown). Eddies are initiated with a Gaussian shape with an initial swirl speed, V_i , in each layer i , where $V_i < 0$ is anticyclonic and $V_i > 0$ is cyclonic. These parameters represent strongly baroclinic and moderately non-linear⁴ anticyclonic eddies similar to those observed in the eastern tropical Pacific. Radius and swirl velocities were based on satellite observations (see Section 5.3.1) and published values. Published studies on eddies in the eastern tropical Pacific covered 1979-1980, 1984-85, 1985-86 [34], and 1992-2004 [3, 17, 22, 24, 37, 55] using a variety of techniques: sea surface temperature (advanced very high resolution radiometer, AVHRR), chlorophyll a concentrations (coastal zone color scanner, CZCS, and SEAWiFS ocean color), altimetry, ADCP observations, floats, and dynamic height measurements (Table 5.2). I adopted a set of standard parameters used throughout the experiments unless otherwise noted; *viz.*,

$$l = 100 \text{ km}, \quad V_1 = -75 \text{ cm s}^{-1}, \quad V_2 = 15 \text{ cm s}^{-1}.$$

The lower layer swirl speed was chosen to decrease the radiation of Rossby waves in the lower layer (see Section 5.3.2). A background flow of -5 cm s^{-1} to the west was included in the upper layer to mimic mean flow in the region [18]; no background flow was included in the lower layer. Results were not sensitive to the inclusion of background flow in either layer.

Willett and colleagues [54] suggested that the tropical Pacific eddies are more like frontal-geostrophic eddies than quasi-geostrophic eddies due to the large length scale relative to the radius of deformation and the large depression of the pycnocline relative to the shallow seasonal pycnocline, only 20 - 100 m deep. A quasi-geostrophic approximation was employed here since the $l : R_D$ ratio rarely met the frontal-geostrophic requirement that $l > 3R_D$. Observations of l ranged from 50 - 250 km; the higher end of the range may have been estimates of total radius and thus overestimates of the

⁴The ratio of Rossby numbers associated with nonlinear advection and linear wave propagation, $V_1/\beta l^2$ are moderate between 1 and 5. For example, β is $1.9 \times 10^{-3} \text{ km}^{-1} \text{ d}^{-1}$ at 10° N; V_1 is 65 km d^{-1} ; l is 100 km; Thus, $V_1/\beta l^2 = 3$.

Tehuantepec					
Propagation		Radius [km]	Swirl [cm s ⁻¹]	Data	Ref
Direction	Speed [cm s ⁻¹]			Source	
258°	9-21 (16)	120	–	SST, Color	[34]
–	8.5	150	80	Model	[32]
–	–	50-200	–	SLA	[37]
–	4.7-8	85-200	–	SST, Color	[24]
–	16.7	200	–	SLA, DH	[22]
–	14.6	168	–	Drifters, CTD, SLA	[25]
–	–	100-160	50-100	Model	[55]

Papagayo					
Propagation		Radius [km]	Swirl [cm s ⁻¹]	Data	Ref
Direction	Speed [cm s ⁻¹]			Source	
251°	9-21 (16)	50-190 (140)	70	SST, Color	[34]
~270°	15	–	80	ADCP	[32]
–	11.9	150	110	Model	[32]
~260°	12.6	200	67, 140	Floats	[3]
–	–	50-250	–	SLA	[37]
–	6.8-13.3	85-225	–	SST, Color	[24]

Table 5.2: Characteristics of anticyclonic Tehuantepec and Papagayo eddies from published literature. Propagation direction is degrees from north. SST: Sea Surface Temperature; Color: Ocean Color; SLA: Sea Level Anomaly; DH: Dynamic Height; ADCP: Acoustic Doppler Current Profiler.

e-folding radius. Additionally, the depression of the seasonal pycnocline (~ 100 m) is small compared to the depth of the permanent pycnocline at 500-600 m [18] used here. More importantly here, the frontal-geostrophic approximation assumes an infinitely deep lower-layer, making it inappropriate for questions about flow in the lower layer and interactions with topography. The parameters used here conformed well to the assumptions of the quasi-geostrophic approximation. The largest deviation from the quasi-geostrophic assumptions occurs with the introduction of ridge topography (maximum ridge elevation, 780 m, compared to the lower layer depth, 2625 m).

Ridge topography was modeled from cross-sections of the 9° N segment of the East Pacific Rise. Topographic data from fifteen zonal cross-sections of 256 km of the EPR, obtained using GeoMapApp (<http://www.marine-geo.org>, [8]), were averaged after aligning the ridge axis. Cross-sections were not taken through lines intersecting seamounts. The mean ridge cross-section was projected meridionally in the model domain. Transform faults and lower-order breaks in ridge topography were not in-

cluded. The axial summit trough was smaller than the grid resolution and thus was not included. The 1536 km by 1536 km domain consisted of a flat bottom with depth H , where $H = H_1 + H_2$, and the eastern edge of the ridge topography positioned at the center of the domain extending 256 km to the west, such that the ridge axis (maximum elevation) was 130 km to the west of the domain center. Simulations were run for the reference flat-bottom case (without topography) and with the ridge topography to assess the effect of the ridge on eddy propagation and bottom currents.

Water mass movements in the lower layer were tracked via a tracer. Tracer concentration was initialized in the lower layer with a Gaussian-distribution with e-folding radius, r . The tracer was passively advected in the current velocities simulated in the lower layer, V_2 . Diffusion was not explicitly incorporated, but numerical diffusion contributed to the spread of the tracer.

A series of experiments with the quasi-geostrophic model were performed to investigate the general vertical structure and propagation of the eddies. All experiments had anticyclonic flow in the surface layer. The dynamics of flow in the bottom layer were studied by varying the initial swirl speed in the lower layer, V_2 . Simulations were initiated with anticyclonic flow ($V_2 < 0$), a still layer ($V_2 = 0$), and cyclonic flow ($V_2 > 0$) at depth. Fluid transport in the lower layer was visualized by including tracer patch with a radius $\frac{3}{4}l$ centered at the initial eddy position. Propagation speed and trajectory were first investigated for the reference flat-bottom case for various l and V_1 . Changes in the deep layer flows and surface propagation were then investigated for the ridge topography case. Simulated current velocity records along the ridge axis (at the maximum elevation) were qualitatively compared to the filtered current velocities measured at East Wall at 170 mab.

The potential impact of eddy induced currents on larval transport was considered by introducing small patches of tracer at various positions along the ridge axis. The patches conceptually mimicked production at the 9° N, 11° N, and 13° N vent fields. Tracer patches with an e-folding radius of 10 km were used due to resolution constraints. The spread of the tracer patch along the ridge was recorded over time as an eddy passed over the ridge.

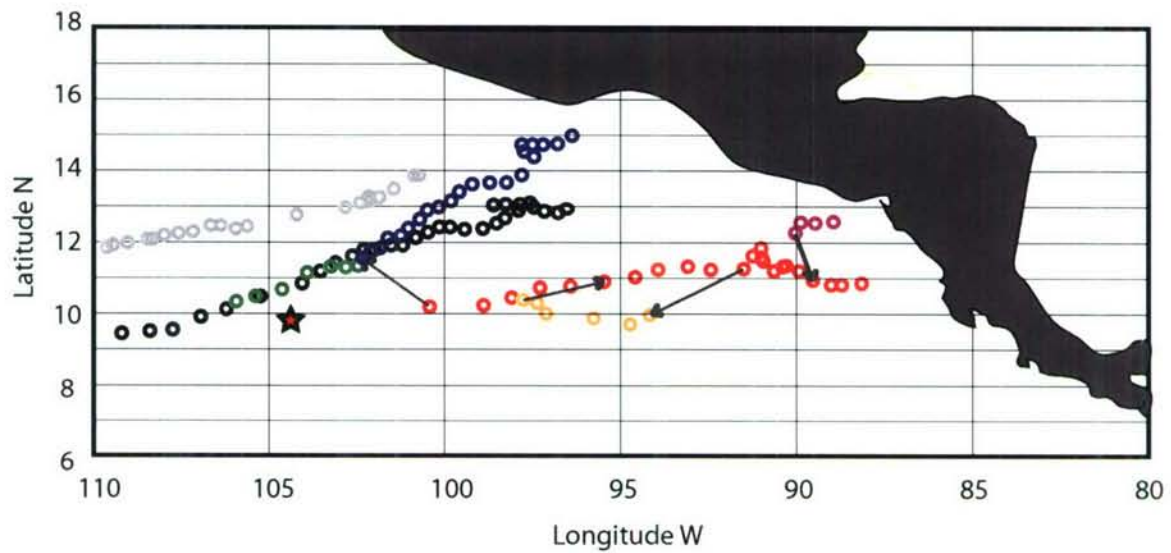


Figure 5-2: Trajectories of the maximum sea-level anomaly (center) of three Tehuantepec eddies (light gray, black and blue) and one Papagayo eddy (red) plotted every 5 days. The Papagayo eddy formed in two locations (purple and red) then merged just off the coast. Fifty days later, the Papagayo eddy split (red and orange), but, the daughter eddy was reabsorbed after another 30 days. The Papagayo eddy merged with one of the Tehuantepec eddies (blue), the resultant mixed eddy is tracked in green. Arrows indicate the direction of absorption between two eddy centers. The location of the near-bottom observations is denoted by the red star.

5.3 Results

5.3.1 Sea Surface Observations

Sea level anomalies indicative of four anticyclonic eddies were observed by satellite altimetry during the period of near-bottom observations, Nov 2004 - Apr 2005 (Fig 5-2). A weak eddy (Teh1), SLA < 10 cm, formed to the north of the Gulf of Tehuantepec in October 2004. Teh1 crossed the EPR near 13° N at the end of November during the first two weeks of near-bottom observations, after which it quickly strengthened and propagated westward at 10.4 cm s⁻¹. A second Tehuantepec eddy (Teh2) formed in the Gulf of Tehuantepec before the observation period began, but did not strengthen until December. Teh2 began crossing the EPR near 11° N at the end of January, but did not cross over 9° N until 10 days later due to the offset in the ridge axis. It took a month and a half to completely cross the EPR. A third Tehuantepec eddy (Teh3) formed at the end of December at approximately the same time as a Papagayo eddy. One eddy formed in the Gulf of Papagayo while another eddy formed ~150 km to the north. The northern eddy was rapidly absorbed into the Papagayo eddy (Pap). Pap split in the middle of February into two rings. The daughter ring was short-lived and began reabsorption into Pap by mid March. Teh3 began influencing the Papagayo eddies as the daughter ring was reabsorbed. Pap and Teh3 merged into a very large eddy (20 cm SLA contour spanning > 600 km) in mid-April as Teh3 began crossing the EPR. The mixed eddy followed the trajectory of Teh3 with only a slight deviation in trajectory when the eddies merged. The mixed eddy began crossing the 9° N segment during the last week of near-bottom larval and current observations.

Two Tehuantepec and the mixed eddy potentially crossed the EPR ridge axis during the near-bottom current observations. Only one eddy, Tehuantepec eddy - Teh2, completely crossed over the study site (9° 50') on the EPR during the period near-bottom observations. Teh2 crossed the ridge just before the large current anomalies were observed on the ridge axis during weeks 14-17 (Fig 4-4). Teh1 passed just to the north of the study site at the beginning of the near-bottom observations but was not evident in the SLA time-series presented in Chapter 4 (Fig 4-10); however, strong near-bottom current velocities observed during the first two weeks may have been due to Teh1. The mixed eddy (Teh3 + Pap) began crossing the ridge during the last week of near-bottom observations.

5.3.2 Quasi-Geostrophic Model

Currents in the Deep

For an eddy with standard parameters, geostrophic cyclonic features developed in the lower layer independent of initial conditions in the lower layer. Initial current conditions for the lower layer, V_2 , were determined over a range of -20 to 20 cm s^{-1} , with no topography. Initial anticyclonic flow ($V_2 \in [-20:5:-5] \text{ cm s}^{-1}$) in the lower layer decayed through the rapid radiation of Rossby waves (Fig 5-3). Rossby waves were seen as ageostrophic flows quickly propagating westward, dissipating the anticyclonic vorticity. A cyclone formed in place of the anticyclone and strengthened as it propagated as a coherent feature (Fig 5-3). Initiation of a still lower layer ($V_2 = 0$) developed into paired vortices with an anticyclone to the west and a cyclone to the east (data not shown). The anticyclone again radiated as Rossby waves, leaving a cyclonic eddy in the lower layer associated with the anticyclonic eddy in the surface layer. A weaker anticyclonic feature formed in the wake of the cyclonic eddy. V_2 was optimized to reduce the radiation of Rossby waves, because the development of the anticyclonic feature in the wake could have been due to the Rossby waves wrapping around the domain. Cyclonic flow of 15 to 20 cm s^{-1} reduced the radiation to near zero. The cyclone propagated as a cohesive geostrophic feature and transported tracer within its core (data not shown). The anticyclonic feature still developed in the wake of the cyclone but developed more slowly (Fig 5-4). All subsequent simulations were performed with an initial cyclonic swirl speed $V_2 = 15 \text{ cm s}^{-1}$, unless otherwise noted.

Propagation

Variation of the radius, l , and swirl speed, V_1 , from the standard parameters resulted in different propagation trajectories and speeds. Increasing the radius increased the trajectory angle⁵ and increased the propagation speed (Fig 5-5a). Increasing the swirl speed resulted in decreased trajectory angle and increased propagation speed (Fig 5-5b). Propagation speeds ranged from 11.2 - 16.2 cm s^{-1} , within the range of observed propagation speeds (Tables 5.2 and 5.1). Trajectory angles varied between 246° and 254° , within the range observations for Tehuantepec eddies but not for Papagayo eddies (Tables 5.1 and 5.2).

The upper and lower layers did not propagate as a cohesive unit. For an eddy with

⁵Trajectory angle was measured from north.

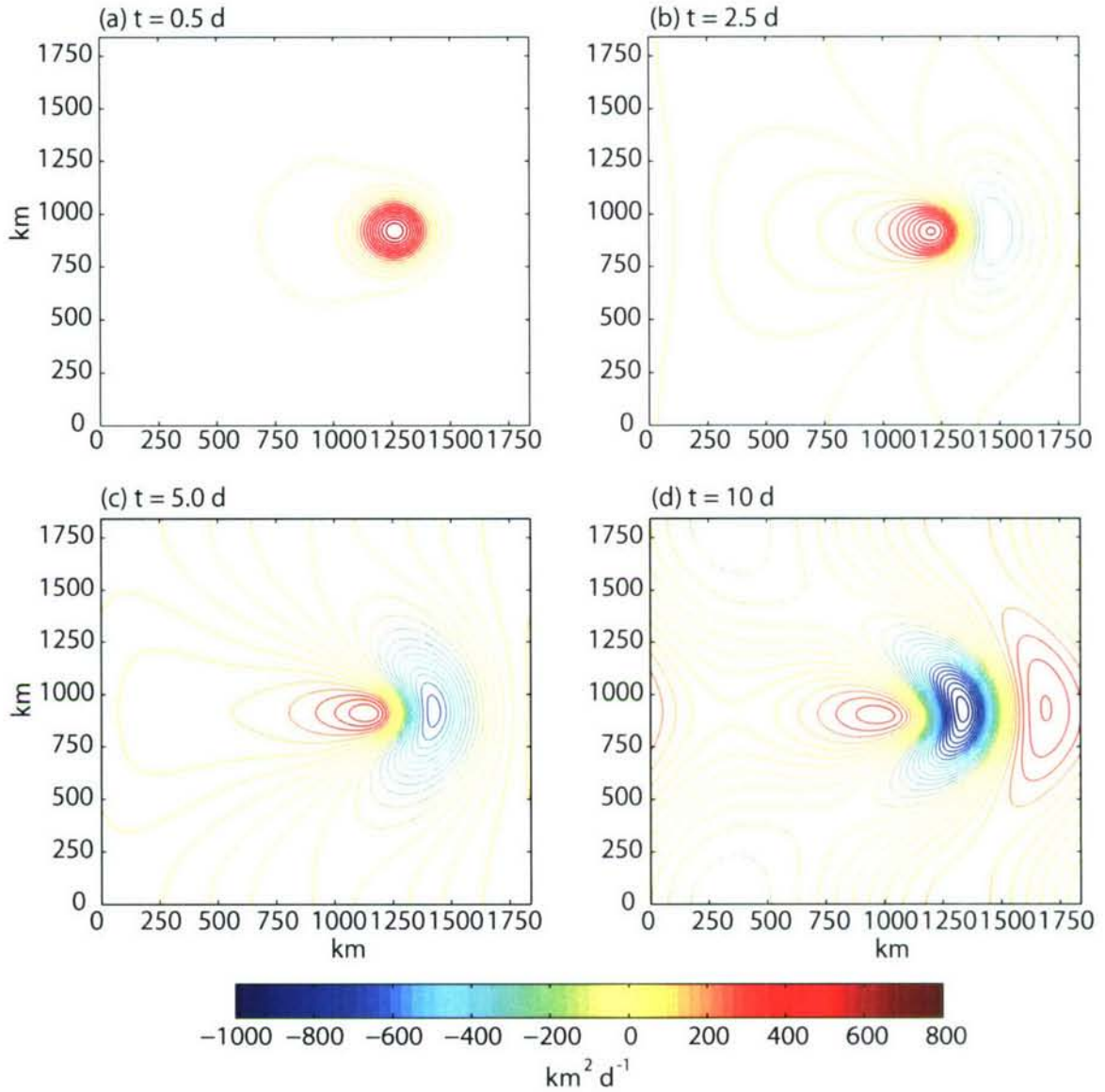


Figure 5-3: Contours of the stream function in the lower layer $\psi_2(x, y, t)$ using standard upper layer parameters and an initial anticyclonic swirl $V_2 = -5 \text{ cm s}^{-1}$ in the lower layer at (a) $t = 0.5$ d, (b) $t = 2.5$ d, (c) $t = 5$ d, and (d) $t = 10$ d. Note the rapid decay and propagation of the initial anticyclonic feature (positive ψ - warm colors) and the development and strengthening of a cyclonic feature (negative ψ - cool colors). The contour interval was $50 \text{ km}^2 \text{d}^{-1}$ for all plots.

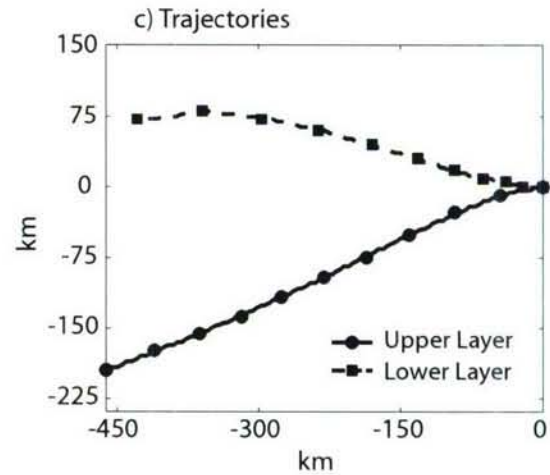
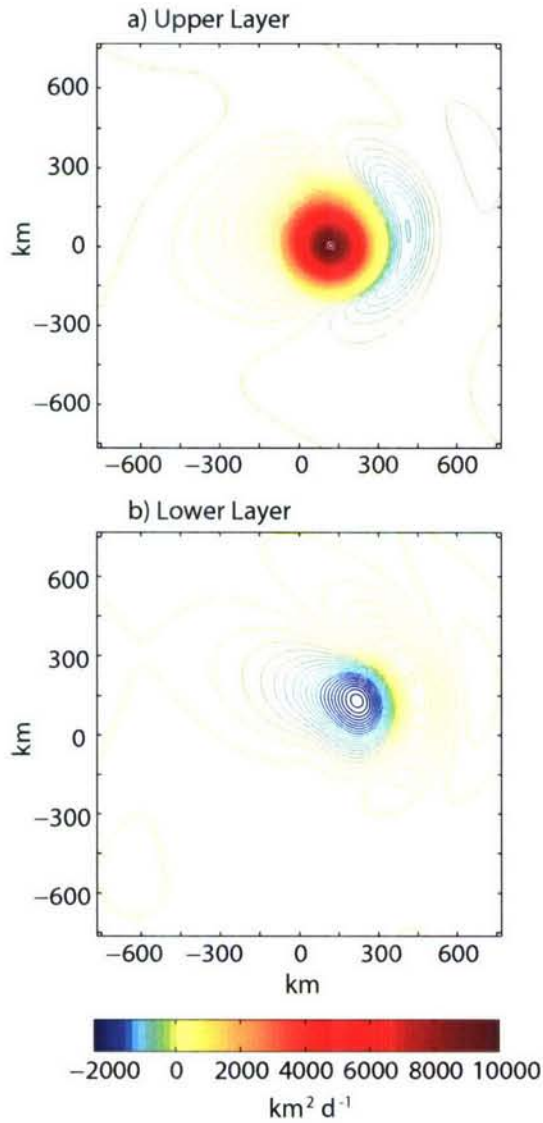


Figure 5-4: Contours of the stream function at day 25 in the upper (a) and lower (b) layers using standard parameters. Note the offset between the centers of the surface anticyclone and the cyclone at depth. The contour interval was $125 \text{ km}^2 \text{ d}^{-1}$ for both plots. (c) Trajectories of the spatial maximum of ψ in the upper layer (solid line, circles) and of the spatial minimum lower layer (dashed line, square) over 50 days. Dots indicate positions every $\Delta t = 5.0 \text{ d}$.

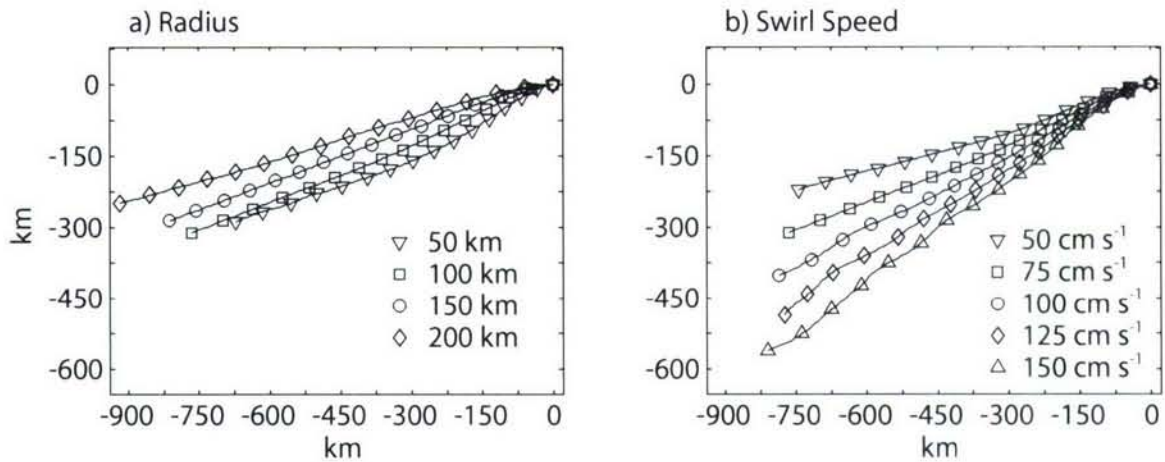


Figure 5-5: Trajectories of the spatial maximum for ψ_1 in the upper layer over 75 days for standard parameters varying (a) e -folding radius, l , and (b) swirl speed, V_1 . Symbols mark every 5 days.

standard parameters, the upper layer propagated west-southwest (248°) at 11.5 cm s^{-1} , while the lower layer propagated more slowly (6.2 cm s^{-1}) in the direction of 282° (Fig 5-4c). After 25 days of propagation, there was a distinct lag between the cyclone in the lower layer and the anticyclone in the upper layer (Fig 5-4a, b). Despite the differences in trajectories, the spatial extent of the vortices in the upper and lower layers overlapped continuously.

Topographic Effects

Introduction of topography only subtly changed propagation and swirl speed of the surface vortex. Using standard parameters, propagation speed decreased from 12.9 cm s^{-1} to 12.8 cm s^{-1} with the addition of topography, close to the limit of detection based on grid size. The trajectory also changed only slightly from 249.4° over a flat bottom to 249.7° over the ridge (Fig 5-6a), again close to the limit of detection based on grid size. Ridge topography had a larger effect on the swirl speed. When the eddy began interacting with the ridge topography ($t \simeq 35 \text{ d}$), the maximum absolute swirl speed decreased. Once the center of the eddy crossed the ridge axis on $\sim \text{day } 50$, the maximum absolute swirl speed increased again (Fig 5-6b).

Topography altered the cyclonic eddy in the lower layer (Fig 5-7) compared to the reference flat bottom (Fig 5-8). The cyclone became elongated along the ridge and deflected towards the south upon initial contact with the topography. On the eastern ridge flank, the topography compressed the fluid which added anticyclonic vorticity.

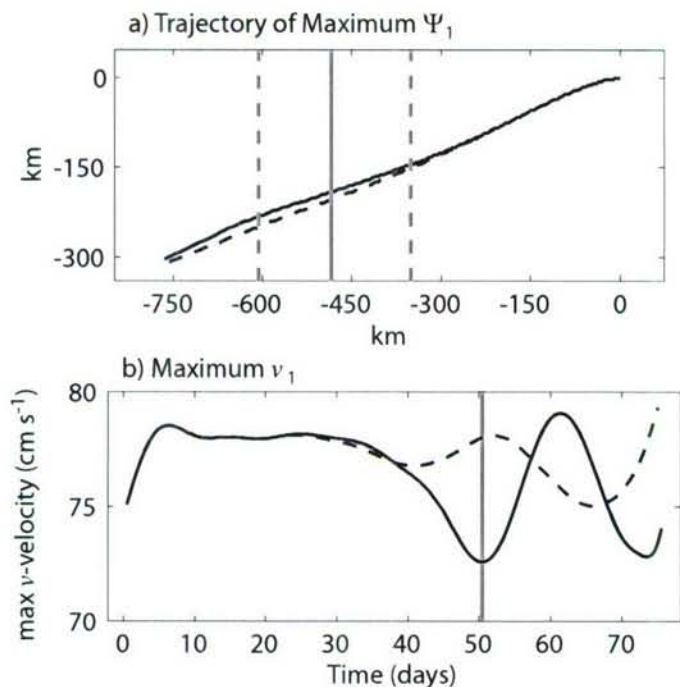


Figure 5-6: (a) Trajectories of the spatial maximum of ψ_1 , upper layer, over 75 days for standard parameters with (solid line) and without (dashed line) ridge topography. Solid gray line denotes the ridge axis. Dashed gray lines denote the extent of the ridge topography. (b) Maximum meridional velocity, v_1 , over time in the upper layer over 75 days for the standard parameters with (solid line) and without (dashed line) ridge topography. Solid gray line denotes approximate time when the center of the anticyclone was over the ridge axis.

The anticyclonic vorticity weakened the cyclone and later strengthened the trailing anticyclone. Contours of the stream function showed the propagation of the northern half of the cyclone over the ridge, leaving a southern portion on the eastern side of the ridge (Fig 5-7c, d). The tracer indicated that the core of the cyclone deformed but did not split (Fig 5-9). The tracer was transported over the ridge in a coherent mass with deformation from elongation and stretching induced by the ridge. The tracer trajectory did not significantly deviate from the reference tracer trajectory in the flat bottom case (Fig 5-10). The water mass elongated along the ridge to the south was likely from the annulus of the eddy surrounding the core [47]. Once over the ridge axis, the decrease in elevation added cyclonic vorticity and strengthened the cyclone (Fig 5-7 e, f).

Simulated current velocities along the ridge for the standard parameters were compared to observed near-bottom current velocities (Fig 5-11). The direction of the current velocities corresponded well between the two records. The simulated current velocities were stronger when northward, during weeks 16 to 19 as the trailing edge of the cyclone passed the ridge, than when southward, during weeks 12 to 15 as the leading edge of the cyclone passed the ridge. Strong simulated southward current velocities during weeks 20 and 21 were associated with the anticyclone in the wake

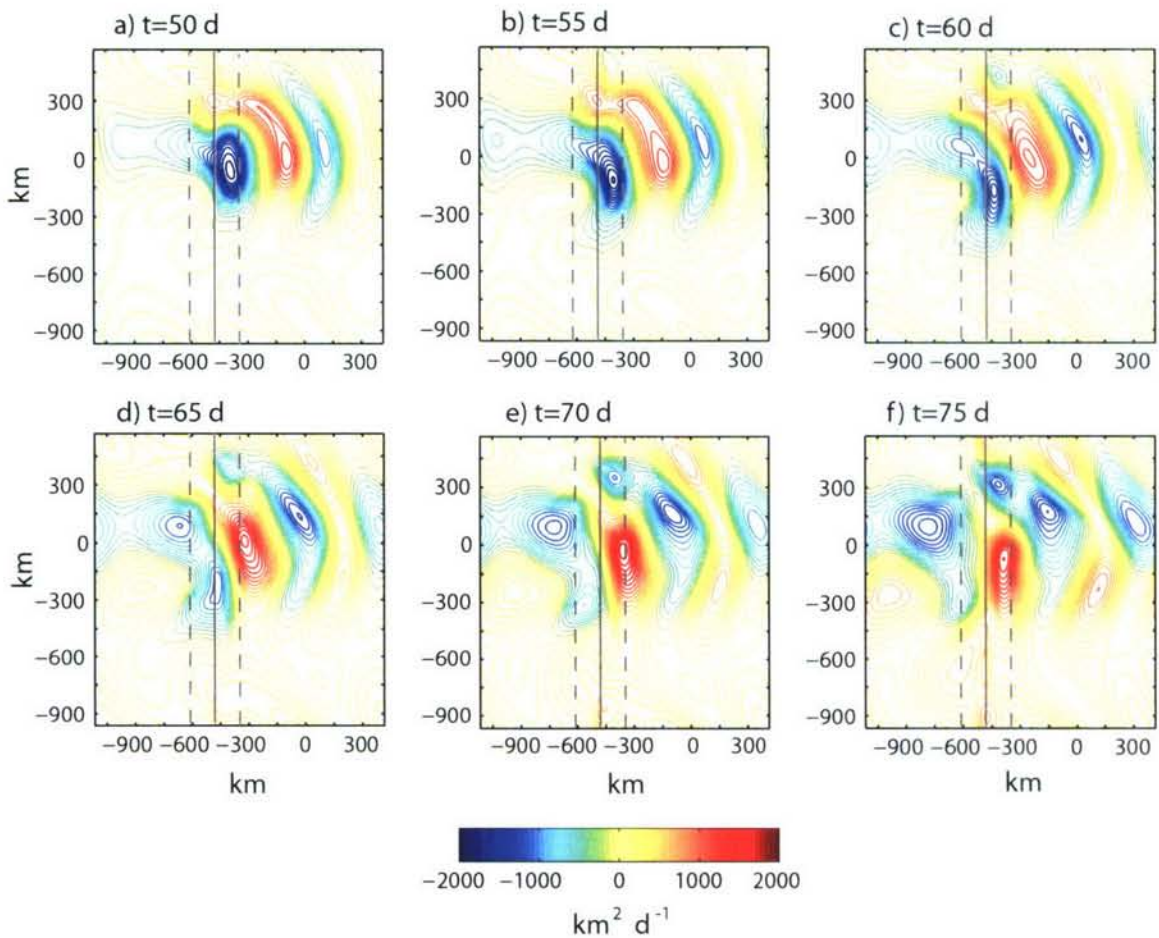


Figure 5-7: Plan views of the stream function in the lower layer ψ_2 showing the evolution of the cyclone (dark blue) with standard parameters as it crosses the ridge topography every 5 days from day 45 to day 70. Anticyclones and cyclones develop to the east in the eddy wake. The contour interval was $100 \text{ km}^2 \text{ d}^{-1}$ for all plots. The solid gray line denotes the ridge axis. The dashed gray lines denote the extent of the topography.

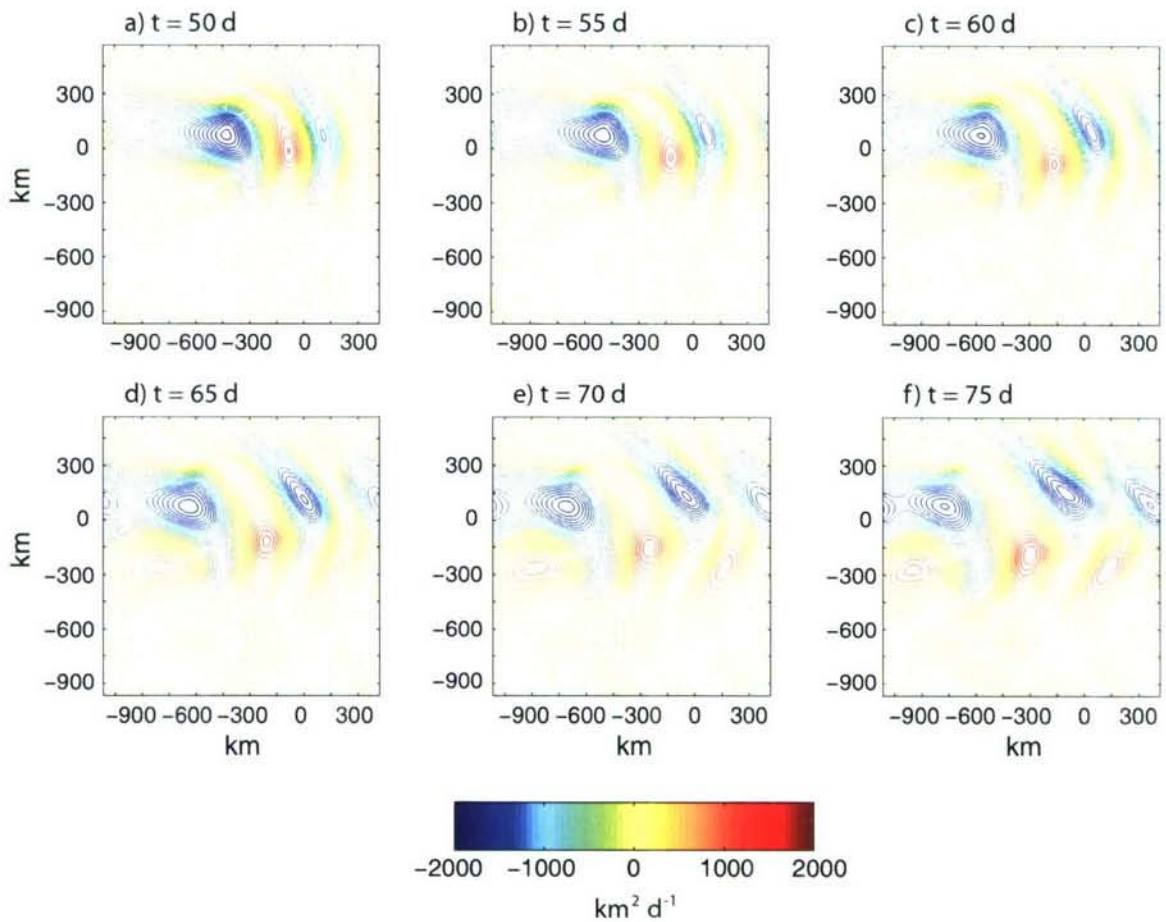


Figure 5-8: Plan views of the stream function in the lower layer ψ_2 showing the evolution of the cyclone (dark blue) with standard parameters over a flat bottom every 5 days from day 45 to day 70. Anticyclones and cyclones develop to the east in the eddy wake. The contour interval was $100 \text{ km}^2 \text{ d}^{-1}$ for all plots.

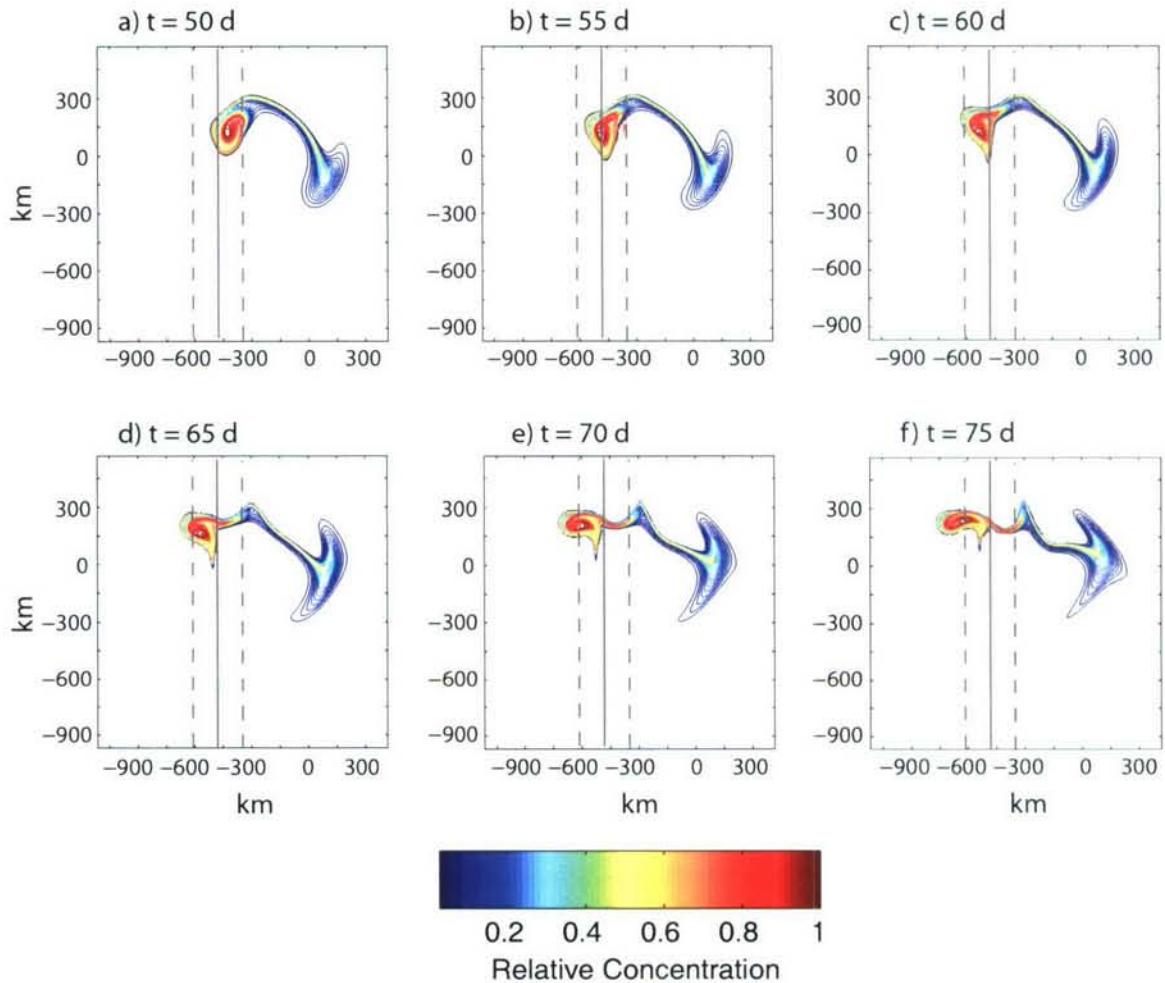


Figure 5-9: Plan views of the concentration of tracer (normalized to the maximum) in the lower layer showing the movement of water in the cyclone core as it crosses the ridge every 5 days from day 45 to day 70. Some tracer was not transported within the cyclone, leaving a trail of tracer with low concentration (cool colors) compared to tracer in the core (warm colors). The contour interval is 0.025 for all plots. The solid gray line denotes the ridge axis. The dashed gray lines denote the extent of the topography.

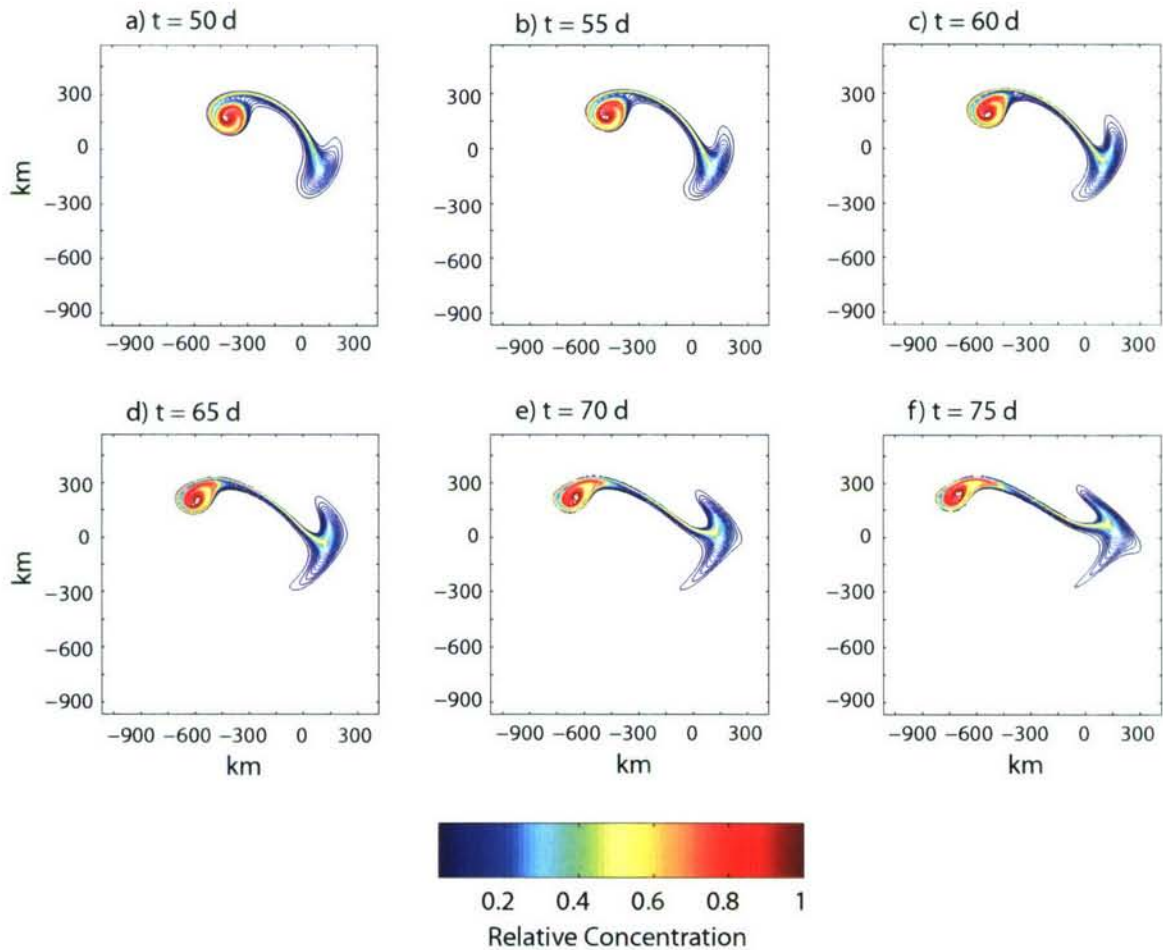


Figure 5-10: Plan views of the concentration of tracer (normalized to the maximum) in the lower layer showing the movement of water in the cyclone core over a flat bottom every 5 days from day 45 to day 70. Some tracer was not transported within the cyclone, leaving a trail of tracer with low concentration (cool colors) compared to tracer in the core (warm colors). The contour interval is 0.025 for all plots.

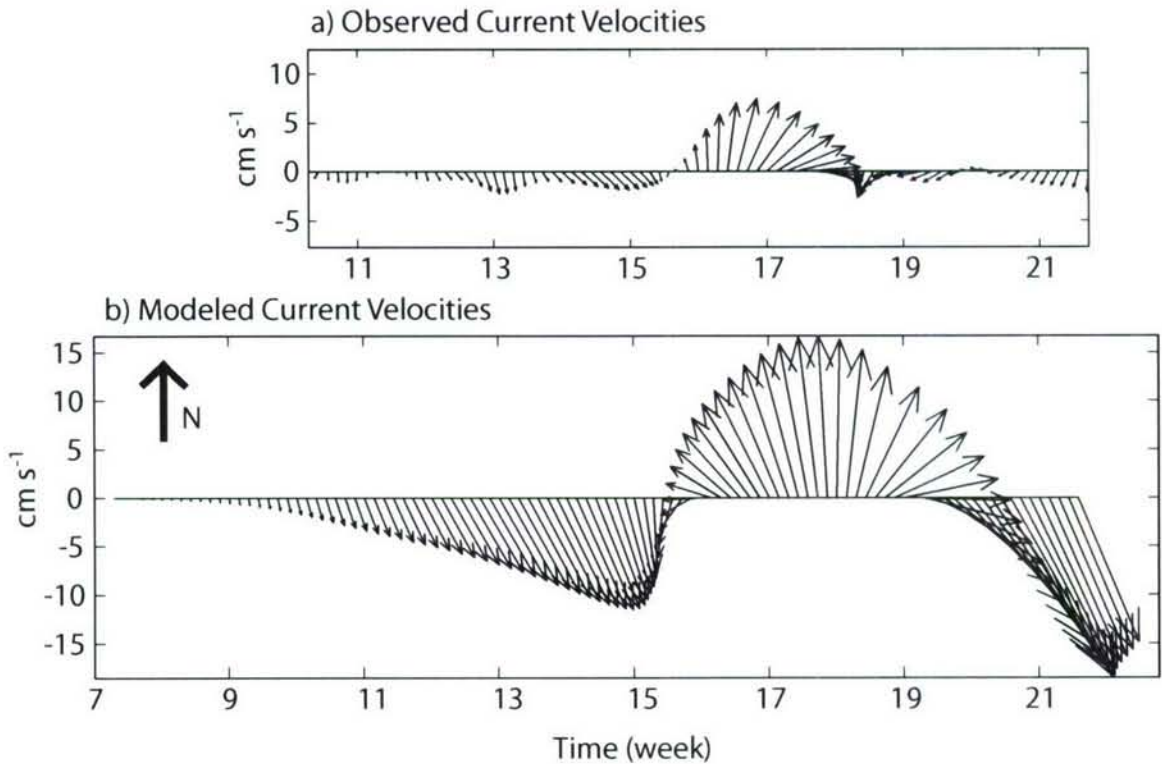


Figure 5-11: (a) Observed current velocities at East Wall 170 mab low-pass filtered, cut off 150 hours compared to (b) modeled current velocities.

of the cyclone. The observed current velocities also were stronger when northward, during weeks 16 to 18 as the trailing edge of the cyclone passed the ridge, than when southward, during weeks 13 to 15 as the leading edge of the cyclone passed. Simulated current velocities were overall higher than observed current velocities by 5 to 10 cm s⁻¹. The simulated northward current anomaly also lasted approximately twice as long as the observed anomaly.

Tracer Dispersal

Larval dispersal potential was assessed by advecting tracer patches placed at various locations along the location of the ridge axis, with ridge topography (Fig 5-12 & 5-14) and with a flat-bottom (Fig 5-13 & 5-15), in an eddy with standard parameters. The end result for tracer within the influence of an eddy crossing ridge topography was dilution and displacement off of the ridge axis. However, before final transport off of the ridge axis some of the tracer was advected more than 100 km along the ridge axis. Transport of the tracer depended on the initial position relative to the path of the cyclone (Fig 5-12 & 5-14). Tracer patches were initially positioned on the ridge axis at

the center of the eddy's path, and 100 km to the north and south of the eddy's path. For the flat-bottom case, tracer returned to the initial longitudinal position only for the patch positioned 100 km to the north of the eddy center (Fig 5-13). When ridge topography was included, the tracer patches were sheared and portions returned to the ridge axis (Fig 5-12 & 5-14). The tracer patch initially near the center of the eddy was first sheared to the southeast and advected to the south with a large portion of the tracer remaining on the ridge. Tracer was sheared and advected southward a maximum of ~ 250 km from the release point. The trailing edge of the eddy then advected the tracer back to the north and west, bringing a large concentration of tracer back onto the ridge axis. The tracer patch 100 km to the south of the center also was advected initially to the south and east. Tracer was quickly transported off axis, partially because the patch was not sheared as much by the slower swirl speeds in the periphery of the eddy core. Tracer was quickly advected to the north then west and a large 'blob' was brought back onto the ridge ~ 150 km to the north of the starting point. The tracer patch released 100 km north was advected off axis in strong westward currents. A thin and dilute filament of tracer was advected back onto the ridge initially ~ 100 km north of the starting point and then extended southward to ~ 50 km south of the starting point.

5.4 Discussion

5.4.1 Applicability to Tehuantepec and Papagayo Eddies

Despite the simplifications associated with the quasi-geostrophic model, the propagation characteristics of simulated eddies were similar to surface observations of Tehuantepec eddies. Propagation speeds were faster than those observed in the satellite time-series in this study but were within the range of observations in the literature. The simulated trajectories were generally oriented more to the south, but by less than a 5° difference in direction. Interactions with the Tehuantepec Ridge topography (Fig 5-1) may account for this minor discrepancy in trajectory angle.

Simulated eddies did not correspond as closely to surface observations of Papagayo eddies. Papagayo eddies of all sizes were observed to propagate almost directly west with little to no southward displacement. Eddies simulated with parameters in the range of observations propagated west-southwest due to non-linear dynamics. Eddies propagated more westerly as the radius increased and/or the swirl speed decreased

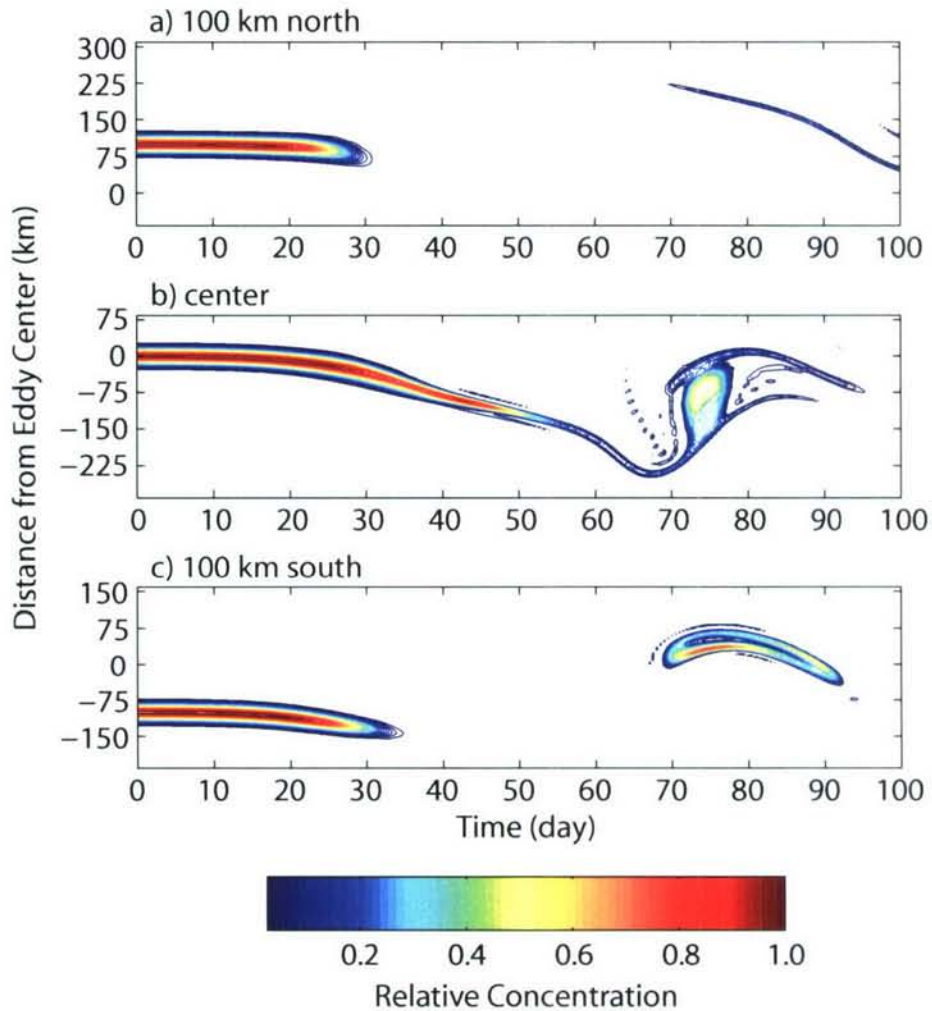


Figure 5-12: Time-series of the concentration of tracer, relative to the initial maximum, on the ridge axis for tracer patches starting on the ridge axis (a) 100 km to the north of the center of the eddy path, (b) at the center of the eddy path, and (c) 100 km to the south of the center of the eddy path. The eddy was modeled using the standard parameters.

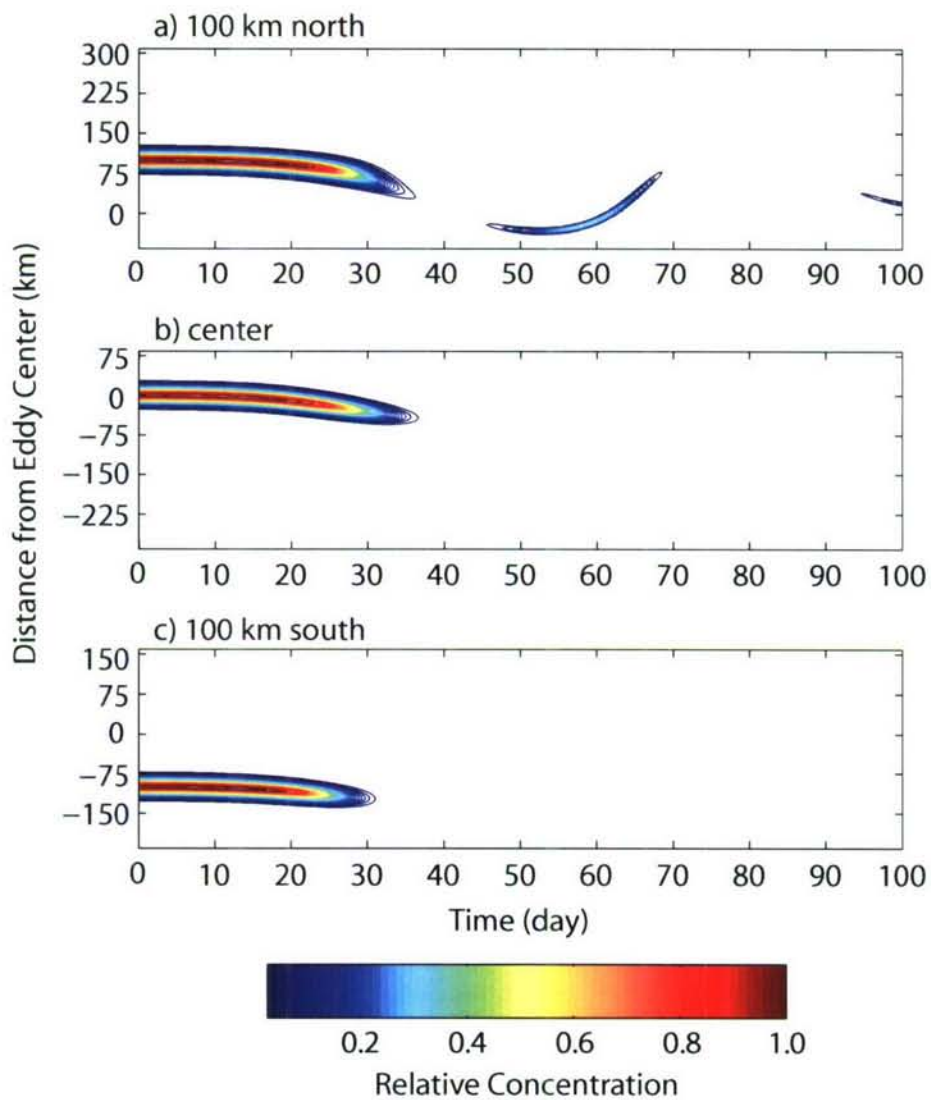


Figure 5-13: Time-series of the concentration of tracer over a flat-bottom, relative to the initial maximum, at the same location as the ridge axis in Figure 5-12 for tracer patches starting (a) 100 km to the north of the center of the eddy path, (b) at the center of the eddy path, and (c) 100 km to the south of the center of the eddy path. The eddy was modeled using the standard parameters.

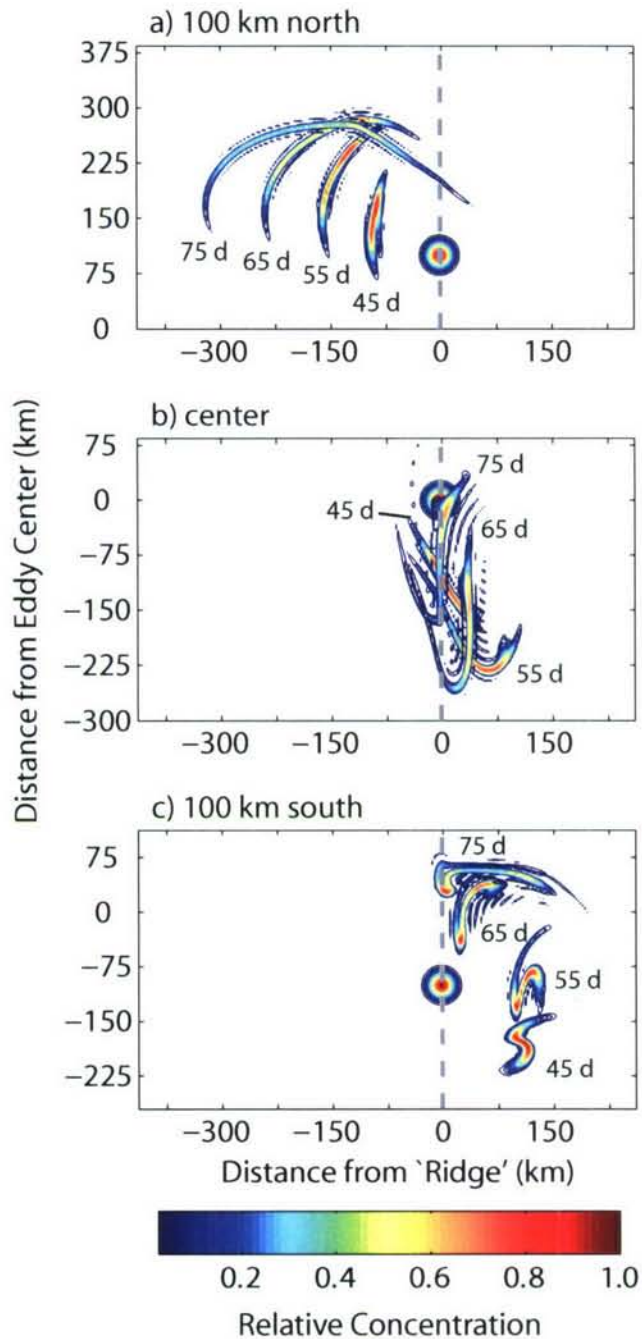


Figure 5-14: Spatial distribution of tracer patches over ridge topography at their initial position and every 10 days from day 45 to day 75. Tracer patches had starting positions on the ridge axis (a) 100 km to the north of the center of the eddy path, (b) at the center of the eddy path, and (c) 100 km to the south of the center of the eddy path. The eddy was modeled using the standard parameters.

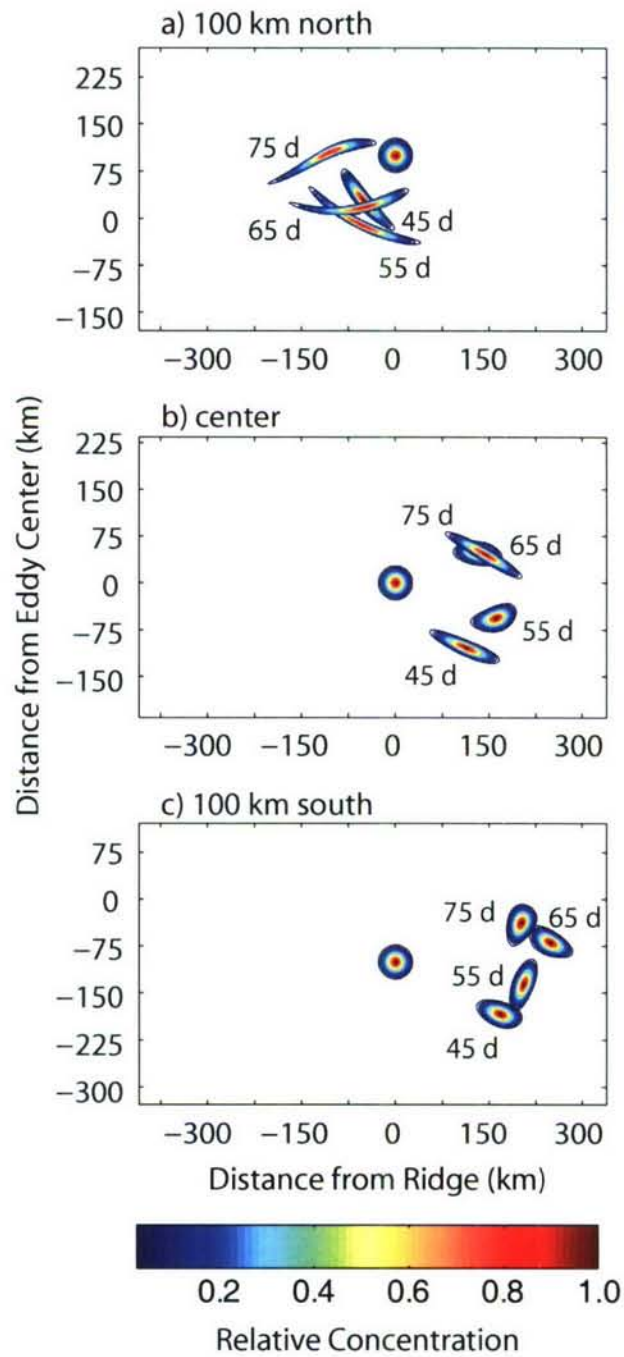


Figure 5-15: Spatial distribution of tracer patches over a flat bottom at their initial position and every 10 days from day 45 to day 75. Tracer patches had starting positions at the same location as the ridge axis in Figure 5-14 (a) 100 km to the north of the center of the eddy path, (b) at the center of the eddy path, and (c) 100 km to the south of the center of the eddy path. The eddy was modeled using the standard parameters.

(Fig 5-5), i.e. as the eddies became more linear. However, observations of Papagayo eddies do not suggest that these are weak, linear eddies. The length scale and swirl speeds were comparable to those of Tehuantepec eddies.

Surrounding currents may be influencing the propagation and dynamics of Papagayo eddies. The quasi-geostrophic model utilized here included a weak background flow to the west at 5 cm s^{-1} , but otherwise assumed minimal influence by the surrounding fluid. However, baroclinic instabilities in the North Equatorial Counter Current (NECC) and the Costa Rica Coastal Current (CRCC) have been proposed to greatly influence the development of Tehuantepec and Papagayo eddies [3, 17, 39, 55]. Generation of Papagayo eddies occurs closer to the NECC and thus may be influenced more by variations in the NECC compared to Tehuantepec eddies. Interactions with the NECC may limit the southward movement of Papagayo eddies. Additionally, interactions with the unstable NECC may account for the stretching, splitting, and merging of Papagayo eddies during the satellite observations (Fig 5-2). Similar eddy instability was not observed in the Tehuantepec eddies which were further north of the NECC. Due to the discrepancies between the model results and observations of Papagayo eddies, the remaining discussion is likely more applicable to the case of Tehuantepec eddies.

5.4.2 Vertical Structure

Simulated eddies formed vertical dipoles with flows in each layer acting largely independent of each other. The surface layer maintained the initial anticyclonic eddy, while the lower layer developed a cyclonic eddy. Dimensional analysis using the Burger number ($\text{Bu} = (\frac{NH}{fl})^2 = (\frac{R_D}{l})^2$), where N is the buoyancy frequency, is useful in determining the relative contributions of vorticity and vertical stretching to the flow. For an eddy with standard parameters, $R_D = 90 \text{ km}$ and $l = 100 \text{ km}$, vorticity and vertical stretching contribute roughly equally to the dynamics of the flow. The flow is partially barotropic, as evidenced by the development of flow in the lower layer and changes in swirl speed in the upper layer over topography. However, the flow has a strong baroclinic component, as the layers are also partially decoupled by the stratification; flow in the deep layer is the opposite direction and the trajectories of the anticyclone and cyclone deviate from each other.

Although dipole vortices have not been observed in eddies formed from current meanders [11, 33, 52], their presence in simulated Tehuantepec eddies is surprising

in the context of ring observations but is consistent with geophysical fluid dynamic theory. Flierl and colleagues [21, 19] proposed the ‘no net angular momentum theory’ in which a slowly varying, isolated disturbance on the beta plane must have zero net relative angular momentum to satisfy

$$\beta \int \int \psi = 0. \quad (5.4)$$

Therefore, an isolated feature should consist of both negative and positive potential vorticity. The simplest way to achieve this condition on a β -plane is via a dipole. Although the theory was initially applied to barotropic vortices with horizontal (2-D) dipoles, vertical dipoles such as those observed in this study also satisfy the condition for baroclinic vortices. Furthermore, Flierl et al [21] argued that barotropic Rossby waves would be generated to dissipate any unbalanced angular momentum. Simulations in the present study showed that all initial anticyclonic flows in the lower layer were quickly radiated as barotropic Rossby waves. Cyclonic flow in the lower layer was relatively stable over the multiple months of simulation, likely due to the balance with the anticyclonic flow in the upper layer. The modeled cyclonic eddy was a coherent structure able to carry a patch of tracer within its core with minimal loss. Since equation 5.4 is dependent upon β , one would expect monopoles on a f -plane (where β is zero) to be stable. Indeed, when β was set to zero, the anticyclonic flows in the deep layer were stable as a monopole and did not radiate as Rossby waves (data not shown).

The primary mechanism proposed for the generation of Tehuantepec and Papagayo eddies is consistent with the development of a vertical dipole pair (heton). Wind jets initially generate a pair of anticyclonic and cyclonic eddies on either side of the jet [32] creating a horizontal dipole. However, upwelling along the coast virtually eliminates the cyclonic eddy through entrainment and by limiting the layer thickness [32]. I speculate that a cyclonic eddy may then develop in the lower layer to satisfy the no net angular momentum theory. Vertical stretching as the eddy moves off of the shelf may further contribute to the development of the cyclonic eddy at depth.

The model results supported the hypothesized connection between the observed cyclonic current velocities near-bottom and the anticyclonic Tehuantepec eddy (Teh2) on the surface. Both the model and observations were consistent with a vertical dipole with anticyclonic flow in the upper layer and a slightly lagged cyclonic flow in the lower layer. Additionally, the simulated currents at a point on the ridge axis showed

the same asymmetry between the meridional flows with northward flow being stronger than southward flow. However, there were discrepancies between the simulated and observed current velocities. The modeled current velocities were stronger than the observed current velocities. While, the observed current velocities suggested that the cyclone took 4-5 weeks to pass over the ridge, simulated current velocities suggested that the cyclone took much longer, 8-9 weeks, to pass over the ridge. These discrepancies may be due to numerous factors that were not included in the model. For example, the differences in translation speed in the lower layer may have been because the lower layer did not include a mean background flow. Alternatively, Teh2 may have been influenced by the mixed eddy (Teh3 + Pap) that passed shortly thereafter (Fig 4-10). The Tehuantepec Ridge could have influenced the cyclone to move further south rather than to the north. Despite these differences, the major conclusion that the cyclone at depth was associated with the surface Tehuantepec anticyclone remains extremely plausible. This would then represent one of only a few field observations of hetons (vertical dipoles) that are hypothesized to be important in the transport of heat [27], salinity and particles, including larvae.

5.4.3 Ridge Interactions

The simulated dipole eddies interacted with the ridge topography relatively weakly compared to previous studies []. This result differed from previous experiments and modeling which found strong interactions between eddies similar to Agulhas rings interacting with a meridional ridge (e.g. [4, 44, 53]). Depending on the initial starting position and conditions, these previous studies showed that the ridge destroyed, reflected, or trapped the eddies. While deformation of the cyclone in the lower layer was observed in the present experiments, the surface anticyclone crossed the ridge with little deviation in its path and the deep cyclone did cross the ridge after some deformation and weakening. The vertical structure may account for the differences between the present study and some of the Agulhas studies. The Agulhas studies considered barotropic vortices or monopoles with the flow at depth in phase with flow at the surface. Beismann et al [4] found that eddies could cross the ridge if the flow in the lower layer had decayed sufficiently through the radiation of Rossby waves. Kamenkovich and colleagues [29] suggested that baroclinic Agulhas rings could cross ridge topography but barotropic or near-barotropic (little to no shear) could not cross the ridge. The eddies considered here were strongly baroclinic. The shear and decou-

pling between the two layers was likely the primary reason these eddies crossed the ridge with little change in the surface eddy trajectory.

5.4.4 Implications for Dispersal

Mesoscale eddies may have a significant impact on the dispersal of larvae along the East Pacific Rise (EPR). Model results supported the connection between strong currents on the ridge and the passage of a Tehuantepec eddy, suggesting that the influence of the eddies extends to at least the depth of the ridge, and likely to the abyssal seafloor. Simulated current velocities often exceeded 25 cm s^{-1} on the ridge axis, even higher than those already observed. These strong currents could significantly increase the potential dispersal distance of a larva. If larvae act as passive particles, the tracer results can be applied to gain insight into larval dispersal. Interactions with ridge topography enhanced tracer dispersal along the ridge axis through shearing and elongation of the eddy core. The end result of the eddy passing was the loss of the tracer patches from the ridge axis. The modeled loss of tracer is consistent with the observed decrease in larval flux (Chapter 4), and total particulate flux (data not shown), into the sediment traps while eddies passed over the vent sites.

While overall larval abundance at a site may decrease, dispersal between vent fields may be enhanced by the eddies. The observed eddy took over a month to pass and the modeled eddies took even longer. During that time, tracer (larval) concentrations were diluted on the ridge but also were advected in eddy induced currents up and down the ridge, sometimes distances greater than 150 km. Larger eddies have the potential to advect passive particles including larvae even greater distances. Depending on the location of the patch relative to the path of the eddy, the larvae could be advected to the north and/or to the south. Advection due to the eddy would be sufficient to transport, albeit a small proportion of, larvae both directions between the 9° N , 11° N , and 13° N vent fields, approximately 150 to 200 km apart. The benefits of the transport between the vent fields may counterbalance the loss of larvae from the ridge axis.

Bibliography

- [1] Alessi, C., Beardsley, R., Limeburner, R., Rosenfeld, L., Lentz, S. J., Send, E., Winant, C., Allen, J., Halliwell, G., Brown, W., & Irish, J. (1985). CODE-2:

- moored array and large-scale data report. Technical Report WHOI 85-35, Woods Hole Oceanographic Institution.
- [2] Backus, R. H., Flierl, G. R., Kester, D. R., Olson, D. B., Richardson, P. L., Vastano, A. C., Wiebe, P. H., & Wormuth, J. H. (1981). Gulf Stream cold-core rings: Their physics, chemistry, and biology. *Science*, 212(4499):1091–1100.
- [3] Ballestero, D. & Coen, J. (2004). Generation and propagation of anticyclonic rings in the Gulf of Papagayo. *International Journal of Remote Sensing*, 25:2217–2224.
- [4] Beismann, J., Käse, R., & Lutjeharms, J. (1999). On the influence of submarine ridges on translation and stability of Agulhas rings. *Journal of Geophysical Research*, 104(C4):7897–7906.
- [5] Boehlert, G., Watson, W., & Sun, L. (1992). Horizontal and vertical distributions of larval fishes around an isolated oceanic island in the tropical Pacific. *Deep Sea Research Part A. Oceanographic Research Papers*, 39:439–466.
- [6] Bograd, S. J., Rabinovich, A. B., LeBlond, P. H., & Shore, J. A. (1997). Observations of seamount-attached eddies in the North Pacific. *Journal of Geophysical Research. C. Oceans*, 102(C6):12,441–12,456.
- [7] Canuto, C., Hussaini, M., Quarteroni, A., & Zang, T. (1988). *Spectral methods in fluid mechanics*. Springer-Verlag.
- [8] Carbotte, S., Arko, R., Chayes, D., Haxby, W., Lehnert, K., O’Hara, S., W.B.F., R., Weissel, R., Shipley, T., Gahagan, L., Johnson, K., & Shank, T. (2004). New integrated data management system for Ridge2000 and MARGINS research. *EOS*, 85:553, 559.
- [9] Carter, E. & Robinson, A. (1987). Analysis models for the estimation of oceanic fields. *Journal of Atmospheric and Oceanic Technology*, 4:49–74.
- [10] Chelton, D., deSzoeke, R., Schlax, M., El Naggar, K., & Siwertz, N. (1998). Geographical variability of the first-baroclinic Rossby radius of deformation. *Journal of Physical Oceanography*, 28:433–460.
- [11] Clement, A. & Gordon, A. (1995). The absolute velocity field structure of Agulhas eddies and the Benguela Current. *Journal of Geophysical Research*, 100:22591–22601.
- [12] Cushman-Roisin, B., Chassignet, E., & Tang, B. (1990). Westward motion of mesoscale eddies. *Journal of Physical Oceanography*, 20:758–768.
- [13] de Ruijter, W., van Aken, H., Beier, E., Lutjeharms, J., Matano, R., & Schouten, M. (2004). Eddies and dipoles around South Madagascar: formation, pathways and large-scale impact. *Deep-Sea Research I*, 51:383–400.

- [14] Dewar, W. (1983). *Atmospheric Interactions with Gulf Stream Rings*. PhD thesis, Massachusetts Institute of Technology.
- [15] Doty, S. & Oguri, M. (1965). The island mass effect. *Journal du Conseil*, 22:33–37.
- [16] Emery, A. (1972). Eddy formation from an oceanic island: ecological effects. *Caribbean Journal of Science*, 12:121–128.
- [17] Farrar, J. & Weller, R. (2006). Intraseasonal variability near 10° N in the eastern tropical Pacific Ocean. *Journal of Geophysical Research*, 111:doi:10.1029/2005JC002989.
- [18] Fiedler, P. & Talley, L. (2006). Hydrography of the eastern tropical Pacific: A review. *Progress in Oceanography*, 69:143–180.
- [19] Flierl, G. (1987). Isolated eddy models in geophysics. *Annual Review of Fluid Mechanics*, 19:493–530.
- [20] Flierl, G. (1994). Semicoherent oceanic features. *Chaos*, 4:355–367.
- [21] Flierl, G., Stern, M., & Whitehead, J. (1983). The physical significance of modons: laboratory experiments and general integral constraints. *Dynamics of Atmospheres and Oceans*, 7:233–263.
- [22] Giese, B., Carton, J., & Holl, L. (1994). Sea level variability in the eastern tropical Pacific as observed by TOPEX and Tropical Ocean-Global Atmosphere Tropical Atmosphere-Ocean Experiment. *Journal of Geophysical Research*, 99(C12):24,739–24,748.
- [23] Goni, G., Garzoli, S., Roubicek, A., Olson, D., & Brown, O. (1997). Agulhas ring dynamics from TOPEX/POSEIDON satellite altimeter data. *Journal of Marine Research*, 55:861–883.
- [24] Gonzalez-Silvera, A., Santamaria-del Angel, E., Millán-Nunez, R., & Manzo-Monroy, H. (2004). Satellite observations of mesoscale eddies in the Gulfs of Tehuantepec and Papagayo (Eastern Tropical Pacific). *Deep-Sea Research II*, 51:587–600.
- [25] Hansen, D. & Maul, G. (1991). Anticyclonic current rings in the eastern tropical Pacific Ocean. *Journal of Geophysical Research*, 96(C4):6965–6979.
- [26] Heywood, K., Stevens, D., & Bigg, G. (1996). Eddy formation behind the tropical island of Aldabra. *Deep Sea Research I*, 43:555–578.
- [27] Hogg, N. & Stommel, H. (1985). The heton, an elementary interaction between discrete baroclinic geostrophic vortices, and its implications concerning eddy heat-flow. *Proceedings of the Royal Society of London*, 397:1–20.

- [28] Hopfinger, E. & Vanheijst, G. (1993). Vortices in rotating fluids. *Annual Review of Fluid Mechanics*, 25:241–289.
- [29] Kamenkovich, V., Leonov, Y., & Nechaev, D. (1996). On the influence of bottom topography on the Agulhas eddy. *Journal of Physical Oceanography*, 26:892–912.
- [30] Lee, T., Clarke, M., Williams, E., Szmant, A., & Berger, T. (1994). Evolution of the Tortugas Gyre and its influence on recruitment in the Florida Keys. *Bulletin of Marine Science*, 54:621–646.
- [31] Lobel, P. & Robinson, A. (1988). Larval fishes and zooplankton in a cyclonic eddy in Hawaiian waters. *Journal of Plankton Research*, 10:1209–1223.
- [32] McCreary, J., Hyong, S., & Enfield, D. (1989). The response of the coastal ocean to strong offshore winds: with application to circulations in the Gulfs of Tehuantepec and Papagayo. *Journal of Marine Research*, 47:81–109.
- [33] Mulhearn, P., Filloux, J., Lilley, F., Bindoff, N., & Ferguson, I. (1986). Abyssal currents during the formation and passage of a warm-core ring in the East Australian Current. *Deep-Sea Research*, 33:1563–1576.
- [34] Müller-Karger, F. & Fuentes-Yaco, C. (2000). Characteristics of wind-generated rings in the eastern tropical Pacific Ocean. *Journal of Geophysical Research*, 105(C1):1271–1284.
- [35] Nakata, H., Kimura, S., Okazaki, Y., & Kasai, A. (2000). Implications of meso-scale eddies caused by frontal disturbances of the Kuroshio Current for anchovy recruitment. *Ices Journal of Marine Science*, 57(1):143–151.
- [36] Nof, D. (1981). On the β -induced movement of isolated baroclinic eddies. *Journal of Physical Oceanography*, 11:1662–1672.
- [37] Palacios, D. & Bograd, S. (2005). A census of Tehuantepec and Papagayo eddies in the northeastern tropical Pacific. *Geophysical Research Letters*, 32:doi:10.1029/2005GL024324.
- [38] Pedlosky, J. (1996). *Ocean Circulation Theory*. Springer.
- [39] Périgaud, C. (1990). Sea level oscillations observed with Geosat along the two shear fronts of the Pacific North Equatorial Countercurrent. *Journal of Geophysical Research*, 95(C5):7239–7248.
- [40] Richardson, P. & Fratantoni, D. (1999). Float trajectories in the deep western boundary current and deep equatorial jets of the tropical Atlantic. *Deep Sea Research II*, 46:305–333.
- [41] Richardson, P. & Tychensky, A. (1998). Meddy trajectories in the Canary Basin measured during the SEMAPHORE experiment, 1993-1995. *Journal of Geophysical Research*, 103:25029–25045.

- [42] Sale, P. (1970). Distribution of larval Acanthuridae off Hawaii. *Copeia*, pages 765–766.
- [43] Sangrá, P., Pelegrí, J., Hernández-Guerra, A., Arregui, I., Martín, J., Marrero-Díaz, A., Martínez, A., Ratsimandresy, A., & Rodríguez-Santana, A. (2005). Life history of an anticyclonic eddy. *Journal of Geophysical Research*, 110:doi:10.1029/2004JC002526.
- [44] Sansón, L. (2002). Vortex-ridge interaction in a rotating fluid. *Dynamics of Atmospheres and Oceans*, 35:299–325.
- [45] Schmitz, W. (1996). On the eddy field in the Agulhas Retroflection, with some global considerations. *Journal of Geophysical Research*, 101(C7):16,259–16,271.
- [46] Schouten, M., de Ruijter W.P.M., van Leeuwen, P., & Lutjeharms, J. (2000). Translation, decay and splitting of Agulhas rings in the southeastern Atlantic Ocean. *Journal of Geophysical Research*, 105(C9):21913–21925.
- [47] Shi, C. & Nof, D. (1993). The splitting of eddies along boundaries. *Journal of Marine Research*, 51:771–795.
- [48] Siegel, D., McGillicuddy, D., & Fields, E. (1999). Mesoscale eddies, satellite altimetry, and new production in the Sargasso Sea. *Journal of Geophysical Research*, 104:13,359–13,379.
- [49] Sponaugle, S., Lee, T., Kourafalou, V., & Pinkard, D. (2005). Florida current frontal eddies and the settlement of coral reef fishes. *Limnology and Oceanography*, 50(4):1033–1048.
- [50] Stammer, D., Böning, C., & Dieterich, C. (2001). The role of variable wind forcing in generating eddy energy in the North Atlantic. *Progress in Oceanography*, 48:289–311.
- [51] Tracey, K., Watts, D., Meinen, C., & Luther, D. (2006). Synoptic maps of temperature and velocity within the Subantarctic Front south of Australia. *Journal of Geophysical Research*, 111:doi:10.1029/2005JC002905.
- [52] van Aken, H., van Veldhoven, A., Veth, C., de Ruijter, W., van Leeuwen, P., Drijfhout, S., Whittle, C., & Rouault, M. (2003). Observations of a young Agulhas ring, Astrid, during MARE in March 2000. *Deep-Sea Research II*, 50:167–195.
- [53] van Geffen, J. & Davies, P. (2000). A monopolar vortex encounters a north-south ridge or trough. *Fluid Dynamics Research*, 26:157–179.
- [54] Willett, C., Leben, R., & Lavín, M. (2006). Eddies and tropical instability waves in the eastern tropical Pacific: A review. *Progress in Oceanography*, 69:218–238.
- [55] Zamudio, L., Hurlburt, H., Metzger, E., Morey, S., O'Brien, J., Tilburgh, C., & J., Z.-H. (2006). Interannual variability of Tehuantepec eddies. *Journal of Geophysical Research*, 111:doi:10.1029/2005JC003182.

Chapter 6

Conclusion

6.1 Summary of Results

The goals of this thesis were to quantify the spatial and temporal variation in the larval supply of vent gastropods near $9^{\circ} 50' N$ on the East Pacific Rise and to investigate the hydrodynamic processes that contribute to the observed variations. These goals were achieved through a combination of concurrent near-bottom observations of larval flux and current velocities supplemented with satellite observations and a modeling study. Fluxes of hydrothermal vent gastropods to two vent sites, East Wall and Choo Choo (separated by 1.6 km), varied both spatially and temporally on daily and weekly timescales. The variation in larval flux was significantly correlated with transport in currents. Results suggested that the larval flux towards the benthos originated primarily from neighboring vent communities with 1-2 km. Vents with multiple neighboring vents to the north and south may receive uninterrupted high larval flux, while larval flux to isolated vents may be limited. Larval loss in cross-axis current flows and during the passing of a mesoscale eddy created regional (> 1.6 km) decreases in larval flux. While these larvae were lost from the $9^{\circ} 50' N$ area, transport in eddy-induced currents or off-axis currents may have increased the overall connectivity of the northern East Pacific Rise.

In Chapter 2, I developed an approach to identify hydrothermal vent gastropods in a labor and cost efficient manner using a combination of molecular and morphological techniques. While the approach was developed for identification of the larval stage, the sequence database can be used to identify any stage of vent gastropod species. Embryos and developing veligers within egg capsules laid near $9^{\circ} 50' N$ were identified

as *Gymnobela* sp. A using the sequence database. This represents a larval development strategy that has hence been rare at hydrothermal vents. Egg capsules only have been reported for three other unidentified taxa at the Galapagos Rift and Juan de Fuca [9]. Comparison of the genetics and population dynamics of *Gymnobela* sp. A to turrids with planktotrophic larvae and the many gastropods with non-planktotrophic lecithotrophic larvae may provide insights into the role of larval dispersal and the evolutionary constraints on hydrothermal vent species. Results from Chapter 2 were used in Chapters 3 and 4 to morphologically identify gastropod larvae to the lowest possible taxonomic level.

In Chapter 3, daily larval flux and current velocity observations suggested that larval supply to hydrothermal vents could be highly variable and was dependent upon proximity to the nearest vents to the north and south. East Wall received uninterrupted larval flux independent of the currents, whereas Choo Choo received lower larval flux punctuated with an episode of increased larval flux during southward current flows. A distance of 4.5 km was sufficient to impede the transport of detectable numbers larvae from V vent to Choo Choo in northward currents. The irregular distribution of vents along the ridge axis meant that larval flux was contingent upon the variation in the direction of the along-axis current velocities.

In Chapter 4, larval loss from the ridge was the dominant factor in the generation of variation in larval flux to East Wall and Choo Choo. Variation in larval supply has been focused largely on the periods of increased larval supply. However, the mechanisms for decreasing larval supply may be just as important in controlling population and community dynamics. Cross-axis currents on the ridge axis were correlated with the decrease in larval flux at both sites. There was no evidence that larvae transported off-axis returned to the vent sites.

In Chapter 5, modeling and satellite observations were combined with the observations from Chapter 4 to show that an anticyclonic eddy originating in the Gulf of Tehuantepec extended to the seafloor where it influenced current velocities and larval fluxes. Tehuantepec and Papgayo eddies formed vertical dipoles in the model with strong anticyclonic flow at the surface, also observed via satellite altimetry, and weaker cyclonic flow at depth, also observed in near-bottom current velocities. The passing Tehuantepec eddy created strong current velocities on the ridge axis during which time larval flux to both East Wall and Choo Choo decreased. While eddies decreased local larval flux, the passing of an eddy could have enhanced larval dispersal

and population connectivity along 100 - 300 kilometers of the nEPR. Tracer (a proxy for passive larvae) advected in simulated currents was transported tens to hundreds of kilometers along the ridge axis. Shear in the swirl also stretched tracer patches such that the tracer spread over 50 - 250 km. Larvae transported to spread over that area could interact with numerous vents in multiple fields during the passing of a single eddy.

6.2 Recovery from Disturbance

The results of this thesis present a hypothesis to explain the two, apparently contradictory, realities of larval supply based on benthic observations and work on larval dispersal: 1) an abundant larval supply remains close to vent sites and 2) larvae are dispersed long distances (within the scale of a ridge segment ~ 100 km). Point estimates of larval abundances were highest near a vent site, near bottom (1 m above bottom) compared to away from a vent site and off bottom (≥ 20 m above bottom) [13]. I propose that the larval supply is primarily locally driven with frequent periods of loss corresponding to long-distance dispersal events. Chapter 3 demonstrated that larval supply was primarily from neighboring vents. Larval transport between neighboring vents would keep larval supply high, facilitating the rapid establishment of a dominant species. However, initial colonists must develop quickly in order to generate a local larval supply. The time to reproduction would be the rate-limiting step for initial establishment local abundance. The growth rate and maturation of most vent species are currently unknown. Estimated growth rates of the vent tubeworm, *Riftia pachyptila*, are 4 cm yr^{-1} [5] to 85 cm yr^{-1} [10], supporting the hypothesis of rapid growth and development to maturation. Frequent long-distance dispersal events via mesoscale eddies and/or off-axis currents could provide initial colonists. Tehuantepec and Papagayo eddies could transport larvae from vent communities hundreds of kilometers away. An average of 3.5 Tehuantepec and 2.2 Papagayo eddies form each year with the potential to interact with the ridge and vent larvae [15]. Additionally, larvae may be transported long distances in proposed off-axis jets on the eastern and western flanks. The combination of local larval transport and dispersal events would provide sufficient initial colonists and ample subsequent recruits to rapidly establish high biomass and dominance.

A preliminary test of part of this hypothesis is underway on the 9° N segment.

The majority of the benthic and larval studies to date focused on the cluster of vents near $9^{\circ} 50' \text{ N}$. For areas with multiple vents clustered together, larval supply is expected to be uninterrupted and high. This is consistent with the observations of strong benthic interactions [6, 7, 12, 14] and rapid establishment of species [16]. However, the hypothesis of a local larval supply can be tested at isolated vent sites where larval supply is expected to be infrequent and limiting. Recruitment studies and successional time-series have not been done at isolated vent sites, partially due to logistical constraints on submarine time. However, recruitment substrate, current meters and sediment traps currently deployed at K vent ($9^{\circ} 29.7' \text{ N}$) and in the $9^{\circ} 50' \text{ N}$ area as part of the LADDER study will soon provide information on the different factors contributing to population and community dynamics at isolated and clustered vent communities.

Additionally, monitoring of the recolonization of nascent vents and early succession is underway in the $9^{\circ} 50' \text{ N}$ area. In January 2006, relatively soon after the field program for this thesis finished, an extensive magmatic and tectonic event obliterated most of the hydrothermal vents between $9^{\circ} 48' \text{ N}$ and $9^{\circ} 50.5' \text{ N}$ in lava flows extending from $9^{\circ} 46' \text{ N}$ to $9^{\circ} 56' \text{ N}$ [18]. As part of the first response cruise to the site in May 2006, I deployed two sediment traps and a current meter near $9^{\circ} 50' \text{ N}$ to assess the availability and the species composition of larvae settling towards the nascent vents. Thus, monitoring of larval flux is ongoing in collaboration with numerous interdisciplinary efforts that will better characterize the physical, chemical and biological succession after this large disturbance.

6.3 Mesoscale Eddies

The observation and characterization of a vertical dipole interacting with the seafloor represents a contribution of potentially broad importance to oceanography. Mesoscale eddies have been shown to be important in mixing and transporting heat, chemical constituents and biology in surface waters. Results from this thesis suggest that they may also play an important role in mixing and transporting heat, chemical constituents and biology in the deep-sea near hydrothermal vents. Heat transfer and chemical alterations during the generation of hydrothermal fluids accounts for large percentages of both the oceanic heat budget [1, 2, 8, 11, 17] and oceanic chemical composition [4, 3, 19]. Globally, the interaction of mesoscale eddies with the mid-

ocean ridge could be important in the distribution of the heat and chemical anomalies produced at hydrothermal vents.

Bibliography

- [1] Anderson, R. & Hobart, M. (1976). The relation between heat flow, sediment thickness, and age in the eastern Pacific. *Journal of Geophysical Research*, 81:2968–2989.
- [2] Converse, D., Holland, H., & Edmond, J. (1984). Flow rates in the axial hot springs of the East Pacific Rise (21° N): implications for the heat budget and the formation of massive sulfide deposits. *Earth and Planetary Science Letters*, 69:159–175.
- [3] Edmond, J., Measures, C., McDuff, R., Chan, L., Collier, R., Grant, B., Gordon, L., & Corliss, J. (1979). Ridge crest hydrothermal activity and the balances of the major and minor elements in the ocean: the Galapagos data. *Earth and Planetary Science Letters*, 46:1–18.
- [4] Edmond, J. M., von Damm, K. L., McDuff, R. E., & Measures, C. I. (1982). Chemistry of hot springs on the east pacific rise and their effluent dispersal. *Nature*, 297(5863):187–191.
- [5] Gaill, F., Shillito, B., Ménard, F., Goffinet, G., & Childress, J. (1997). Rate and process of tube production by the deep-sea hydrothermal vent tubeworm *Riftia pachyptila*. *Marine Ecology Progress Series*, 148:135–143.
- [6] Govenar, B., Freeman, M., Bergquist, D. C., Johnson, G. A., & Fisher, C. R. (2004). Composition of a one-year-old *Riftia pachyptila* community following a clearance experiment: Insight to succession patterns at deep-sea hydrothermal vents. *Biological Bulletin*, 207(3):177–182.
- [7] Govenar, B., Le Bris, N., Gollner, S., Glanville, J., Aperghis, A. B., Hourdez, S., & Fisher, C. R. (2005). Epifaunal community structure associated with *Riftia pachyptila* aggregations in chemically different hydrothermal vent habitats. *Marine Ecology Progress Series*, 305:67–77.
- [8] Green, K. & von Herzen, R. (1981). The Galapagos spreading center at 86°W; a detailed geothermal field study. *Journal of Geophysical Research*, 86:979–986.
- [9] Gustafson, R. G., Littlewood, D. T. J., & Lutz, R. A. (1991). Gastropod egg capsules and their contents from deep-sea hydrothermal vent environments. *Biological Bulletin*, 180(1):34–55.
- [10] Lutz, R., Shank, T., Fornari, D., Haymon, R., M., L., Von Damm, K., & Desbruyères, D. (1994). Rapid growth at the deep-sea vents. *Nature*, 371:663–664.

- [11] MacDonald, K. C., Becker, K., Spiess, F. N., & Ballard, R. D. (1980). Hydrothermal heat flux of the 'black smoker' vents on the East Pacific Rise. *Earth Planet Sci. Lett.*, 48(1):1–7. English.
- [12] Mullineaux, L. S., Mills, S. W., & Goldman, E. (1998). Recruitment variation during a pilot colonization study of hydrothermal vents (9° 50' N, East Pacific Rise). *Deep Sea Research*, 45:1–3.
- [13] Mullineaux, L. S., Mills, S. W., Sweetman, A. K., Beaudreau, A. H., Metaxas, A., & Hunt, H. L. (2005). Vertical, lateral and temporal structure in larval distributions at hydrothermal vents. *Marine Ecology Progress Series*, 293:1–16.
- [14] Mullineaux, L. S., Peterson, C. H., Micheli, F., & Mills, S. (2003). Successional mechanism varies along a gradient in hydrothermal fluid flux at deep-sea vents. *Ecological Monographs*, 73(4):523–542.
- [15] Palacios, D. & Bograd, S. (2005). A census of Tehuantepec and Papagayo eddies in the northeastern tropical Pacific. *Geophysical Research Letters*, 32:doi:10.1029/2005GL024324.
- [16] Shank, T. M., Fornari, D. J., Von Damm, K. L., Lilley, M. D., Haymon, R. M., & Lutz, R. A. (1998). Temporal and spatial patterns of biological community development at nascent deep-sea hydrothermal vents (9° 50' N, East Pacific Rise). *Deep-Sea Research (Part 2, Topical Studies in Oceanography)*, 45:465–515.
- [17] Sleep, N. & Wolery, T. (1978). Egress of hot water from mid-ocean ridge hydrothermal systems: some thermal constraints. *Journal of Geophysical Research*, 83:5913–5922.
- [18] Tolstoy, M., Cowen, J., Baker, E., Fornari, D., Rubin, K., Shank, T., Waldhauser, F., Bohnenstiel, D., Forsyth, D., Holmes, R., Love, B., Perfit, M., Weekly, R., Soule, S., & Glazer, B. (2006). A sea-floor spreading event captured by seismometers. *Science*, 314(5807):1920–1922.
- [19] Von Damm, K. L., Grant, B., & Edmond, J. M. (1983). Preliminary report on the chemistry of hydrothermal solutions at 21 degree North, East Pacific Rise. *Hydrothermal Processes At Seafloor Spreading Centers*, 12:369–390.

REPORT DOCUMENTATION PAGE	1. REPORT NO. MIT/WHOI 2007-16	2.	3. Recipient's Accession No.
4. Title and Subtitle Influence of Hydrodynamics on the Larval Supply to Hydrothermal Vents on the East Pacific Rise		5. Report Date June 2007	
7. Author(s) Diane K. Adams		6.	
9. Performing Organization Name and Address MIT/WHOI Joint Program in Oceanography/Applied Ocean Science & Engineering		8. Performing Organization Rept. No.	
		10. Project/Task/Work Unit No. MIT/WHOI 2007-16	
		11. Contract(C) or Grant(G) No. (C) OCE0424953 (C) OCE9712233 (G)	
12. Sponsoring Organization Name and Address National Science Foundation National Defense Science and Engineering Graduate Fellowship Woods Hole Oceanographic Institution		13. Type of Report & Period Covered Ph.D. Thesis	
15. Supplementary Notes This thesis should be cited as: Diane K. Adams, 2007. Influence of Hydrodynamics on the Larval Supply to Hydrothermal Vents on the East Pacific Rise. Ph.D. Thesis. MIT/WHOI, 2007-16.		14.	
16. Abstract (Limit: 200 words) Examination of the scales at which larval supply varies spatially and temporally, and correlation with concurrent physical observations can provide insights into larval transport mechanisms that contribute to structuring marine benthic communities. In order to facilitate field studies, this thesis first provides new morphological and genetic identifications for hydrothermal vent gastropod larvae along the northern East Pacific Rise. Daily and weekly variability in the supply of hydrothermal vent gastropod larvae to two hydrothermal vents, 1.6 km apart on the East Pacific Rise, were quantified concurrently with current velocity observations. The magnitude and temporal pattern of larval supply differed between vent sites, despite their close proximity. A strong correlation between along-axis flow and daily larval supply suggested that larval supply occurred primarily via along-axis transport between local sources 1-2 km apart. However, weekly larval supply appeared to be driven by larger spatial scales through losses associated with cross-axis flows and the passage of mesoscale eddies. Tracer movement within a quasi-geostrophic eddy model was consistent with the observations of decreased larval supply concurrent with an eddy observed via satellite altimetry. The tracer movement also indicated that deep eddy-induced flow could facilitate a long-distance dispersal event, enhancing dispersal between vents 100s km apart.			
17. Document Analysis a. Descriptors hydrothermal vents larvae hydrodynamics b. Identifiers/Open-Ended Terms c. COSATI Field/Group			
18. Availability Statement Approved for publication; distribution unlimited.		19. Security Class (This Report) UNCLASSIFIED	21. No. of Pages 164
		20. Security Class (This Page)	22. Price